Fast Link Adaptation for 802.11n

Jensen, Tobias; Kant, Shashi

AALBORG UNIVERSITET

Fast Link Adaptation for IEEE 802.11n

Institute of Electronic Systems
Signal and Information Processing in Communications
Shashi Kant · Tobias Lindstrøm Jensen

The Faculty of Engineering and Science

Aalborg University

Master's Thesis

TITLE:

Fast Link Adaptation for
IEEE 802.11n

PROJECT PERIOD:

P10,
February 5, 2007
- August 6, 2007

PROJECT GROUP:

1091

GROUP MEMBERS:

Shashi Kant
Tobias Lindstrøm Jensen

SUPERVISORS:

Dr. Joachim Wehinger,
Wipro-NewLogic Technologies,
Sophia Antipolis,
France.

Prof. Dr. Bernard Fleury
Aalborg University,
Denmark.

NUMBER OF COPIES: 5

REPORT PAGE COUNT: 130

APPENDIX PAGE COUNT: 10

TOTAL PAGE COUNT: 140

ABSTRACT:

For fast link adaptation (FLA) algorithm, link quality metrics (LQMs) are presented for IEEE 802.11n WLAN systems with convolutional coding and higher order modulations. The LQMs estimate the PER of an instantaneous fading channel such that the FLA technique can dynamically select a suitable modulation and coding scheme (MCS) which fulfills a PER objective. The presented LQMs are Raw-BER, EESM and MIESM, and MMIBM which utilize the post processing SINRs to compute the uncoded bit error probability, effective SNR and mutual information, respectively. We also present a novel LQM, MMIRM, which is derived from the reliability of the generated LLRs and it can be useful when linear receivers like MMSE are not employed. However, more research in MMIRM has to be carried out to bring the performance up to the same level as the other presented methods. We also give a useful upper bound of the performance of any fast link adaptation scheme which is obtained by simulation. It is shown that the best LQM achieves a throughput that is at most $1\,\mathrm{dB}$ and $1.25\,\mathrm{dB}$ from the practical upper bound in SISO and MIMO systems, respectively.

Preface

This thesis report serves as a documentation for the project work of the group 1091 in the period from February 5, 2007 to August 6, 2007. It is to comply with the demands at Aalborg University for the SIPCom specialization in the 10^{th} semester. The project is executed in cooperation with Wipro-NewLogic Technologies, Sophia-Antipolis, France, as a part of their modem development for IEEE 802.11n.

Structure

The report is divided into a number of chapters whose contents are outlined here.

- "Introduction" part contains the introduction to the project and the problem scope.

- "Channel" chapter provides a general concept of wireless channels and introduces the IEEE channel models for 802.11n.

- "MIMO-OFDM" introduces the basic concepts of orthogonal frequency division multiplexing (OFDM), bit interleaved and coded modulation (BICM), and multiple input and multiple output (MIMO). The MIMO receivers are briefly discussed with softbit generation to make the reader familiar with the notations to be used in the FLA algorithms.

- The chapter "Link Adaptation Algorithms" explains link adaptation mechanism in general and gives a foundation for the possibilities to use link adaptation for IEEE 802.11n. This is followed by a survey of possible link quality metrics (LQMs) for fast link adaptation and 3 LQMS are chosen for further investigation.

- "Fast Link Adaptation Algorithms" considers the different methods selected in the previous chapter. Further, it considers general parts of the FLA algorithm common to all the methods.

- In the chapter "Numerical Results", the simulation results are presented and discussed for the considered LQMs. The estimation accuracy, throughput and PER performances are evaluated for 1×1 and 2×2 under ideal and non-ideal conditions. The results of the throughput and delay simulations are also provided for different settings. Finally, the methods are compared with each other and analyzed to find a robust LQM which should be implemented in the modem.

- "Conclusions" summarizes the results obtained throughout the report.

Reading Guidelines

Chapter 2 "Channel" and Chapter 3 "MIMO-OFDM" are considered as the background information for the rest of the report. If the reader is familiar with these concepts he/she can skip these chapters.

Nomenclature

References to various publications are denoted by brackets as [] and may also contain a reference to a specific page or section where the information appears. The identification in the brackets refers to the bibliography which can be found at the back of the main report on p.125 . Reference to figures (and tables) are denoted by "Figure/Table x.y" and equations by "Equation (x.y)" where x is a chapter number and y is a counting variable for the corresponding element in the chapter.

A vector is denoted by small bold face letters "$\boldsymbol{a}$" and matrix by "$\mathbf{A}$", always capital. Acronyms are given on p.11 and mathematical conventions are given on p.13.

The words in the *italic* form are used in the text to accentuate the matter.

Enclosed Material

A CD ROM contain a Postscript, DVI and PDF version of this report. A version with hyperlinks is also included in DVI and PDF.

Tobias Lindstrøm Jensen

Shashi Kant

Contents

Acronyms

AWGN	Additive White Gaussian Noise
BER	Bit Error Rate
BICM	Binary Interleaved Coded Modulation
BPSK	Binary Phase Shift Keying
CSI	Channel State Information
CP	Cyclic Prefix
DC	Direct Current
DIFS	Distributed Inter Frame Space
EESM	Exponential Effective SNR Mapping
FFT	Fast Fourier Transform
FLA	Fast Link Adaptation
GI	Guard Interval
HDTV	High Definition TV
HT	High Throughput
HTC	High Throughput Control
IEEE	Institute of Electrical and Electronics Engineers
IFFT	Inverse Fast Fourier Transform
LA	Link Adaptation
LLR	Log-Likelihood Ratios
LOS	Line of Sight
LQM	Link Quality Metric
MAC	Medium Access Control
MAI	MCS request / Antenna selection Identifier
MCP	Modulation and Coding Product
MCS	Modulation and Coding Scheme
MFB	MCS Feedback
MFSI	MCS feedback Sequence Identifier
MI	Mutual Information
MIBM	Mutual Information Bit Mapping
MIESM	Mutual Information Effective SNR Mapping
MIMO	Multiple Input Multiple Output
ML	Maximum Likelihood
MMIBM	Mean Mutual Information per coded Bit Mapping
MMIRM	Mean Mutual Information Reliability Mapping
MMSE	Minimum Mean Square Error

MRQ	MCS Request
MSI	MCS request Sequence Identifier
NLOS	Non Line of Sight
NDP	Null Data Packet
PDF	Probability Density Function
PEP	Pair wise Error Probability
PER	Packet Error Rate
PHY	Physical Layer
PL	Packet Length
PLCP	Physical Layer Convergence Protocol
PPDU	PLCP Packet Data Unit
PSDU	Physical layer Service Data Unit
QAM	Quadrature Amplitude Modulation
QoS	Quality of Service
QPSK	Quadrature Phase Shift Keying
Rx	Receiver
SDM	Space Division Multiplexing
SIFS	Short Inter Frame Space
SINR	Signal to Interference and Noise Ratio
SISO	Single Input Single Output
SLA	Slow Link Adaptation
SM	Spatial Multiplexing
SNR	Signal to Noise Ratio
STA	Station
TP	Throughput
TRQ	Training (sounding) Request
Tx	Transmitter
TXOP	Transmit Opportunity
VoIP	Voice over Internet Protocol
WLAN	Wireless Local Area Networks
WSS	Wide Sense Stationarity
ZF	Zero Forcing

Mathematical Conventions

$\mathcal{CN}$	Circularly Symmetric Complex Gaussian Noise
$h[n, \ell]$	Channel impulse response
$H[n, f]$	Channel transfer function
$\mathbf{H}[k]$	Channel transfer function for the kth subcarrier
W_{c}	Coherence bandwidth with correlation level 0.9
τ_s	Delay spread
T_{c}	Coherence time with correlation level 0.9
D_s	Doppler spread
$R[\Delta f]$	Frequency Correlation Function
$R[\Delta n]$	Time Correlation Function
$\mathbf{H}^H$	Hermitian (complex conjugate) transpose of $\mathbf{H}$
$\mathit{SINR}_j[k]$	Symbol SINR for the jth stream and kth subcarrier
$\mathit{SNR}_{\mathrm{eff}}$	Effective SNR
$\mathit{SNR}_{\mathrm{instant}}$	Instantaneous SNR
$\mathrm{RawBER}_j[k]$	RawBER for the jth stream and kth subcarrier
N_{T}	Number of transmit antennas
N_{R}	Number of receive antennas
N_{ss}	Number of spatial streams
N_{sd}	Number of data subcarriers
N_{sc}	Number of used subcarriers (data and pilot subcarriers)
N_{symb}	Number of OFDM symbols
R_{c}	Code rate
$\mathbb{E}\{\cdot\}$	Expectation operator
$\log$	Natural Logarithm
$\log_2$	Logarithm of base 2
$\log_{10}$	Logarithm of base 10
$\mathbb{P}\{x\}$	Probability of a random variable $X = x$
$p(x)$	PDF of a random variable $x \in X$
L	Log-Likelihood Ratio (LLR)
$\lfloor x \rfloor$	Floor operator
$\mathcal{F}\{\cdot\}$	Fourier transform
$\mathit{var}\{X\}$	variance of a random variable X, i.e., $\mathbb{E}\{(X - \mathbb{E}\{X\})^2\}$

1 Introduction

A wireless communication standard like IEEE802.11 or HiperLAN/2 is always envisaged to provide ubiquitous high-speed access to data or information. The zeal for a higher data rate communication system has challenged the wireless researchers all over the world. Thus, the data rate offered by the current wireless communication systems has increased tremendously. The current wireless local area networks (WLAN) such as IEEE 802.11a/g standard offers data rate at physical (PHY) layer up to $54\,\mathrm{Mbps}$ (cf. Figure 1.1). The advent of new applications such as video transmission to high definition TV (HDTV), streaming of video, video phones, etc., demand very high data rates. The latest digital communication techniques can be used to increase the data rate. The basic ways to increase the data rate are larger channel bandwidth with utilization of a higher number of data subcarriers, larger size of constellation, higher coding rate and use of multiple antennas.

Therefore, the thirst of higher data rate and range can be quenched by the techniques employed in the IEEE standard 802.11 [IEEE802.11n]. The PHY of 802.11n employs multiple antennas at the transmitter with orthogonal frequency division multiplexing (OFDM) to render higher data rates and range [IEEE802.11n]. Furthermore, 802.11n's PHY can offer a maximum data rate up to $600\,\mathrm{Mbps}$ by including 64 quadrature amplitude modulation (QAM) with coding rate $5/6$, four spatial streams, short guard interval of $400\,\mathrm{ns}$ and $40\,\mathrm{MHz}$ channel bandwidth [IEEE802.11n] (cf. Figure 1.1). The IEEE 802.11n standard is supposed to be finalized in 2008.

In real world scenarios, the wireless channel varies over time. Thus, link adaptation (LA) can be used to cope with a varying channel in order to sustain a reliable communication and to increase throughput of a system. The IEEE standard 802.11n defines a protocol (i.e., LA) that allows to adjust the modulation and coding scheme (MCS) according to current channel condition in order to increase throughput.

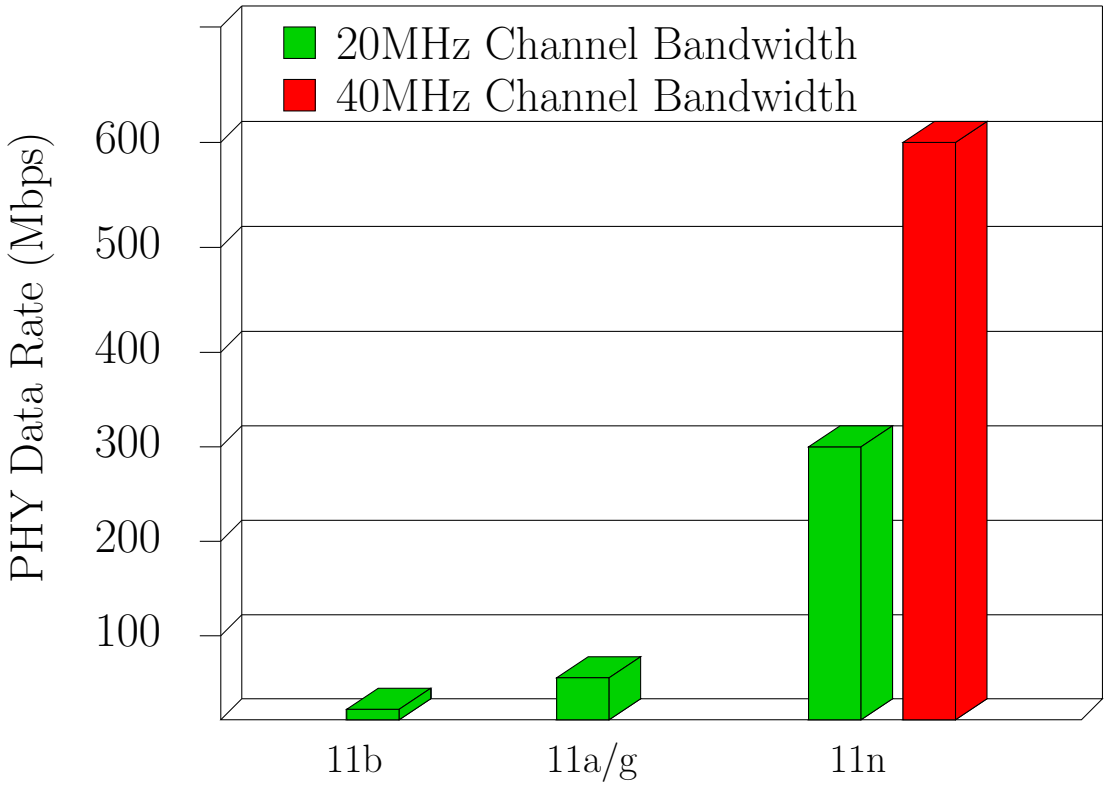

Figure 1.1: *Comparison of data rates of IEEE 802.11 WLAN standards*

A basic principle of LA is to select one of the MCS according to a channel condition or channel state information (CSI) [1] at the receiver [2]. The scenario in Figure 1.2 is contemplated where two stations (STAs) A and B communicate by some predefined protocols. Stations (STAs) A and B are assumed to be a transmitter and receiver, respectively. If STA A wants to transmit data or packets reliably to STA B, then STA B can estimate and recommend a MCS n $\left(n \in \{0, 1, \cdots, 76\}\right)$ to STA A such that the transmission is reliable under the current channel condition. Hence, LA can assist STA A to transmit packets reliably and exploit maximum data throughput at STA B by dynamically adjusting its MCS recommended by STA B. Furthermore, the MCS can be estimated by CSI available at STA B under some quality of service (QoS) constraint.

The IEEE 802.11n standard has both High Throughput (HT) and non-HT fea-

[1] A CSI provides some knowledge about the channel. It can include instantaneous signal to noise plus interference ratio (SINR) for MIMO , signal to noise ratio (SNR) for SISO, estimated channel, etc. [Gesbert et al., 2002].

[2] It is worth to mention that CSI can also be available at the transmitter for instance by assuming reciprocity of the channel. The principle of reciprocity implies that the channel is identical for forward and reverse link as long as the channel is measured at the same time instant and frequency with identical antenna locations. For detailed information on the reciprocity and its implications, refer [Paulraj et al., 2005].

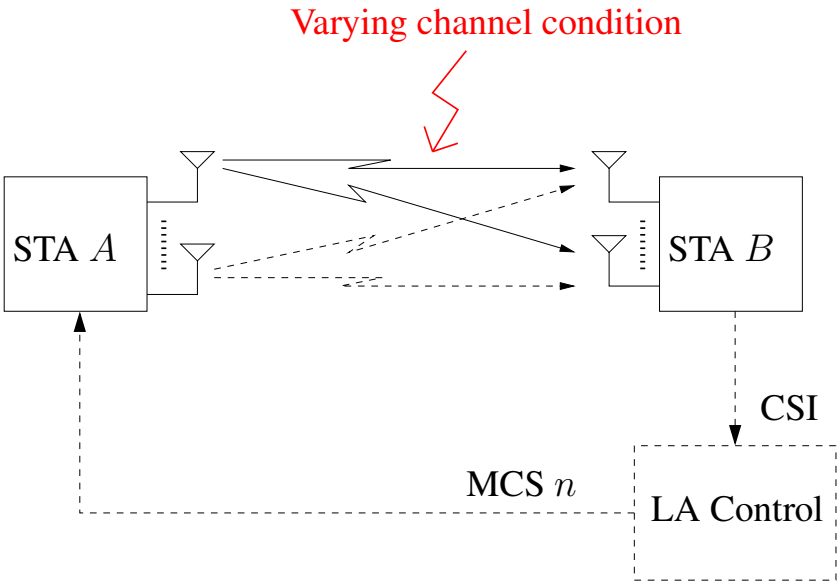

Figure 1.2: *Basic scheme for link adaptation.*

tures. Non-HT features mean that it supports legacy devices i.e., 802.11a/g. An HT STA (High Throughput Station) comprises features like MIMO techniques, LDPC (Low Density Parity Check) coding, and link adaptation to provide high throughput [IEEE802.11n]. There are some mandatory and optional features in the 802.11n. Some of the new MAC features of IEEE 802.11n compared to 802.11a/g are frame aggregation, reverse direction protocol (i.e., allows a STA to share its TXOP (transmit opportunity) with another STA). The main mandatory PHY features are single spatial stream, 20 MHz channel bandwidth, interoperability with legacy devices (i.e., legacy and mixed mode) and convolutional code. Some of the optional PHY features are support of $2, 3, 4$ spatial streams, short guard interval, 40 MHz channel bandwidth, support of only HT features (greenfield mode), transmit beamforming, LDPC codes, STBC (Space Time Block Coding) and LA.

1.1 Project Scope

The main objective of this project work is to investigate various link quality metrics (LQMs) for fast link adaptation (FLA) algorithms for IEEE 802.11n and to assess their performance. Only MIMO systems up to 2x3 is considered. An IEEE 802.11n modem simulator in MATLAB is available at Wipro-NewLogic which is used to assess the performance of different algorithms designed by the signal processing team. The simulator can simulate a one-way link for a block fading channel. The simulator is the starting point for assessing the throughput associated to a particular fast link adaptation

algorithm. Our contributions to the simulator chain are to make changes to the current simulator such that it supports a feedback mechanism for FLA with a time varying channel as illustrated in Figure 1.2. Further, to add a fast link adaptation algorithm to the simulator chain.

Channel 2

This chapter deals with the channel models considered relevant for this project. If the reader is familiar with the fundamentals of channels, then he or she can skip this chapter. Firstly, a short introduction is given in Section 2.1 and 2.2 which will help to clarify concepts and notation. In Section 2.3, the IEEE channel models are introduced which are used for this project work. Important parameters for the used IEEE models will be given to help in the design of an FLA algorithm. For convenience only discrete models are considered in this chapter.

2.1 Physical Propagation Channel Model

Consider a setup as shown in Figure 2.1 with a single receive and transmit antenna and a number of obstacles in the area. These could be buildings, walls, furniture etc. The signal is scattered by these obstacles. This causes a multiple of possible propagation paths. A propagation path can also be the unscattered direct Line of Sight (LOS) path.

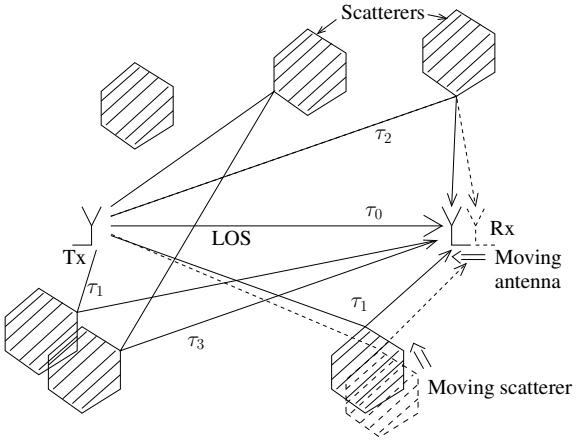

Figure 2.1: *Transmitter and receiver in an area with scatterers. The received signal comes from different paths including the LOS path. The paths change because the scatterers and/or the receiver moves.*

This setup will yield the equivalent discrete baseband model [Tse et al., 2005, p.26].

$$y[n] = \sum_{\ell=\emptyset}^{\mathbb{L}-1} h[n,\ell]x[n-\ell] \tag{2.1}$$

where $x[n]$ is the transmitted signal at time n, and $y[n]$ is the received signal. The channel impulse response $h[n,\ell]$ is the gain and phase shift for the tap ℓ of the paths with the same delay. There are for example two paths with the same delay τ_1 in Figure 2.1. A simple model for the channel impulse response is to assume [Tse et al., 2005, p.36];

- The phase of the signal paths are uniformly distributed $[0; 2\pi)$.
- The phase of the signal paths are independent.
- The amplitude of the signal paths are of the same order.
- There are many paths.

Then the channel impulse response can be modelled as a Rayleigh distribution for a NLOS channel as given in Equation (2.2).

$$P_{|h[n,\ell]|}(z) = \frac{z}{\sigma_\ell^2} \exp\left(-\frac{z^2}{2\sigma_\ell^2}\right). \tag{2.2}$$

Further, the argument is uniformly distributed as $\arg\{h[n,\ell]\} = 1/2\pi$. For a LOS channel the amplitude of the signal paths are not necessarily of the same order. The impulse response can then be modelled as having a Rician distribution.

$$|h[n,\ell]| \sim \sqrt{\frac{\kappa}{\kappa+1}}\sigma_\ell \exp(j\theta) + \sqrt{\frac{1}{\kappa+1}}\mathcal{CN}(0,\sigma_\ell^2) \tag{2.3}$$

where the first term corresponds to the LOS impinging with the angle θ and the second term is the other scattered paths distributed as circular symmetric. The parameter κ determines the power ratio between the LOS component and all NLOS components of the channel. The IEEE channel model which we will consider later uses cluster modelling where the signal is scattered by the groups of scatterers. Further, it also assumes that the amplitude of the signal paths are exponential decaying and not of the same order of amplitude.

2.2 Time Variant Channels

Now let us consider the time variant channel with the example shown in Figure 2.2. Consider two groups of effects that will make a channel time variant [Tse et al., 2005, p.10].

- **Small scale fading –** Small scale displacements over time causing constructive and destructive interference of the different paths.
- **Large scale fading –** Large scale displacement significantly changing/creating/destroying the different signal paths.

The small and large scale fading will influence the SNR or the link quality as a function of time. In Figure 2.2, the fast fluctuation is due to small scale fading, and the slow fluctuations due to large scale fading effects.

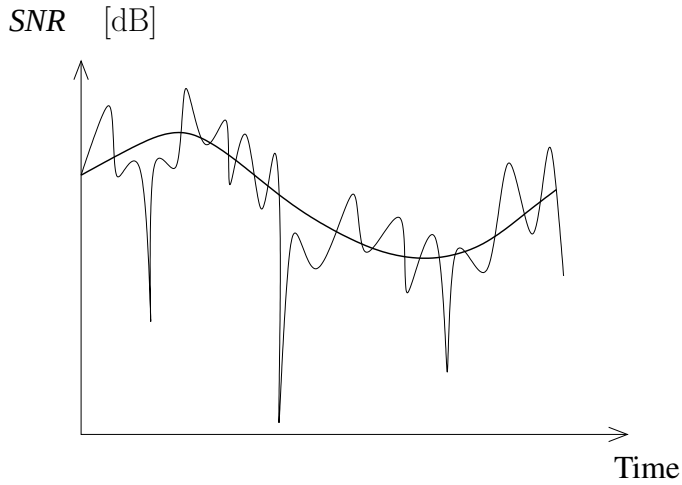

Figure 2.2: *Varying SNR or link quality as a function of time. Idea from [Tse et al., 2005, p.11].*

Reconsider Figure 2.1, and notice how the scatterers and the receive antenna are moving. Especially the phase of the received signal changes when the length of the propagation path changes. The phase change creates constructive/deconstructive superposition which results in fading. Small scale displacements of scatterers and the receive antenna change the length of the propagation paths causing small scale fading. This means that the channel impulse response is varying over time. Figure 2.3 shows an example of an impulse response $|h[n, \ell]|$ which changes during time $n = m$ to $m + 2$.

2.2.1 Time Selective Fading

In time selective fading, the channel gain varies over time which is represented in Figure 2.4(b). Due to the different relative velocities on individual paths Doppler frequencies are introduced. The Doppler frequency D_i for the ith path with relative angle to the LOS angle α_i and velocity v is [Fleury, 2006, p.10]

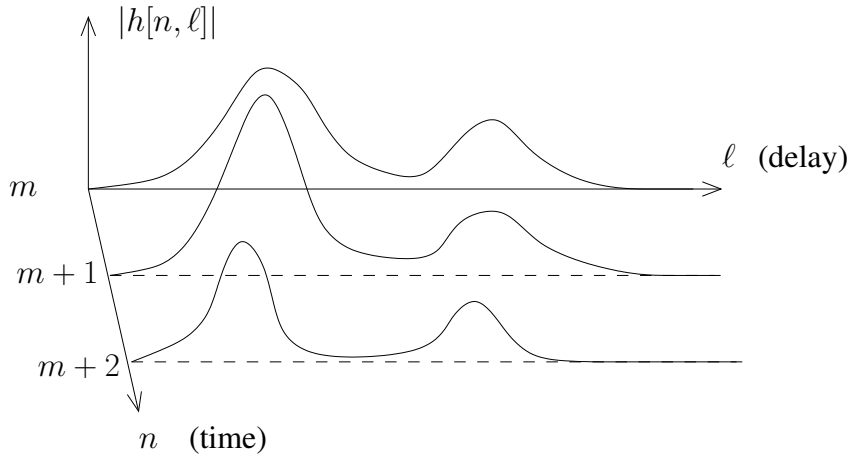

Figure 2.3: *Example which showing how $|h[n,\ell]|$ changes between $n = m$ and $m + 2$.*

$$D_i = \frac{v}{\lambda}\cos(\alpha_i)\,. \tag{2.4}$$

with λ the wavelength. With different paths, the Doppler shift varies as a function of velocity and relative angle. Let's define D_s as the maximum Doppler spread of all Doppler frequencies [Tse et al., 2005, p.30].

$$D_s = \max_{i,j} |D_{f,i} - D_{f,j}| \tag{2.5}$$

The Doppler spread is shown in Figure 2.4(a). Consider now the coherence time T_c as the time duration such that the channel can be considered as "almost" time invariant or "flat". This is shown in Figure 2.4(b). A small coherence time will indicate that the channel is changing rapidly, a fast varying channel. A large coherence time T_c will indicate a slowly varying channel.

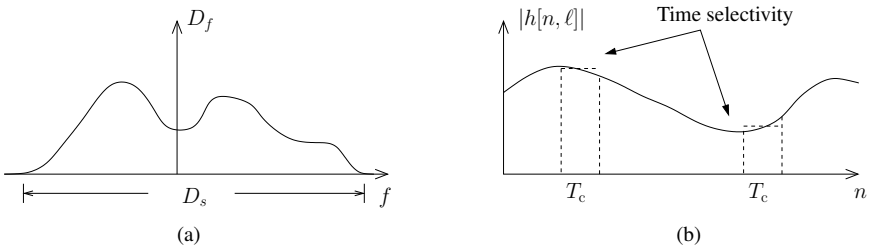

Figure 2.4: *Examples of the notion of doppler spread D_s and coherence time T_c.*

To define coherence time more properly, let $H[n,f] = \mathcal{F}_\ell\{h[n,\ell]\}$ be the Fourier transform of the channel impulse response. Assuming wide sense stationary (WSS) $R[\Delta n] = E\{H^H[n,f]H[n+\Delta n,f]\}$, let the coherence time then be defined as

$$T_{\mathrm{c}} = \underset{T}{\operatorname{argmin}} \{|R[T]| = 0.9\,|R[0]|\} \tag{2.6}$$

where 0.9 is the coherence level. Figure 2.5 explains Equation (2.6). The coherence level for coherence time can be defined differently [Paulraj et al., 2005, p.16] [Rappaport, 2002, p.165]. But, for future use in the report we want to consider the time where the channel can be considered almost constant and a level of 0.9 is appropriate for this use [Fleury, 2007].

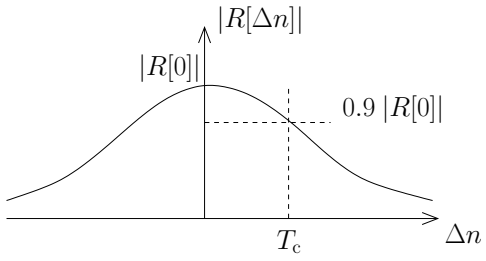

Figure 2.5: *Example of the coherence bandwidth W_{c}.*

The relation between Doppler spread and coherence time can be described as [Paulraj et al., 2005, p.15],

$$T_{\mathrm{c}} \approx \frac{1}{D_s}\,. \tag{2.7}$$

There are also other definitions where coherence time T_{c} and Doppler spread D_s are inversely proportional (No approximation in Equation (2.7) and multiplied with a constant) [Rappaport, 2002, p.163][Tse et al., 2005, p.33]. However, the important notion is that coherence time and Doppler spread forms a reciprocal relation.

2.2.2 Frequency Selective Fading

Now, for convenience let us consider the time invariant channel model with $h[n, \ell] = h[\ell]$. Consider the example shown in Figure 2.6 which describes a channel in delay and frequency.

From Figure 2.6(a) we can see that the attenuation of the paths with different delays changes. The channel acts like a filter, see Equation (2.1), so the channel will attenuate some frequencies more than others as shown in Figure 2.6(b). This effect is called frequency selectivity.

How is it possible to describe the effects of time and frequency selectivity? Let us introduce the delay spread τ_s as the spread which captures "most" of the energy of the filter. This "definition" of the delay spread τ_s is not precise so an RMS measure

can be used to define the delay spread more properly [Rappaport, 2002, p.160]. Let $P(\ell) = E\{h[n,\ell]^2\}$, then the RMS delay spread is defined as

$$\tau_{\mathrm{RMS,s}} = \sqrt{\overline{\tau^2} - (\bar{\tau})^2}\,, \tag{2.8}$$

where,

$$\overline{\tau^2} = \frac{\sum_{\ell} \tau(\ell)^2 P(\ell)}{\sum_{\ell} P(\ell)}\,, \qquad \bar{\tau} = \frac{\sum_{\ell} \tau(\ell) P(\ell)}{\sum_{\ell} P(\ell)}\,, \tag{2.9}$$

and $\tau(\ell)$ is the delay of tap ℓ. Figure 2.6(a) shows an example of a delay spread.

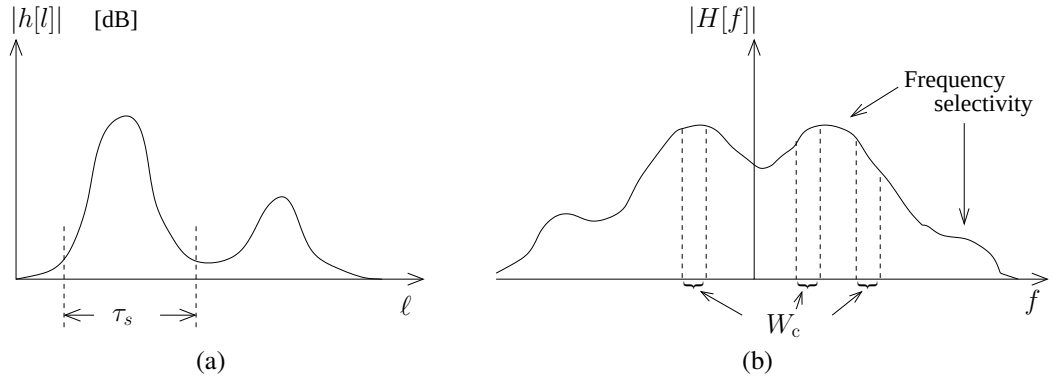

Figure 2.6: *Example of the notion of delay spread τ_s and coherence bandwidth W_{c}.*

Consider the coherence bandwidth W_{c} in Figure 2.6(b) as a measure of the average bandwidth where the amplitude in frequency can be considered almost constant/flat. To define it more properly, let $H[f] = \mathcal{F}_{\ell}\{h[\ell]\}$ be the Fourier transform of the impulse response in delay domain and assuming WSS $R[\Delta f] = E\{H^H[f]H[f+\Delta f]\}$. Let the coherence bandwidth be defined as

$$W_{\mathrm{c}} = \underset{W}{\operatorname{argmin}} \left\{ |R[W]| = c\,|R[0]| \right\}\,. \tag{2.10}$$

Figure 2.7 explains Equation (2.10). The relation between the delay spread and coherence bandwidth is [Paulraj et al., 2005, p.16]

$$W_{\mathrm{c}} \approx \frac{1}{\tau_s}\,. \tag{2.11}$$

There are also other definitions where coherence bandwidth W_{c} and delay spread τ_s are inversely proportional (No approximation in Equation (2.11) and multiplied with a constant) [Rappaport, 2002, p.163] [Tse et al., 2005, p.33]. However again, the important observation is that the coherence bandwidth and delay spread are reciprocal. If

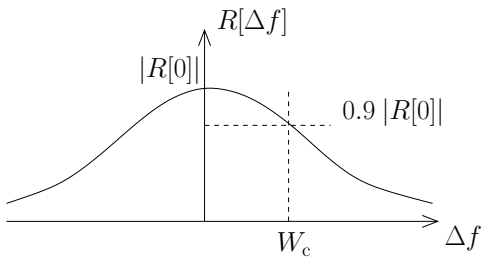

Figure 2.7: *Example of the coherence bandwidth W_c.*

the signal bandwidth is larger than the coherence bandwidth, the channel is considered to be frequency selective [Paulraj et al., 2005, p.16].

2.3 IEEE Channel Models

This section briefly reviews specific channel models for IEEE 802.11n which will be used in this project work.

The implementation of the IEEE channel model is based on a Matlab source code provided in [Schumacher, 2003]. The channel models are incorporated in the simulator chain of Wipro-Newlogic and used to evaluate the link level performance of the IEEE 802.11n modem. The simulator chain was originally designed such that it could only draw independently generated channel samples for a given channel model. The simulator was modified such that it was possible to save and load continuous time varying channel over long time intervals (cf. Figure 2.3). Further, channel samples can be selected with a certain space in time to simulate the behavior of the FLA algorithm as a function of delay in the feedback link.

The simulator generates taps in the delay domain at the sampling frequency 100 MHz, resampled to $20/40/240\,\mathrm{MHz}$ to fit the internal design of the simulator. The temporal sampling frequency is approx. $2.6\,\mathrm{kHz}$ which means that there is a new channel realization available every $T \approx 0.4\,\mathrm{ms}$. Only scatterers are moving to create the time varying channel [TGn IEEE802.11, p.17]. The transmitter and receiver are supposed to remain at the same position. Table 2.1 gives a description of the type of environment for the models A-F. The models A-C are Non Line of Sight (NLOS) models and D-F are Line of Sight (LOS) models.

For this project we will focus mostly on two models, B and E. Model B is selected because it has the lowest delay spread, i.e., highest coherence bandwidth. So, if the channel is in fade almost the entire signal bandwidth will experience fading. It will render the highest PER for the same nominal SNR compared to the models (C-F),

Table 2.1: *Overview of the IEEE channel models [TGn IEEE802.11].*

Channel Model	RMS Delay Spread [ns]	Number of clusters	κ-Factor LOS/NLOS	Description
A	0	1tap	0/-∞	Occurs small percentage of time
B	15	2	0/-∞	Smaller environments (residential homes and small offices)
C	30	2	0/-∞	Smaller environments (residential homes and small offices)
D	50	3	3/-∞	Typical office environment
E	100	4	6/-∞	Typical large open space and office environments
F	150	6	6/-∞	Large open space (indoor and outdoor)

and it will be an interesting channel to design the FLA algorithm for. Model A is a flat fading channel with a single tap and should not be considered for performance comparison [TGn IEEE802.11, p.6]. Channel model E is selected as the second used model because it has low coherence bandwidth as opposed to channel B and includes fluorescent light effect causing an additional Doppler frequency [TGn IEEE802.11, p.21].

Models B-F include scatterers moving at $1.2\,\mathrm{km/h}$ [TGn IEEE802.11, p.17] but it will be beneficial to evaluate the performance of the FLA algorithm for scatterers moving at higher speed, i.e., having lower coherence time. The channel generator [Schumacher, 2003] is altered such that it is possible to change the speed of the scatterers. The effect of changing velocity of the scatterers are given in Section 2.3.3.

To ensure the correct SNR, the taps must fulfill the energy requirement in Equation (2.12).

$$\mathbb{E}\left\{\sum_{\ell=\emptyset}^{\mathbb{L}-1}|h[n,\ell]|^2\right\}=1 \tag{2.12}$$

with $\mathbb{E}\{\cdot\}$ the expectation operator.

2.3.1 Time Variant Transfer Function

Figure 2.8 and 2.9 show the time-variant transfer function for channel model B and E, respectively. Clearly the channel changes over time. It is also possible to see that the coherence bandwidth of channel E is much smaller than that of channel B as expected.

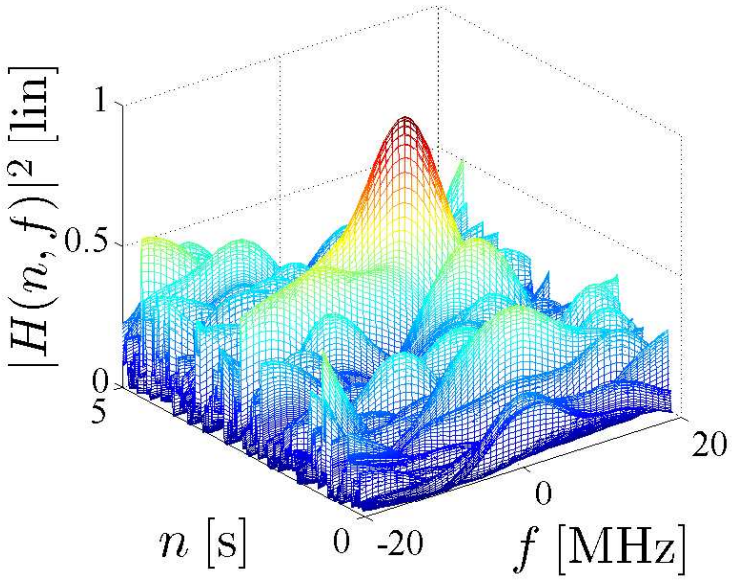

Figure 2.8: *Time-variant transfer function for channel B. Normalized to* $\max_{n,f}\{|H(n,f)|^2\}$. $N_{\mathrm{FFT}} = 128$, *windowed in* $\pm 20\,\mathrm{MHz}$. *The discrete step size in the time domain is* $\Delta n \approx 1.2\,\mathrm{ms}$.

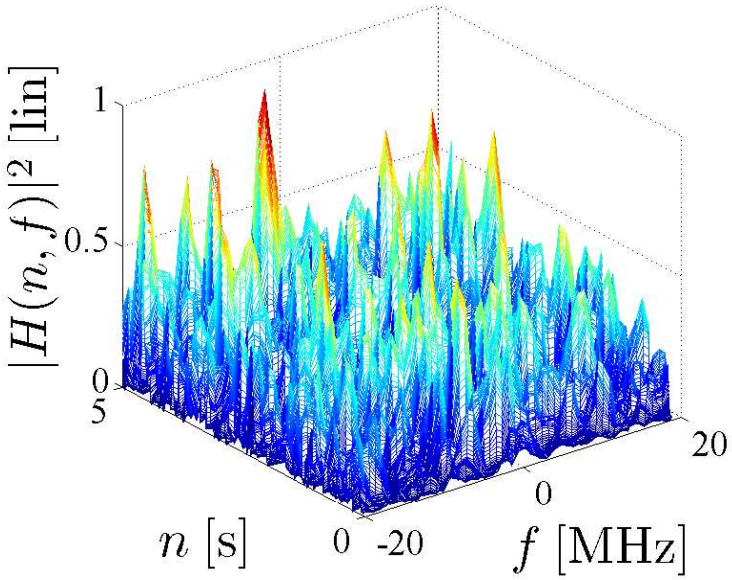

Figure 2.9: *Time-variant transfer function for channel E. Normalized with respect to* $\max_{n,f}\{|H(n,f)|^2\}$. $N_{\mathrm{FFT}} = 128$, *windowed in* $\pm 20\,\mathrm{MHz}$. *The discrete step size in the time domain is* $\Delta n \approx 1.2\,\mathrm{ms}$.

Figure 2.10 shows the instantaneous channel power over time calculated as

$$P[n] = \mathbb{E}_f \left\{ |H[n, f]|^2 \right\} \quad \text{for } f \in \text{ channel bandwidth}\,. \tag{2.13}$$

The dynamics is in the order of $60\,\mathrm{dB}$ for channel B shown in Figure 2.10(a). Link adaptation can be beneficial for this channel. The dynamics in channel E shown in Figure 2.10(b) is smaller than for channel B because of the higher frequency diversity.

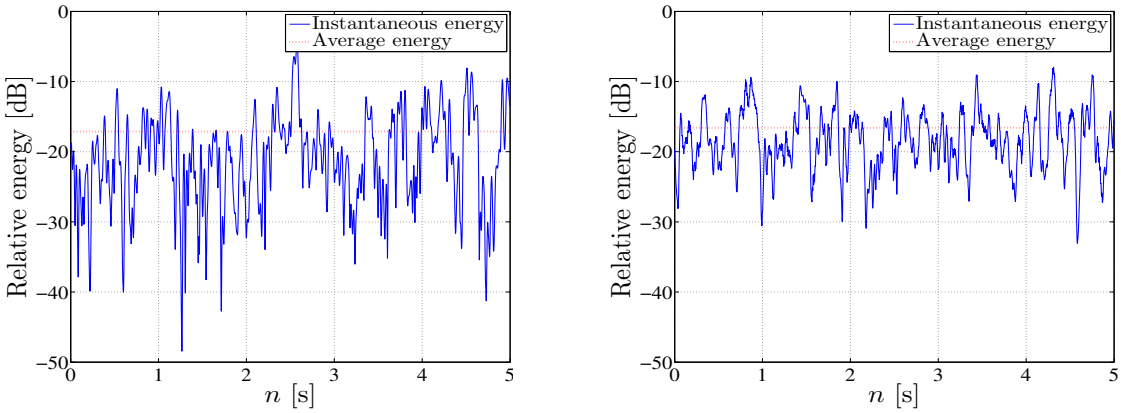

(a) **(b)**

Figure 2.10: *Instantaneous and average energy for channel (a) B and (b) E over a window of* $5\,\mathrm{s}$ *for channel bandwidth* $20\,\mathrm{MHz}$.

2.3.2 Coherence Bandwidth

Figure 2.11 shows the coherence bandwidth with $c = 0.9$. As expected, the coherence bandwidth is much smaller in channel E than in channel B.

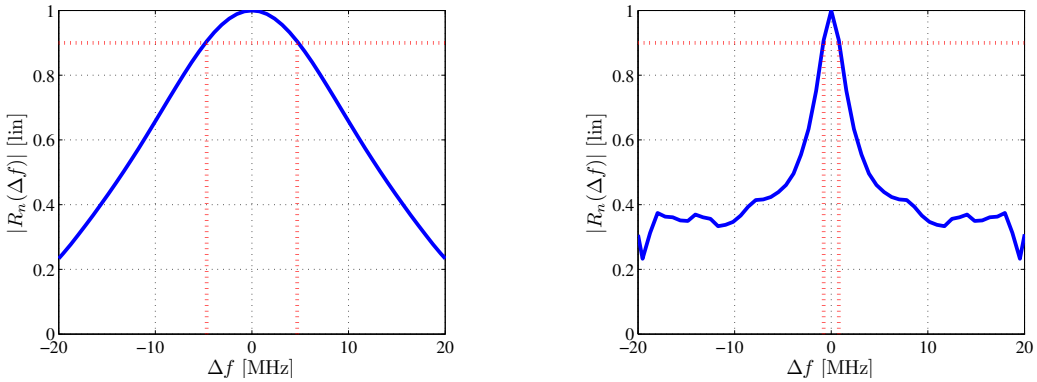

(a) **(b)**

Figure 2.11: *Coherence bandwidth for (a) channel B and (b) channel E to the right.* $W_c = 4.9\,\mathrm{MHz}$ *for channel B and* $W_c = 0.9\,\mathrm{MHz}$ *for channel E. Resolution in frequency is* $0.1\,\mathrm{MHz}$. *Normalized with respect to* $\max_{\Delta f}\{|R(\Delta f)|\}$.

2.3.3 Coherence Time

Figure 2.12 depicts the coherence time of channel B and E. Channel E has a LOS component with strong time correlation so the coherence time is a bit larger than for channel B even though it includes a Doppler effect from fluorescent lights. Also, the correlation does not drop as low in channel E as in channel B for large Δn, i.e., for the range $\pm 0.25 \rightarrow 0.5$.

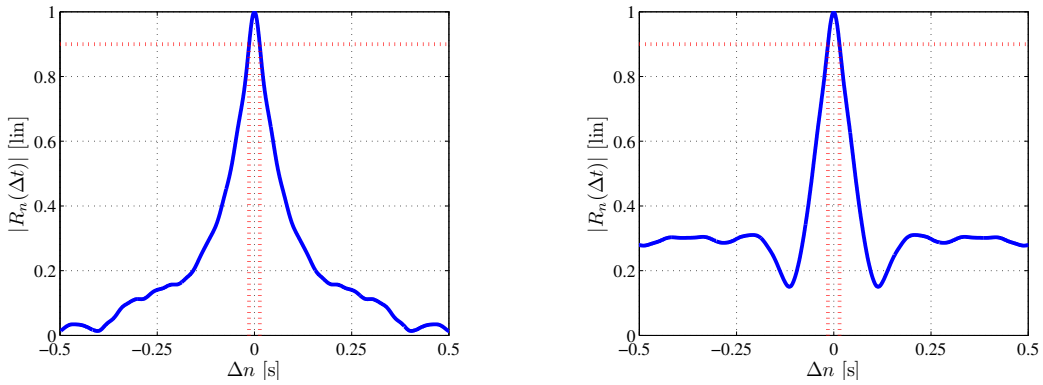

Figure 2.12: *Coherence time for (a) channel B and (b) channel E.* $T_s = 13.8\,\mathrm{ms}$ *for channel B and* $T_s = 14.9\,\mathrm{ms}$ *for channel E. Resolution in time is* $\approx 0.4\,\mathrm{ms}$*. Normalized with respect to* $\max_{\Delta n}\{|R(\Delta n)|\}$.

For channel B we also evaluate the coherence time for different velocity. Figure 2.13 shows the effect of increasing the scatterers' velocity. The correlation falls more rapidly when the velocity is increased. In Table 2.2 the results for coherence time and bandwidth are summarized.

Table 2.2: *Coherence bandwidth and coherence time for the most frequently used models in our study. Resolution in time is* $\approx 0.4\,\mathrm{ms}$ *for coherence time and* $\approx 0.2\,\mathrm{MHz}$ *for coherence bandwidth. Coherence level* $c = 0.9$.

Channel Model	Velocity [km/h]	Coherence Time [ms]	Coherence Bandwidth [MHz]
B	1.2	13.8	4.7
B	2.0	8.0	4.7
B	3.0	5.3	4.9
B	4.0	4.2	4.7
E	1.2	14.9	0.9

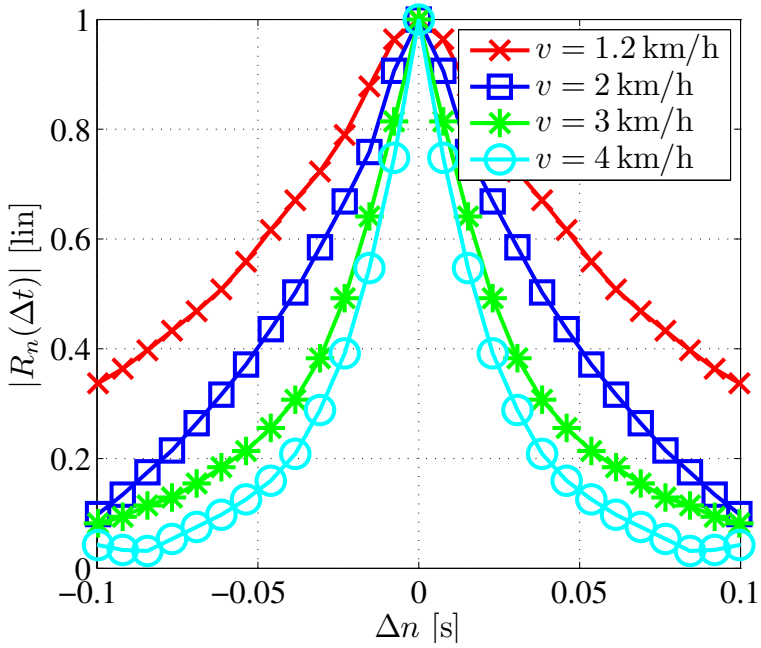

Figure 2.13: *Comparison of time correlation for different velocities using channel model B. The velocity* $v = 1.2\,\mathrm{km/h}$ *is the standard setting for the IEEE models. Normalized with respect to* $\max_{\Delta n}\{|R_v(\Delta n)|\}$.

From Table 2.2 we can *not* conclude that the feedback interval for FLA shall be less than $13.8\,\mathrm{ms}$ for channel model B with scatterers' velocity of $1.2\,\mathrm{km/h}$. The definition of coherence time and the relation to a change in modulation and coding is simply too weak to make such a conclusion. However, it can be apprehended that for a doubling of scatterers' velocity, the feedback frequency should be twice as high.

2.4 Summary

In this chapter we first discussed the physical propagation, the signal paths and simple stochastic models for the channel filter taps. Thereafter, we moved on to the time variant channels and discussed time and frequency selective fading. The first part gave a background to study the IEEE channel models where time and frequency selectivity were studied for the two channel models B and E. It was also shown, how the speed of the scatterers change the coherence time. The change of coherence time will be used for the evaluation of the FLA algorithm when a delay in the side channel is introduced.

MIMO-OFDM 3

If the reader is familiar with the basic concepts of OFDM and MIMO, then he or she can skip this chapter. In the preceding chapter, a multipath propagation channel and its characteristics were described briefly. To mitigate the effects of frequency selective fading, orthogonal frequency division multiplexing (OFDM) can be employed to gain frequency diversity [Prasad et al., 2000]. Due to this reason, OFDM has already been adopted in standards such as IEEE 802.11a/g, IEEE 802.16 (Wireless MAN)[1] and DVB-T (Digital Video Broadcasting - Terrestrial). OFDM is a special case of multicarrier modulation [Prasad et al., 2000] where the data stream is transmitted over a large number of subcarriers. If a single carrier system is employed in a frequency selective fading channel, then the entire packet transmission can fail for a single fade in the channel. However, if a multicarrier modulation, i.e., OFDM, is adopted, then only a small percentage of subcarriers in the multicarrier will be affected. Moreover, the data may be retrieved successfully using error correction coding. However, if a delay spread of a channel is very small, then the coherence bandwidth will be quite large. If the coherence bandwidth is larger than the channel bandwidth, then all the subcarriers will be affected similarly even for a single fade which may fail the entire packet transmission. However, it is very susceptible to phase noise and frequency offset, besides the aforementioned benign characteristics of OFDM. [Prasad et al., 2000].

On the other hand, the use of multiple antennas in wireless systems increases the capacity of a system significantly compared to a SISO system [Bolcskei et al., 2002].

In this chapter, OFDM, MIMO and MIMO-OFDM will briefly be described without channel coding to make the reader familiar with the notations to be used in this report.The interested reader can refer [Prasad et al., 2000] for detailed description of OFDM and [Paulraj et al., 2005] [Zelst, 2004] for detailed description of MIMO and MIMO-OFDM. In Section 3.1, SISO-OFDM, i.e., Single Input Single Output - OFDM

[1] Wireless Metropolitan Area Networks

will briefly be introduced with the signal model. SISO means that the system has got a single antenna at both the transmitter and receiver. In Section 3.2, the concept of MIMO will be introduced with its benign features like diversity and array gain. Thereafter, OFDM is associated with MIMO, thanks to the properties of OFDM which decouples the frequency selective channel into parallel flat-fading channels [Paulraj et al., 2005] [Zelst, 2004]. In Section 3.3, the signal model of MIMO-OFDM is briefly described. In Section 3.2.2, a block diagram of a system model for MIMO BICM-OFDM is presented. Thereafter, in the following Section, the soft bit generation is introduced.

In IEEE 802.11n, convolutional encoding as forward error correction (FEC) is mandatory and the generator polynomials are same as in IEEE 802.11a/g. The FEC of IEEE 802.11 is having generators in octal $[133, 171]_8$ with basic code rate $1/2$. Puncturing is employed to increase the code rate to $2/3, 3/4$ and $5/6$ [IEEE802.11n]. The encoded data is interleaved at bit level [IEEE802.11n]. Thereafter, the bit interleaved coded data is modulated. The IEEE 802.11n standard defines four signal constellations as BPSK (binary phase shift keying), QPSK (quadrature phase shift keying), 16QAM (16 quadrature amplitude modulation) and 64QAM. Thus, the standard IEEE 802.11a/g/n implements bit interleaved coded modulation (BICM). The BICM was firstly introduced by Zehavi [Zehavi, 1992] and he designed codes that separated coding and modulation which performed better in Rayleigh fading channel compared to codes designed using the combined coding and modulation approach. Thereafter, a comprehensive study was done on Zehavi's findings by Caire, et. al. [Caire et al., 1998] and they noted that even though BICM is sub-optimal in the aspect of information theory, it has several properties to be a better choice for practical code design in wireless fading channel.

3.1 Signal Model of SISO-OFDM

The Figure 3.1 shows a SISO-OFDM model with a single antenna at both transmitter and receiver. Let $x[k]$ $(k = 0, 1, 2, \cdots, N-1)$ be a sequence of N modulated (complex) data symbols and $h[\ell]$ $(\ell = 0, 1, 2, \cdots, L-1)$ be a channel response having length L. The transmitter converts the data sequence $\boldsymbol{x}$ from serial to parallel such that it can be represented as an $N \times 1$ vector $\boldsymbol{x} = [x[0]\ x[1]\ \cdots x[N-1]]^T$. Thereafter, the transmitter performs an inverse fast Fourier transform (IFFT) on the data sequence $\boldsymbol{x}$ to be transmitted. After performing IFFT, the sequence vector can be represented as $\widetilde{\boldsymbol{x}} = [\widetilde{x}[0]\ \widetilde{x}[1]\ \cdots \widetilde{x}[N-1]]^T$, i.e.,

$$\widetilde{\boldsymbol{x}} = \mathbf{D}^H \boldsymbol{x} \tag{3.1}$$

where $\mathbf{D}$ is an $N \times N$ matrix whose (k,m)th $\Big((k,m) = 0, 1, \cdots, N-1\Big)$ element is

$$\Big[\mathbf{D}\Big]_{k,m} = \frac{1}{\sqrt{N}} \exp\left(j\frac{2\pi km}{N}\right) \tag{3.2}$$

where $1/\sqrt{N}$ is a normalization factor such that the average power of $\widetilde{\boldsymbol{x}}$ is equal to $\boldsymbol{x}$ [Zelst, 2004] .

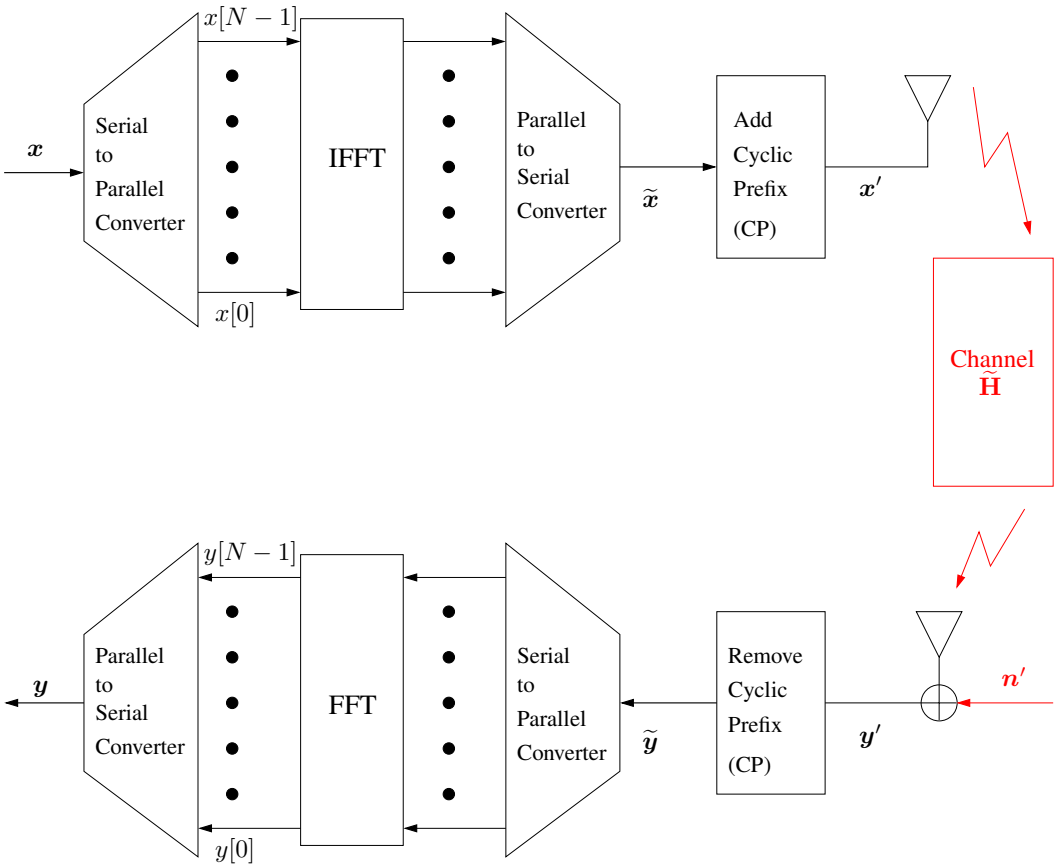

Figure 3.1: *Schematic of SISO-OFDM transmission.*

The above Equation (3.1) can be rewritten as,

$$\widetilde{x}[m] = \frac{1}{\sqrt{N}} \sum_{k=0}^{N-1} x[k] \exp\left(j\frac{2\pi km}{N}\right) \qquad \forall\, m = 0, 1, \cdots, N-1\,. \tag{3.3}$$

Furthermore, in practical systems, N is chosen to be a power of 2 for an efficient implementation of IFFT [Prasad et al., 2000] [Paulraj et al., 2005, p.179]. In 802.11n,

the total number of subcarriers are $N_{\text{sc}} = 54$ out of $N = 64$ for $20\,\text{MHz}$ channel bandwidth and $N_{\text{sc}} = 114$ out of $N = 124$ for $40\,\text{MHz}$ channel bandwidth [IEEE802.11n]. The total number of subcarriers N_{sc} used in the communication system are equally distributed around the 0th subcarrier [Zelst, 2004, p.125]. If N_{sc} subcarriers are used out of N, then the rest of the subcarriers will be padded with zeros which render extra guard space among the adjacent subcarriers and the normalization factor in Equation (3.2) and (3.3) will be $1/\sqrt{N_{\text{sc}}}$. However, in this report N_{sc} will be considered equal to N for simplicity unless stated explicitly.

A new sequence vector $\boldsymbol{x}'$ is considered after adding a cyclic prefix (CP) of length $L-1$ to the vector $\widetilde{\boldsymbol{x}}$. The CP introduces a guard time. Hence, if the guard time introduced by CP is more than the delay spread, the CP will eliminate the inter carrier interference (ICI) and inter symbol interference (ISI) [Prasad et al., 2000, p.39]. The CP consists of the last $L-1$ symbols of the N data sequence vector after IFFT $\widetilde{\boldsymbol{x}}$. Thus, the transmitted sequence vector $\boldsymbol{x}' = [\widetilde{x}[N-(L-1)] \cdots \widetilde{x}[N-1]\, \widetilde{x}[0] \cdots \widetilde{x}[N-1]]^T$ is having length $N+L-1$. The vector $\boldsymbol{x}'$ is referred as an OFDM symbol having a duration $T = (N+L-1)(T_s)$, where T_s is the sampling time period of the channel impulse response.

The OFDM receiver basically performs the inverse operation of the transmitter with some additional tasks like synchronization and frequency offset estimation. The received data sequence $\boldsymbol{y}'$ consists of the transmitted data sequence having length $N+L-1$ convolved with the channel impulse response having length L. So, the received sequence vector $\boldsymbol{y}'$ will have length $N+2L-2$. The receiver will remove the CP from the received sequence $\boldsymbol{y}'$ and collect N data samples such that $\widetilde{\boldsymbol{y}} = \left[y'[0]\; y'[1] \cdots\; y'[N-1]\right]^T$ fulfills,

$$\widetilde{\boldsymbol{y}} = \sqrt{E_s}\, \widetilde{\mathbf{H}}\, \boldsymbol{x}' + \widetilde{\boldsymbol{n}} \tag{3.4}$$

where $\sqrt{E_s}$ is the average symbol energy, $\widetilde{\boldsymbol{n}}$ is the additive zero mean circularly symmetric complex Gaussian noise vector [Paulraj et al., 2005] with covariance matrix $N_0\mathbf{I}_N$ and $\widetilde{\mathbf{H}}$ is a $N \times (N+L-1)$ Toeplitz matrix which is represented as,

$$\widetilde{\mathbf{H}} = \begin{bmatrix} h[L-1] & \cdots & h[1] & h[0] & 0 & 0 & \cdots & 0 \\ 0 & h[L-1] & \cdots & h[1] & h[1] & 0 & \cdots & 0 \\ \vdots & 0 & \ddots & \ddots & \ddots & \ddots & \ddots & \vdots \\ 0 & \vdots & 0 & h[L-1] & \cdots & h[1] & h[0] & 0 \\ 0 & 0 & 0 & 0 & h[L-1] & \cdots & h[1] & h[0] \end{bmatrix}. \tag{3.5}$$

It is worth to mention here that a complex Gaussian random variable will be circularly

symmetric say $Z = X + jY$ which is distributed as $\mathcal{CN}(0, N_0)$, if X and Y, random variables, are independent and identically distributed (i.i.d.) as $\mathcal{N}(0, N_0/2)$.

Since, the first $L-1$ samples of $\boldsymbol{x}'$ are identical to the last $L-1$ samples because of the addition of CP, the above Equation (3.4) can be simplified as,

$$\widetilde{\boldsymbol{y}} = \sqrt{E_s}\, \mathbf{H}_{\mathrm{c}}\, \widetilde{\boldsymbol{x}} + \widetilde{\boldsymbol{n}} \tag{3.6}$$

where $\mathbf{H}_c$ is a $N \times N$ circulant matrix which is a special type of Toeplitz matrix [Paulraj et al., 2005, p.180],

$$\mathbf{H}_c = \begin{bmatrix} h[0] & 0 & \cdots & 0 & 0 & h[L-1] & \cdots & h[1] \\ h[1] & h[0] & 0 & \cdots & 0 & 0 & \ddots & \vdots \\ \vdots & h[1] & h[0] & 0 & 0 & \ddots & 0 & h[L-1] \\ h[L-1] & \vdots & h[1] & \ddots & 0 & \ddots & 0 & 0 \\ \vdots & 0 & h[L-1] & \ddots & h[1] & h[0] & 0 & 0 \\ \vdots & \vdots & 0 & \ddots & \vdots & \ddots & \ddots & 0 \\ 0 & 0 & \cdots & 0 & h[L-1] & \cdots & h[1] & h[0] \end{bmatrix} . \tag{3.7}$$

Thus, the eigendecomposition of the circulant matrix $\mathbf{H}_{\mathrm{c}}$ can be written as [Paulraj et al., 2005, p.180],

$$\mathbf{H}_{\mathrm{c}} = \mathbf{D}^H \mathbf{\Lambda} \mathbf{D} \tag{3.8}$$

where, $\mathbf{D}$ is given in Equation (3.2) and

$$\mathbf{\Lambda} = \begin{bmatrix} H[0] & 0 & \cdots & 0 & 0 \\ 0 & H[1] & 0 & \cdots & 0 \\ \vdots & 0 & \ddots & \ddots & \vdots \\ 0 & 0 & \ddots & H[N-2] & 0 \\ 0 & 0 & \cdots & 0 & H[N-1] \end{bmatrix} \tag{3.9}$$

with

$$H[k] = \sum_{\ell=0}^{L-1} h[\ell]\, \exp\left(-j\frac{2\pi k \ell}{N}\right) \qquad \forall\, k = 0, 1, \cdots, N-1\ . \tag{3.10}$$

$H[k]$ $(k = 0, 1, \cdots, N-1)$ is the sampled channel frequency response of the kth subcarrier. After removing CP and collecting N symbols from the received sequence $\boldsymbol{y}'$ to render $\widetilde{\boldsymbol{y}}$, the receiver performs an FFT on $\widetilde{\boldsymbol{y}}$ to detect the received symbols such that

$$\boldsymbol{y} = \mathbf{D}\widetilde{\boldsymbol{y}}\ . \tag{3.11}$$

Now, plugging Equations (3.1), (3.6) and 3.8 in the above Equation (3.11) to render,

$$\boldsymbol{y} = \sqrt{E_s}\mathbf{D}\mathbf{D}^H\mathbf{\Lambda}\mathbf{D}\mathbf{D}^H\boldsymbol{x} + \mathbf{D}\widetilde{\boldsymbol{n}} \tag{3.12}$$

$$= \sqrt{E_s}\mathbf{\Lambda}\boldsymbol{x} + \boldsymbol{n} \tag{3.13}$$

where $\boldsymbol{n} = \mathbf{D}\widetilde{\boldsymbol{n}}$ is the additive zero mean circularly symmetric complex Gaussian noise vector with covariance matrix $N_0\mathbf{I}_N$ and $\mathbf{D}$ is a unitary matrix, i.e., $\mathbf{D}\mathbf{D}^H = \mathbf{I}_N$. The above Equation (3.13) is an input-output relation in the frequency domain. The elements of $\boldsymbol{n}$ are uncorrelated because of the use of CP with IFFT and FFT which decouples the frequency selective channel into N orthogonal channels [Paulraj et al., 2005, p.180]. Moreover, Equation (3.13) can be rewritten for the kth subcarrier as,

$$y[k] = \sqrt{E_s}H[k]x[k] + n[k] \qquad \forall\, k = 0, 1, \cdots, N-1 \tag{3.14}$$

where $n[k]$ is the kth element of $\boldsymbol{n}$. Thus, it can be construed that OFDM orthogonalizes the multipath fading channel into N orthogonal or parallel flat fading channels because the elements of $\boldsymbol{n}$ are uncorrelated [Paulraj et al., 2005, p.181].

3.2 MIMO

It has been shown that the use of multiple antennas at both ends of a communication system drastically increases the channel capacity and the range over communication systems employing single antenna at both ends [Foschini, 1996]. Furthermore, MIMO systems provide higher diversity [Paulraj et al., 2005] than SISO systems. Diversity is used to combat fading by providing the receiver multiple identical (ideally independent) copies of the transmitted signal. Thus, the multiple identical copies of the signal at the receiver sharply decreases the probability that all the copies of a signal are in fade.

A wireless link having space, time and frequency selective fading can offer diversity in all these dimensions which can be exploited by a wireless communication system. The diversity in the wireless link depends on the codeword dimensions and the channel coherence parameters [Paulraj et al., 2005]. The codeword dimensions are dependent on the number of transmit and receive antennas, the time duration of the codeword and the signal bandwidth. The channel coherence parameters are like coherence bandwidth and time which were defined in Chapter 2.

Diversity available at the receiver is called receive diversity whereas at the transmitter it is called transmit diversity. The receive or transmit diversity has got array and diversity gain which is shown in Figure 3.2 to illustrate the meaning of these terms. The array gain implies the average increase of SNR at the receiver by the coherent

combining effects of multiple antennas at the receiver or transmitter (requires channel knowledge at the transmitter) or both. Furthermore, the effect of array gain is similar to the coding gain at high SNR regime, i.e., parallel shift of the PER versus SNR curves to the left which is shown in Figure 3.2. Diversity gain implies a change in the slope of the PER versus SNR curve. The magnitude of the slope is proportional to the diversity order, i.e., a $\Delta PER = 10^{-1}$ over $\Delta SNR = 10\,\mathrm{dB}$ is diversity one. The diversity order is equal to the product of the number of receive and transmit antennas. Moreover, the diversity gain increases with the increase of SNR whereas the coding or array gain remains constant with the increase of SNR typically at high SNR regime. The transmit diversity is possible through the transmission of precoded or preprocessed data with or without channel knowledge at the transmitter. If the number of transmit antennas (N_T) and/or receive antennas (N_R) tends to infinity, i.e., N_T and/or $N_R \longrightarrow \infty$, then the fading channel will be perfectly stabilized and approaches AWGN channel. Furthermore, to maximize diversity, space time codes like Alamouti codes can be incorporated. To increase data rate, spatial multiplexing can be used. Space time codes are out of the scope of this project work, however spatial multiplexing is briefly described in the following subsection.

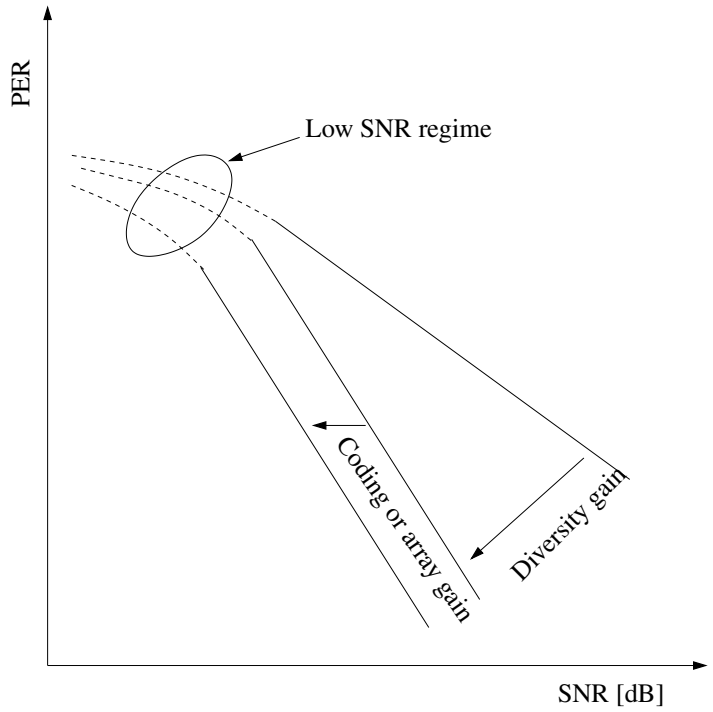

Figure 3.2: *Schematic showing the concepts of diversity and array gain [Paulraj et al., 2005].*

3.2.1 Spatial Multiplexing (SM)

Spatial multiplexing (SM) which is also known as space division multiplexing (SDM), provides a linear increase in data rate [Foschini, 1996]. The basic concept of SM is to demultiplex a bit stream and transmit these demultiplexed streams from different antennas at the same time. Finally, retrieve the original transmitted bit stream by multiplexing all the bit streams retrieved on every spatial streams by a MIMO detector. Various MIMO receivers will be described in Section 3.4. Figure 3.3 shows a basic principle of SM, where a 2×2 system, i.e., 2 transmit antennas and 2 receive antennas, is considered. A data sequence is demultiplexed into 2 spatial streams, modulated (e.g. by BPSK) and transmitted from both transmit antennas simultaneously. The received signals are processed by a MIMO detector to retrieve the transmitted BPSK symbols' sequence on both streams. Finally, the detected symbols' sequence on both spatial streams are multiplexed and thereby an estimation of the original bit stream is obtained.

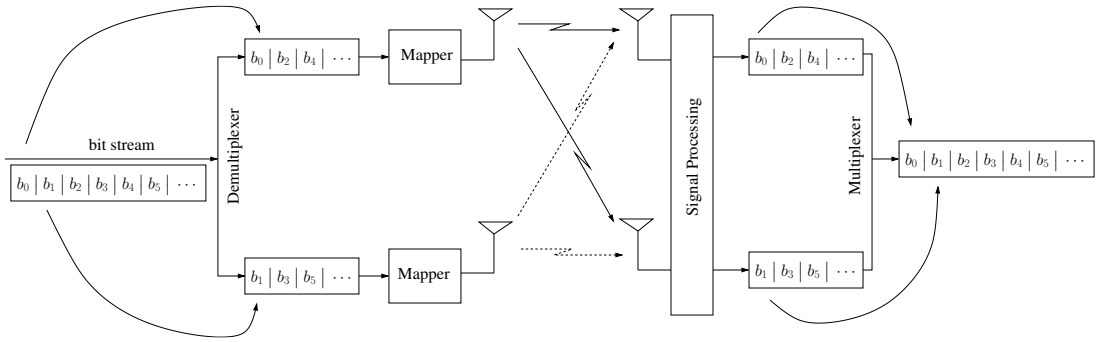

Figure 3.3: *Schematic of spatial multiplexing for a 2×2 system.*

3.2.2 MIMO BICM-OFDM

The signal model of SISO-OFDM was described for uncoded system. The signal model MIMO-OFDM for uncoded system will be described in the following section. However, these models can easily be integrated with BICM. Now, if BICM with convoultional coding is integrated with MIMO-OFDM, then the system model is named as MIMO BICM-OFDM. For instance, IEEE 802.11n is based on a MIMO BICM-OFDM system model. Figure 3.4 shows a block diagram of MIMO BICM-OFDM.

At the transmitter side, firstly, the information bits $\{b\}$ are encoded by the convolutional encoder to render coded bits $\{c\}$. The coded bits would be punctured, if the code rate had to be increased from basic code rate $1/2$ to $2/3$, $3/4$ or $5/6$. Thereafter, the (punctured) coded bits are interleaved, and the interleaved bits are demultiplexed

into spatial streams by a spatial parser. The spatial parser employs spatial multiplexing technique. After spatial parsing of the interleaved bits, the interleaved bits are modulated by a symbol mapper (e.g., 16-QAM) with Gray mapping. The (complex) symbols $\{x\}$ are transmitted using OFDM concept, i.e., FFT operation is performed on the symbols which is followed by an addition of CP as a prefix.

At the receiver side, firstly, CP is removed from the received signal, and thereby the FFT operation is performed. After the FFT operation, the received signal is detected by a MIMO detector (e.g., MMSE receiver). The estimated (complex) symbols are demodulated and thereby soft bits or log-likelihood ratios (LLRs) are generated for each bit by a MaxLog demapper. The soft-decision decoding is employed because it provides a performance gain of $2 - 3$ dB over hard-decision decoding [S. Lin and D. Costello, 1983]. Finally, the generated soft bits (LLRs or L-values) are multiplexed, deinterleaved, and depunctured before feeding it into a Viterbi decoder to estimate the transmitted bits $\{\widehat{b}\}$.

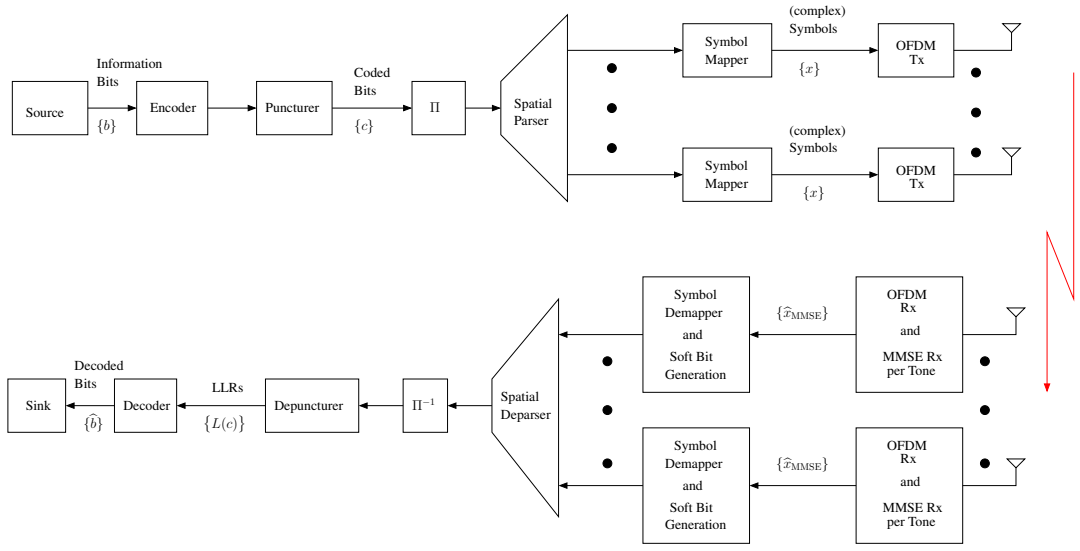

Figure 3.4: *Block diagram of MIMO BICM-OFDM.*

3.3 Signal Model of MIMO-OFDM

In Section 3.1, it was mentioned that OFDM transforms a frequency selective channel into N orthogonal channels. Hence, MIMO techniques like spatial multiplexing can easily be employed with OFDM. In this Section, the uncoded signal model is briefly described for simplicity.

A frequency selective MIMO channel is considered in a communication system

with N_{T} transmit antennas and N_{R} receive antennas. The channel impulse response of length L between the jth transmit antenna and ith receive antenna is considered as $h_{i,j}[\ell]$ $(\ell = 0, 1, 2, \cdots, L-1)$. Suppose $h_{i,j}[\ell]$ represents the i,jth element of the matrix $\mathcal{H}[\ell]$ $(\ell = 0, 1, 2, \cdots, L-1)$, i.e.,

$$\mathcal{H}[\ell] = \begin{bmatrix} h_{1,1}[\ell] & h_{1,2}[\ell] & \cdots & h_{1,N_{\mathrm{T}}}[\ell] \\ h_{2,1}[\ell] & \cdots & \cdots & \vdots \\ \vdots & \cdots & h_{i,j}[\ell] & \vdots \\ h_{N_{\mathrm{R}},1}[\ell] & \cdots & \cdots & h_{N_{\mathrm{R}},N_{\mathrm{T}}}[\ell] \end{bmatrix} . \tag{3.15}$$

The number of spatial streams N_{ss} is equal to the number of transmit antennas N_{T} unless stated explicitly. If a block of sequence of data symbols having dimension $N_{\mathrm{T}} \times N$ is to be transmitted over a frequency selective MIMO channel, then let the sequence of data symbols $x_j[k](k = 0, 1, \cdots, N-1)$ be transmitted from the jth transmit antenna. Furthermore, each sequence of data symbols will be subjected to an IFFT and addition of a CP as a prefix to data sequence before the transmission of each data sequence. After the transmission of a sequence of data symbols, the received sequences at each of the receive antennas will be treated analogous to SISO-OFDM. So, CP is removed from the received sequences followed by an FFT operation. Moreover, the signal received at the ith receive antenna over the kth subcarrier or tone can be represented as similar to SISO-OFDM,

$$y_i[k] = \sqrt{\frac{E_s}{N_{\mathrm{T}}}} \sum_{j=1}^{N_{\mathrm{T}}} H_{i,j}[k] x_j[k] + n_i[k] \quad \forall\, k = 0, 1, \cdots, N-1\ ;\ i = 1, 2, \cdots, N_{\mathrm{R}} \tag{3.16}$$

where E_s is the average symbol energy allocated to the kth tone which is evenly distributed across all the transmit antennas, $n_i[k]$ denotes additive zero mean circularly symmetric complex Gaussian noise having variance N_0 and $H_{i,j}[k]$ is the channel frequency response between the jth transmit antenna and ith receive antenna for the kth subcarrier. Furthermore, $H_{i,j}[k]$ is similar to Equation (3.10) which is given by,

$$H_{i,j}[k] = \sum_{\ell=0}^{L-1} h_{i,j}[\ell]\ \exp\left(-j\frac{2\pi k\ell}{N}\right) \qquad \forall\, k = 0, 1, \cdots, N-1\ . \tag{3.17}$$

Furthermore, the MIMO version of the input-output relation in Equation (3.16) can be represented for the kth subcarrier as,

$$\boldsymbol{y}[k] = \sqrt{\frac{E_s}{N_{\mathrm{T}}}}\, \mathbf{H}[k]\boldsymbol{x}[k] + \boldsymbol{n}[k] \qquad \forall\, k = 0, 1, \cdots, N-1\ , \tag{3.18}$$

where $\boldsymbol{y}[k] = \begin{bmatrix} y_1[k]\ y_2[k]\ \cdots\ y_{N_{\mathrm{R}}}[k] \end{bmatrix}^T$, $\boldsymbol{x}[k] = \begin{bmatrix} x_1[k]\ x_2[k]\ \cdots\ x_{N_{\mathrm{T}}}[k] \end{bmatrix}^T$, $\boldsymbol{n}[k] = \begin{bmatrix} n_1[k]\ n_2[k]\ \cdots\ n_{N_{\mathrm{R}}}[k] \end{bmatrix}^T$ and $\mathbf{H}[k]$ is an $N_{\mathrm{R}} \times N_{\mathrm{T}}$ matrix with $\begin{bmatrix} \mathbf{H}[k] \end{bmatrix}_{i,j} = H_{i,j}[k]$.

The matrix $\mathbf{H}[k]$ is the frequency response of the channel matrix for the kth subcarrier. Furthermore, $\mathbf{H}[k]$ is given by,

$$\mathbf{H}[k] = \sum_{\ell=0}^{L-1} \mathcal{H}[\ell] \, \exp\left(-j\frac{2\pi k\ell}{N}\right) , \tag{3.19}$$

where, $\mathcal{H}[\ell]$ is given in Equation (3.15).

3.4 MIMO Receivers

In this section, MIMO receivers are briefly described in the context of MIMO-OFDM.

3.4.1 ML Receiver

The optimal receiver to estimate the received symbols vector is an ML (maximum likelihood) receiver. The ML receiver estimates the transmitted symbols vector that solves

$$\widehat{\boldsymbol{x}}_{\mathrm{ML}}[k] = \arg\min_{\boldsymbol{x}[k]} \mathbb{E}\left\{\left(\boldsymbol{y}[k] - \sqrt{\frac{E_s}{N_{\mathrm{T}}}}\,\mathbf{H}[k]\boldsymbol{x}[k]\right)^H \left(\boldsymbol{y}[k] - \sqrt{\frac{E_s}{N_{\mathrm{T}}}}\,\mathbf{H}[k]\boldsymbol{x}[k]\right)\right\} \tag{3.20}$$

$$= \arg\min_{\boldsymbol{x}[k]} \left\|\boldsymbol{y}[k] - \sqrt{\frac{E_s}{N_{\mathrm{T}}}}\,\mathbf{H}[k]\boldsymbol{x}[k]\right\|^2 \tag{3.21}$$

where the optimization is performed through an exhaustive search over all the possible symbols vector $\boldsymbol{x}[k]$ in the signal constellation for the most likely transmitted symbols vector. The decoding complexity of the ML receiver increases exponentially with the number of transmit antennas N_{T} [Paulraj et al., 2005]. However, the ML detection problem can be solved with the sphere decoding algorithm [Hassibi and Vikalo, 2005]. Though, the complexity of sphere decoding algorithm is exponential in worst case, its expected complexity is polynomial. On the other hand, sub-optimal receivers are generally employed in practice because of their lower complexity than the ML receiver. In the following section, ZF (zero-forcing) and MMSE (minimum mean square error) linear receivers are briefly described.

3.4.2 ZF Receiver

The ZF receiver inverts the channel matrix to decompose the received signal $\boldsymbol{y}[k]$ (cf. Equation (3.18)) into N_{T} parallel sequence of symbols per subcarrier. So, the received

signal is weighted by the ZF matrix [Paulraj et al., 2005, p.153] which is given as

$$\mathbf{G}_{\mathrm{ZF}}[k] = \sqrt{\frac{N_{\mathrm{T}}}{E_s}}\Big(\mathbf{H}^H[k]\ \mathbf{H}[k]\Big)^{-1}\mathbf{H}^H \qquad \forall\, k = 0, 1, \cdots, N-1 \tag{3.22}$$

where, $\mathbf{H}$ is assumed to have full column rank and $N_{\mathrm{R}} \geq N_{\mathrm{T}}$. The estimated data symbols vector at the kth subcarrier is,

$$\widehat{\boldsymbol{x}}_{\mathrm{ZF}}[k] = \mathbf{G}_{\mathrm{ZF}}[k]\ \boldsymbol{y}[k] \tag{3.23}$$

$$= \boldsymbol{x}[k] + \mathbf{G}_{\mathrm{ZF}}[k]\ \boldsymbol{n}[k]\ . \tag{3.24}$$

However, the disadvantage of ZF receiver is that it enhances the noise by the ZF matrix $\mathbf{G}_{\mathrm{ZF}}[k]$. Moreover, the noise is colored and correlated across the channels. The post-processing SINR available at the output of the ZF receiver is given by

$$\mathit{SINR}_j[k] = \left(\frac{E_s}{N_0}\right)\frac{1}{N_{\mathrm{T}}}\ \frac{1}{\left[(\mathbf{H}^H[k]\ \mathbf{H}[k])^{-1}\right]_{j,j}} \tag{3.25}$$

for $k = 0, 1, \cdots, N-1$ and $j = 1, 2, \cdots, N_{\mathrm{T}}$.

3.4.3 MMSE Receiver

The ZF receiver aims to invert the channel matrix to estimate a transmitted data symbol at the expense of noise enhancement. The MMSE receiver provides a trade-off between the complete decoupling of the channel matrix and noise enhancement. The weighting matrix of the MMSE receiver minimizes the mean square error between the estimated data symbols vector $\widehat{\boldsymbol{x}}_{\mathrm{MMSE}}[k]$ and the transmitted data symbols vector $\boldsymbol{x}[k]$. The objective is formulated as

$$\mathbf{G}_{\mathrm{MMSE}}[k] = \arg\min_{\mathbf{G}[k]}\ \mathbb{E}\left\{\Big(\widehat{\boldsymbol{x}}_{\mathrm{MMSE}} - \boldsymbol{x}[k]\Big)^H\ \Big(\widehat{\boldsymbol{x}}_{\mathrm{MMSE}} - \boldsymbol{x}[k]\Big)\right\} \tag{3.26}$$

$$= \arg\min_{\mathbf{G}[k]}\ \mathbb{E}\left\{\Big(\mathbf{G}[k]\boldsymbol{y}[k] - \boldsymbol{x}[k]\Big)^H\ \Big(\mathbf{G}[k]\boldsymbol{y}[k] - \boldsymbol{x}[k]\Big)\right\} \tag{3.27}$$

The matrix $\mathbf{G}_{\mathrm{MMSE}}[k]$ is found in [Paulraj et al., 2005]

$$\mathbf{G}_{\mathrm{MMSE}}[k] = \sqrt{\frac{N_{\mathrm{T}}}{E_s}}\left(\mathbf{H}^H[k]\ \mathbf{H}[k] + \left(\frac{N_{\mathrm{T}}}{(E_s/N_0)}\right)\mathbf{I}_{N_{\mathrm{T}}}\right)^{-1}\mathbf{H}^H \tag{3.28}$$

for $k = 0, 1, \cdots, N-1$. The output of the MMSE receiver is

$$\widehat{\boldsymbol{x}}_{\mathrm{MMSE}}[k] = \mathbf{G}_{\mathrm{MMSE}}[k]\ \boldsymbol{y}[k] \tag{3.29}$$

$$= \sqrt{\frac{N_{\mathrm{T}}}{E_s}}\left(\mathbf{H}^H[k]\ \mathbf{H}[k] + \left(\frac{N_{\mathrm{T}}}{(E_s/N_0)}\right)\mathbf{I}_{N_{\mathrm{T}}}\right)^{-1}\mathbf{H}^H\ \boldsymbol{y}[k]\ . \tag{3.30}$$

It is worth to mention that $\widehat{\boldsymbol{x}}_{\mathrm{MMSE}}[k]$ is biased. A biased estimation means that

$$\mathbb{E}\left\{\widehat{\boldsymbol{x}}_{\mathrm{MMSE}}[k] - \boldsymbol{x}[k]\right\} \neq 0. \tag{3.31}$$

It is mentioned in [Seethaler et al., 2004] that the biased estimation causes a slight degradation in the performance compared to the unbiased estimation. In our simulator, the unbiased MMSE detector is employed for our project work. The unbiased MMSE estimation description is briefly provided in Appendix A. Furthermore, the post-processing SINR available at every subcarrier is given as [Paulraj et al., 2005],

$$\mathit{SINR}_j[k] = \frac{1}{\left[\left(\left(\frac{E_s}{N_0}\right)\frac{1}{N_{\mathrm{T}}}\,\mathbf{H}^H[k]\,\mathbf{H}[k] \;+\; \mathbf{I}_{N_{\mathrm{T}}}\right)^{-1}\right]_{j,j}} - 1 \tag{3.32}$$

$$\forall\; k = 0, 1, \cdots, N-1; \quad j = 1, 2, \cdots, N_{\mathrm{T}}$$

where "-1" accounts for bias [Cioffi et al., 1995] so as to have unbiased $\mathit{SINR}_j[k]$. The MMSE receiver converges to a ZF receiver at high SNR regime. However, MMSE approximates a matched filter (MF) at low SNR regime and thus, outperforms the ZF receiver.

3.4.4 Gaussian Assumption of the MMSE Output

In general, the output of the MMSE receiver is a multivariate complex Gaussian distribution [Seethaler et al., 2004], however the mixture of Gaussians is modelled by a single Gaussian PDF with same mean and covariance for practical reasons [Kim et al., 2006]. Furthermore, the output of the MMSE receiver has AWGN like characteristics for any IEEE indoor channel [Peng et al., 2007]. So, in this project work, we also assume that the output of the MMSE receiver is equivalent to an AWGN channel. Moreover, the single Gaussian approximation holds well according to our simulations too for low SNR regime because the blend of interference from interfering spatial streams and additive noise all together are observed as a single Gaussian distribution. In case of very high SNR, Figure 3.5 shows that there are two Gaussian clouds at each signal constellation of BPSK transmission for MCS 8 (2×2 system, cf. Table B.1) under IEEE channel model E and SNR $120\,\mathrm{dB}$. It implies that the single Gaussian approximation of the MMSE output is not good for the very high SNR regime. In case of multiple spatial streams, the interference from other streams at high SNR becomes prominent.

Figure 3.6 shows the scatter plots of MMSE output for BPSK and 64QAM constellation for a 2×2 system which represents a single Gaussian distribution at each signal

constellation. Further evaluation of the Gaussian assumption is done in Section 5.2.2, where the assumption is validated.

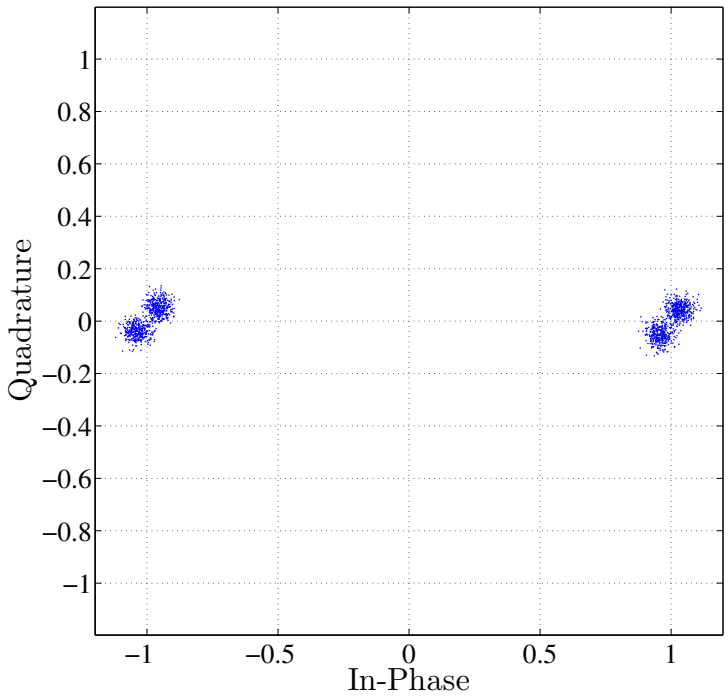

Figure 3.5: *Scatter plot represents bad single Gaussian assumption of the MMSE output at very high SNR* 120 dB *for MCS* 8 *and one channel realization from model E.*

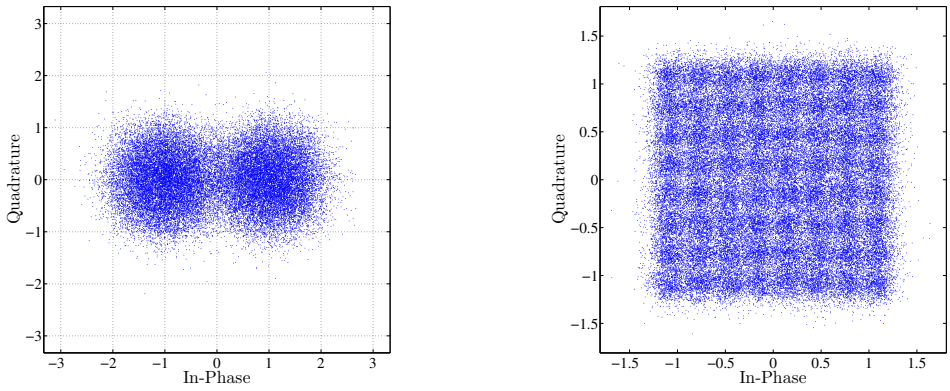

Figure 3.6: *Scatter plots of BPSK and* 64*QAM represent the single Gaussian approximation at each signal constellation of BPSK and* 64*QAM.*

3.5 Soft Bit Generation

The generation of bit LLRs or soft bits are briefly described in this Section. For simplicity, the subcarrier and spatial stream indices are removed from Equation (3.18) assuming an AWGN channel per subcarrier and spatial stream after the MMSE receiver and $\widehat{x}_{\mathrm{MMSE}}$ is replaced with $\widehat{x}$ too. Furthermore, it is assumed that the symbol energy is $E_s = 1$ such that the signal model can be written as,

$$\widehat{x} = G_{\mathrm{MMSE}} y = x + n \,, \tag{3.33}$$

where y, x and n are scalar values, G_{MMSE} is given in Equation (3.28), and n denotes additive zero mean circularly symmetric complex Gaussian noise having post processing variance $\widetilde{N}_0$, i.e.,

$$\widetilde{N}_0 = 1/\mathit{SINR} \tag{3.34}$$

where *SINR* is the post processing signal to interference and noise ratio which is given in Equation (3.32) for the MMSE receiver.

Let us assume that at a particular time instant $\log_2 M$ bits are transmitted in a symbol x, where M represents M-ary signal constellation. For instance, 16QAM has $\log_2 M = \log_2(16) = 4$ bits per symbol. Moreover, it is assumed that c_m ($m = 1, 2, \cdots, \log_2 M$) is the mth coded bit of the transmitted symbol x. Let us also assume that $\mathcal{S} = \{s_1,\ s_2,\ \cdots,\ s_M\}$ denotes the set of (complex) constellation symbols with cardinality $|\mathcal{S}| = M$. So, $\mathcal{S}_0^m \left(m = 1, 2, \cdots, \log_2 M\right)$ denotes the set of (complex) constellation symbols where the mth bit is 0. Similarly, $\mathcal{S}_1^m \left(m = 1, 2, \cdots, \log_2 M\right)$ denotes the set of (complex) constellation symbols where the mth bit is 1. The definition of LLR for each coded bit can be written as,

$$L\left(c_m\right) = \log\left(\frac{\mathbb{P}\Big(c_m = 1\Big|y\Big)}{\mathbb{P}\Big(c_m = 0\Big|y\Big)}\right) \tag{3.35}$$

$$= \log\left(\frac{\mathbb{P}\left(c_m = 1\middle|\widehat{x}\right)}{\mathbb{P}\left(c_m = 0\middle|\widehat{x}\right)}\right) \tag{3.36}$$

$$= \log\left(\frac{\displaystyle\sum_{s\in\mathcal{S}_1^m} \mathbb{P}\left(s\middle|\widehat{x}\right)}{\displaystyle\sum_{s\in\mathcal{S}_0^m} \mathbb{P}\left(s\middle|\widehat{x}\right)}\right) \,, \tag{3.37}$$

using Bayes' rule,

$$L\left(c_m\right) = \log\left(\frac{\displaystyle\sum_{s\in\mathcal{S}_1^m} p\left(\widehat{x}\middle|s\right)\mathbb{P}(s)}{\displaystyle\sum_{s\in\mathcal{S}_0^m} p\left(\widehat{x}\middle|s\right)\mathbb{P}(s)}\right) \,, \tag{3.38}$$

where $p\left(\widehat{x}\middle|s\right)$ is the conditional PDF of the MMSE output and $\mathbb{P}(s)$ is the probability of a symbol in a signal constellation. It is assumed that each symbol in the constellation is equiprobable, i.e., $\mathbb{P}(s) = 1/M$, which leads to

$$L\left(c_m\right) = \log\left(\frac{\sum\limits_{s\in\mathcal{S}_1^m} p\left(\widehat{x}\middle|s\right)}{\sum\limits_{s\in\mathcal{S}_0^m} p\left(\widehat{x}\middle|s\right)}\right) . \tag{3.39}$$

Since the output of the MMSE is approximately Gaussian, the conditional probability density function (PDF) $p\left(\widehat{x}\middle|s\right)$ is Gaussian as well. The conditional PDF is given by

$$p\left(\widehat{x}\middle|s\right) = \frac{1}{\sqrt{2\pi\left(\widetilde{N}_0/2\right)}}\exp\left(-\frac{\left|\widehat{x}-s\right|^2}{2\left(\widetilde{N}_0/2\right)}\right) \tag{3.40}$$

$$= \frac{1}{\sqrt{\pi\widetilde{N}_0}}\exp\left(-\frac{\left|\widehat{x}-s\right|^2}{\widetilde{N}_0}\right) , \tag{3.41}$$

where $\widetilde{N}_0 = 1/\textit{SINR}$. So, Equation (3.39) becomes

$$L\left(c_m\right) = \log\left(\frac{\sum\limits_{s\in\mathcal{S}_1^m}\exp\left(-\frac{\left|\widehat{x}-s\right|^2}{\widetilde{N}_0}\right)}{\sum\limits_{s\in\mathcal{S}_0^m}\exp\left(-\frac{\left|\widehat{x}-s\right|^2}{\widetilde{N}_0}\right)}\right) . \tag{3.42}$$

The computation of $L\left(c_m\right)$ by Equation (3.42) is very complex because it needs to compute the distance for all the constellation symbols. Thus, the max-log approximation is employed to reduce complexity. So,

$$L\left(c_m\right) \approx \log\left(\frac{\exp\left(\max\limits_{s\in\mathcal{S}_1^m}\left\{-\frac{\left|\widehat{x}-s\right|^2}{2(\widetilde{N}_0/2)}\right\}\right)}{\exp\left(\max\limits_{s\in\mathcal{S}_0^m}\left\{-\frac{\left|\widehat{x}-s\right|^2}{2(\widetilde{N}_0/2)}\right\}\right)}\right) \tag{3.43}$$

$$= \frac{1}{\widetilde{N}_0}\left(\min_{s\in\mathcal{S}_0^m}\left\{\left|\widehat{x}-s\right|^2\right\} - \min_{s\in\mathcal{S}_1^m}\left\{\left|\widehat{x}-s\right|^2\right\}\right) . \tag{3.44}$$

Furthermore, a demapper which calculates an LLR using Equation (3.42) is known as LogAPP (logarithmic a-posteriori probability or LogMAP) [Land et al., 2004] demapper whereas a demapper which utilizes Equation (3.43) is known as MaxLog demapper.

3.6 Summary

OFDM is used for the mitigation of the effects of the multipath propagation channels because it decouples the fading channel into parallel flat fading channels. The basic concepts of MIMO was introduced like array gain, diversity gain and spatial multiplexing. The MIMO-OFDM was also introduced with the discussion of MIMO receivers, i.e., ZF and MMSE receivers. The output of the MMSE receiver is considered equivalent to a Gaussian channel which is corroborated with some results in Section 3.4.4. The basic formulas were shown for the computation of the exact and approximate LLR.

Link Adaptation Algorithms 4

A link adaptation (LA) algorithm in general chooses a suitable MCS to increase the throughput of a system while maintaining some quality of service (QoS) objectives. The QoS objectives are, e.g., packet loss, connectivity, packet delivery delay. In this project, the QoS objective is to stay below a target PHY packet error rate (PER) which determines the statistics of retransmissions and ultimately determines the throughput and latency of a system. Thus, LA algorithm with QoS objective will select a suitable MCS value by fulfilling the target PER requirement.

4.1 Slow and Fast Link Adaptation

There are several approaches for LA to predict the PHY PER according to some defined QoS objective [Simoens et al., 2005].

If CSI is available at the transmitter via feedback from the receiver or through the reciprocity principle, then the transmit signal can be preprocessed or precoded prior to transmission in order to exploit spatial diversity [Paulraj et al., 2005]. However, precoding is not the subject of this project work.

If CSI is not available at the receiver, then a simple approach will be to estimate PER by simply dividing the number of erroneous packets by a total number of received packets for a given time period window. However, this approach requires a long time to converge especially at a low PER. This kind of approach is known as slow link adaptation (SLA) because it takes a lot of time to accumulate enough packets to estimate PER. SLA is usually stacked in the MAC layer.

If CSI is available at the receiver, a better and an accurate estimation of PER can also be found which will converge fast. Thus, this kind of LA can be defined as fast link adaptation (FLA) which estimates a suitable MCS that fulfills the QoS constraint for a given CSI. Thereafter, the receiver recommends the estimated MCS via feedback to the transmitter so that the transmitter can transmit data at highest possible rate according

to the current channel conditions. Furthermore, the CSI considered in this project is channel $\mathbf{H}$ and noise variance N_0 (or post-processing SINR) available per subcarrier and per spatial stream after the MMSE detector.

Figure 4.1 shows the difference between SLA and FLA. A transmitter is considered which adapts its data rate with the channel conditions. The two regions are considered in an indoor environment having microwave oven interference. It is considered that any packet in the region of microwave interference will be lost. Thus, the transmitted packet should be modulated and coded according to the varying channel conditions in order to maintain the connectivity of the link. In an AWGN channel a lower MCS causes a lower PER compared to a higher MCS for any given SNR. However, under a fading channel, a higher MCS may cause a lower PER than a lower MCS [Prasad et al., 2000, p.68]. So, the adaptation of MCS in a fading channel should be done cautiously. The throughput or data rate decreases with the choice of a lower MCS. So, a trade off has to be maintained between a low PER and high throughput. Furthermore, it can be seen in the schematic shown in Figure 4.1 that the FLA adapts the MCS according to varying channel conditions in order to have high throughput compared to SLA. FLA is a closed loop mechanism which dynamically selects a suitable MCS value depending on the current channel realization whereas SLA is an open loop mechanism which selects a suitable MCS value depending on long term statistics. In IEEE 802.11n, there are 77 $(0-76)$ MCS [IEEE802.11n]. However, the system we consider is only up to 2x3 which allows 22 different MCS as given in Table B.1.

4.2 Link Adaptation Mechanism in IEEE 802.11n

This Section will introduce the concepts of LA functionality according to the IEEE 802.11n standard.

Table 4.1: *Description of subfields in the LA control field*

Nr. of bits	LA control subfield		Description
1	TRQ		Sounding Request
1	MAI	MRQ	MCS Request
3		MSI	Sequence number of MCS request in the range 0 (000) to 6 (110)
3	MFSI		Sequence number of MCS feedback to pair MRQ; for “unsolicited response” = 7 (111)
7	MFB		MCS feedback

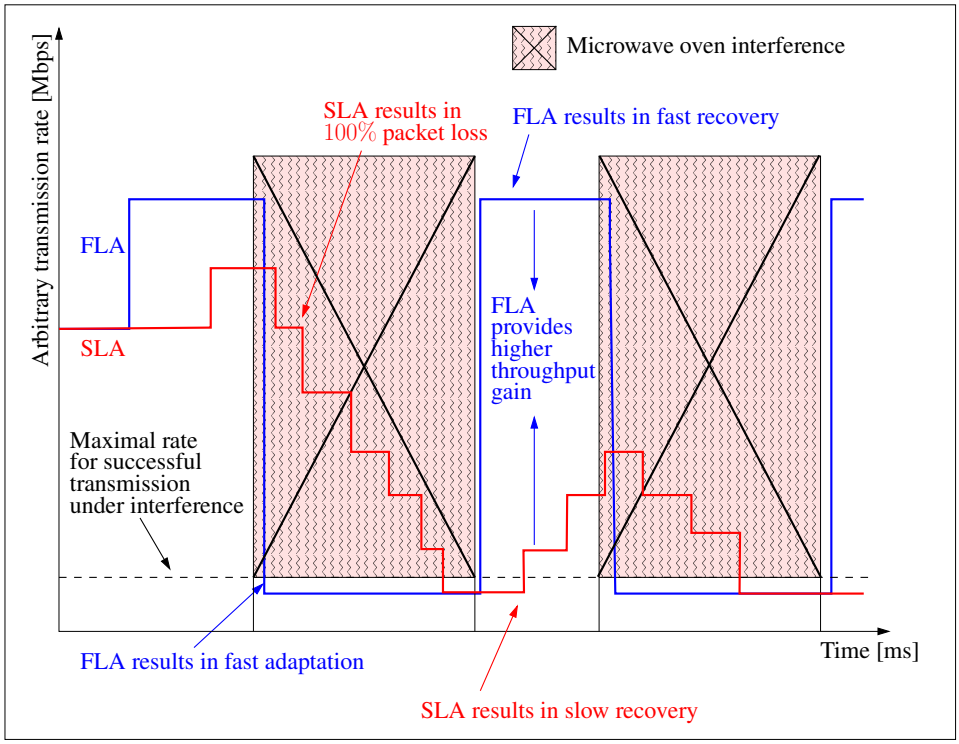

Figure 4.1: *Schematic highlighting the difference between slow link adaptation (SLA) and fast link adaptation (FLA). Inspired from [Globecom, 2003].*

The MAC header shown in Figure 4.2(a) [IEEE802.11n, p.12] consists of frame control, duration, address and HT control (HTC) field . The HTC field shown in Figure 4.2(b) is also referred as +HTC field. The +HTC field consists of the LA control field and other fields [IEEE802.11n, p.17]. The LA control field is shown in Figure 4.2(c). The meaning of subfields in the LA control field are provided in Table 4.1. The same scenario shown in Figure 1.2 can be reconsidered in Figure 4.3 where the two STAs support FLA functionalities. If STA A (MFB requester) requests STA B (MFB responder) for MCS feedback, then STA A will set the MRQ field to 1 in the MAI field of the LA control field. Furthermore, when STA A sets the MRQ field to 1, then it also sets the MSI field which contains a sequence number of MCS request in the range 0 to 6 that identifies the specific MCS request. After the request of MCS feedback from STA A, the STA B can respond in two ways:

Immediate response: If STA B feedbacks the estimated MCS in the TXOP of STA A, then STA A can obtain the benefit of link adaptation in its TXOP. The TXOP is a time duration granted to an STA to use the medium [Hara et al., 2004].

Unsolicited or delayed response: If STA B feedbacks the estimated MCS in the subsequent TXOP obtained by itself rather than the TXOP of STA A.

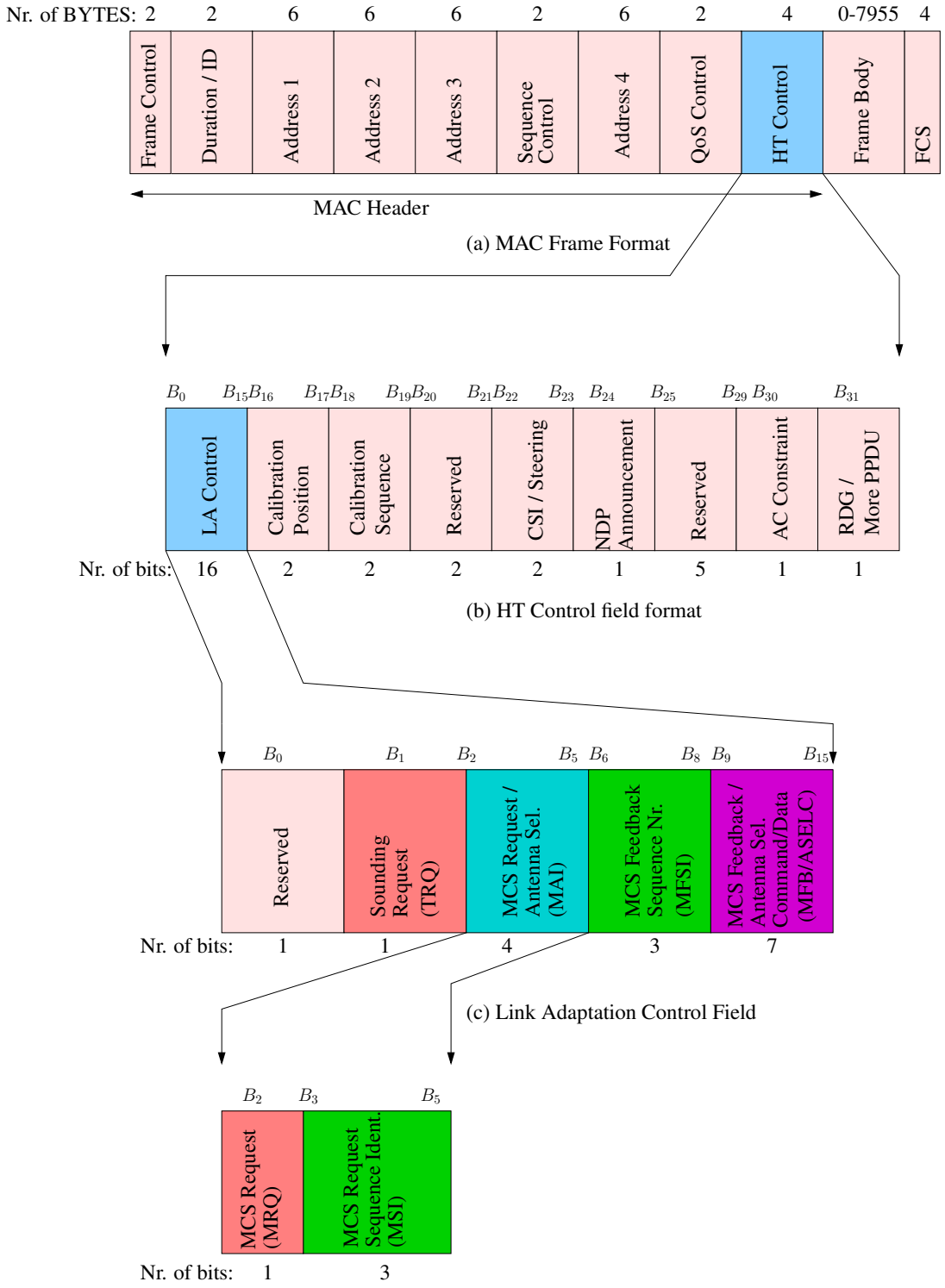

Figure 4.2: *MAC frame, +HTC field and LA control field formats in IEEE* 802.11*n.*

If STA B supports LA in any ways, i.e., immediate or delayed response, then it can feedback the estimated MCS by setting,

- MFB = in the range 0 to 126 and MFSI = sequence number provided in the MSI field of MCS request by STA A [IEEE802.11n, p.19].

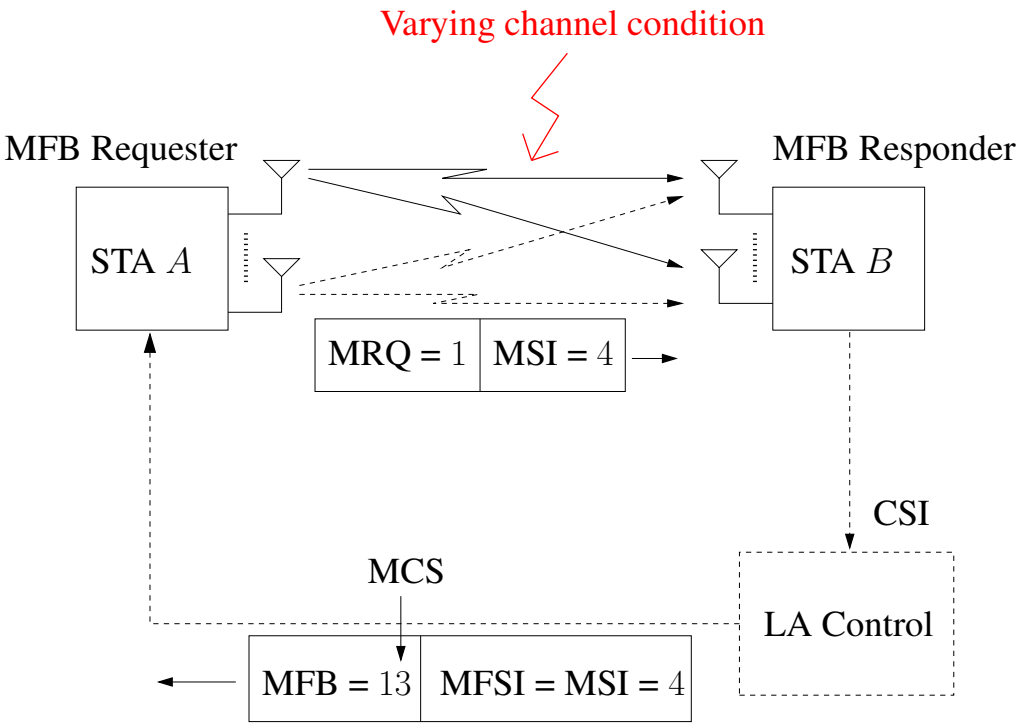

Figure 4.3: *Schematic highlighting the principle of LA in IEEE 802.11n.*

Furthermore, when STA B responds immediately; however it can not feedback the estimated MCS immediately, then it can set

- MFB = 127 ("all ones") and MFSI = 7 which means that STA B does not have the estimated MCS for the current and other pending MCS requests.
- MFB = 127 ("all ones") and MFSI = sequence number provided in the MSI field of MCS request by STA A. By setting these values of MFB and MFSI, STA B would mean to STA A that it would never provide the MCS feedback for the requested sequence [IEEE802.11n, p.19].

STA A can request MFB in two ways from STA B by setting MRQ field to 1 in the MAI field of +HTC frame,

- in a sounding PPDU (PLCP Packet Data Unit, where PLCP - Physical Layer Convergence Protocol).
- with the NDP (Null Data Packet) Announcement field set to 1; thereafter sending a following sounding NDP.

Furthermore, it is worth to mention that STA A sends the sounding PPDU or NDP by sounding all its supported spatial dimensions such that the STA B will have the knowledge of all the spatial dimensions [IEEE802.11n, p.146].

4.3 Survey of Fast Link Adaptation Algorithms

There are numerous publications that have dealt with the PER estimation and link quality metrics (LQMs). The main approaches of FLA can be classified as follows:

$(\mathbf{1})$ Instantaneous SNR [Simoens et al., 2001].

$(\mathbf{2})$ PER indicator method [Lampe et al., 2003].

$(\mathbf{3})$ Raw or uncoded bit error rate mapping (RawBER) [Peng et al., 2007].

$(\mathbf{4})$ Exponential effective SNR mapping (EESM) [Ericsson, 2003B].

$(\mathbf{5})$ Channel capacity and cut-off rate mapping [FITNESS, 2000].

$(\mathbf{6})$ Mutual information per coded bit mapping (MIBM) [Sayana et al., 2007].

Some of these algorithms will briefly be discussed in the following sections. For this project work, we have chosen only three of them: $(\mathbf{3})$ RawBER, $(\mathbf{4})$ EESM and $(\mathbf{6})$ MIBM. The detailed description of the three chosen algorithms are described in the following Chapter 5.

A general FLA mechanism in the context of this project work is shown in Figure 4.4 which comprises an LQM computation and MCS search mechanism. The LQM computation module generally maps the current CSI of the fading channel into a single scalar value (LQM) which then is used to estimate PER for this specific channel state. The calculated scalar *LQM* is then used to estimate PER via the function $\psi_{MCS,PL}\left(LQM\right)$ from AWGN performance for the current MCS value, i.e.,

$$PER_{\text{FadingChannel}}\left(\{\text{CSI}\}\right) \approx \underbrace{PER_{\text{AWGN}}\left(LQM\right)}_{\psi_{MCS,PL}\left(LQM\right)}. \tag{4.1}$$

The function $\psi_{MCS,PL}\left(LQM\right)$ could be a look-up table dependent on the MCS value and packet length (PL). If the estimated PER of the current MCS can not fulfill the target PER, then the MCS value will be changed until the estimated PER is able to fulfill the target PER. Finally, the suitable MCS value will be recommended to the transmitter such that it transmits the signal with the highest possible rate while maintaining the QoS constraint. The above condition (4.1) should be fulfilled for each instantaneous channel realization of any (IEEE) channel models to insure stability of the estimation.

4.3.1 Instantaneous SINR

Instantaneous SINR is a simple and conventional LQM for an FLA algorithm. A look-up table can be prepared before hand by segregating and mapping the SNR range

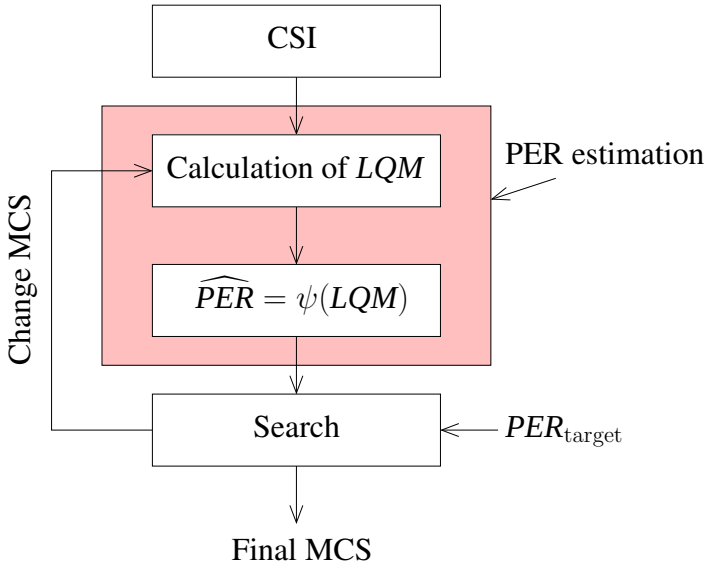

Figure 4.4: *Schematic of a general FLA mechanism.*

according to target PER for respective MCS under AWGN channel. A scalar value (LQM) based on the instantaneous SINR can be calculated in general [Simoens et al., 2005],

$$SNR_{\text{instant}} = \left(\frac{1}{N_{\text{ss}}\, N_{\text{sd}}}\right) \sum_{j=1}^{N_{\text{ss}}} \sum_{k=1}^{N_{\text{sd}}} SINR_j[k] \tag{4.2}$$

where $SINR_j[k]$ is given in Equation (3.32), N_{sd} is a number of the used data subcarriers and N_{ss} is a number of spatial streams.

After the calculation of SNR_{instant} for an instantaneous channel realization at the receiver having channel knowledge, the PER can be estimated for a given MCS and packet length by looking up the table according to the calculated SNR_{instant}. However, it was shown in [Lampe et al., 2003] that the PER curve for each individual multipath channel realizations will be different from the average PER curve for a given channel model, MCS and packet length. Furthermore, for a fixed PER, the *SNR* difference between two individual channel realizations can be quite large, i.e., SNR_{instant} is not an accurate LQM [Simoens et al., 2005]. Thus, if the LQM for the FLA is based on SNR_{instant}, there can be some channel realizations for which the FLA may have fatal adaptation of MCS and render packet losses unless a suitable MCS is used for the transmission. So, an LQM for the FLA based on the instantaneous SINR can not be accurate enough in the estimation of PER.

4.3.2 PER Indicator Method

The PER indicator method introduced in [Lampe et al., 2003] can be used as a link quality metric to estimate PER. This method has higher accuracy than the instantaneous SINR. It is based on a two-dimensional mapping having a PER indicator as one parameter and another parameter as the SNR difference from the AWGN channel. The mapping is parametrized by the target PER, given MCS and packet length [Blankenship et al., 2004]. The PER indicator can be given by [Lampe et al., 2003] [Blankenship et al., 2004],

$$I_{\mathrm{var}\rho} = \frac{1}{N_{\mathrm{sd}} - 1} \sum_{k=1}^{N_{\mathrm{sd}}} \left| \left| H[k] \right| - \left| \widetilde{H} \right| \right|^{\rho} \tag{4.3}$$

where $|H[k]|$ is the magnitude of the channel transfer function on the kth subcarrier and $\left|\widetilde{H}\right|$ is the average of all $|H[k]|$. The value of $\rho = 1.4$ is given in [Lampe et al., 2003]. Thus, the PER can be estimated for the current channel realization by looking up the prepared two dimensional table. However, this method can not easily be extended to MIMO-OFDM because it is unclear in MIMO case for obtaining the matrix average and norm.

4.3.3 Exponential Effective SINR Mapping (EESM)

The EESM method is a technique which is originally used for system-level simulations in [Ericsson, 2003B]. The concept of effective SINR is to calculate an instantaneous effective SINR ($SINR_{\mathrm{eff}}$) such that [Nanda et al., 1998]

$$PER_{\mathrm{AWGN}}(SINR_{\mathrm{eff}}) \;\approx\; PER_{\mathrm{FadingChannel}}\left(\{SINR[1],\, SINR[2],\, \cdots,\, SINR[N_{\mathrm{sd}}]\}\right) \tag{4.4}$$

where N_{sd} is a number of the used data subcarriers.

It means that the set of SINRs $(\{SINR[1],\, SINR[2],\, \cdots,\, SINR[N_{\mathrm{sd}}]\})$ available over all the data subcarriers under any fading channel can be translated to one scalar value (LQM), i.e., $SINR_{\mathrm{eff}}$, such that it yields the same *PER* under an AWGN channel. A look-up table can be prepared beforehand containing *PER* versus *SNR* in an AWGN channel. The $SINR_{\mathrm{eff}}$ can be calculated from Equation (4.5) [Ericsson, 2003B] which is then used to look up the table to estimate *PER* for the current fading channel realization.

$$SNR_{\mathrm{eff}} = -\beta \,\log\left(\frac{1}{N_{\mathrm{ss}}\, N_{\mathrm{sd}}} \sum_{j=1}^{N_{\mathrm{ss}}} \sum_{k=1}^{N_{\mathrm{sd}}} \exp\left(\frac{-SINR_j[k]}{\beta}\right)\right) \tag{4.5}$$

where N_{ss} is a number of spatial streams, $\mathit{SINR}_j[k]$ is given in Equation (3.32) and the parameter β is used to fit the model to the characteristics of the considered MCS. There can be various possible ways to optimize β for each MCS [Brueninghaus et al., 2005]. In this project work, to obtain β, a least squares fit is performed in the $\log(\mathit{PER})$ domain, i.e.,

$$\beta_{\text{opt}} = \arg \min_{\beta} \left\{ \sum_{i=1}^{N_C} |\Delta e_i(\beta)|^2 \right\} , \tag{4.6}$$

where

$$\Delta e_i(\beta) = \log\left(\mathit{PER}^i_{\text{P}}(\beta)\right) - \log\left(\mathit{PER}^i_{\text{M}}\right) \qquad \forall\, i = 1, 2, \cdots, N_C , \tag{4.7}$$

N_C is the number of different channel realizations considered for the optimization process, $\mathit{PER}^i_{\text{M}}$ is the measured PER for the ith channel realization and noise variance, and $PER^i_{\text{P}}(\beta)$ is the estimated PER for the given β, ith channel realization and noise variance.

It has been shown that the EESM has a higher accuracy in terms of PER estimation than PER indicator method discussed in Section 4.3.2 [Blankenship et al., 2004]. In this project work, EESM is selected for further investigation as a link quality metric for PER estimation and will be discoursed extensively in Section 5.3.

4.3.4 Raw or Uncoded Bit Error Rate (RawBER) Mapping

In RawBER mapping, a single scalar value (LQM) is found by averaging over all the probability of uncoded bit errors at each subcarrier. A one dimensional look-up table can be prepared beforehand for an AWGN channel which can take raw (uncoded) bit error rate as an input and corresponding PER as an output for a given MCS and packet length. The LQM in RawBER mapping is given by [Lamarca et al., 2005] [Peng et al., 2007]

$$\mathit{RawBER} = \left(\frac{1}{N_{\text{ss}}\, N_{\text{sd}}}\right) \sum_{j=1}^{N_{\text{ss}}} \sum_{k=1}^{N_{\text{sd}}} \mathit{RawBER}_j[k] \tag{4.8}$$

where, $\mathit{RawBER}_j[k]$ is a raw bit error probability of the jth spatial stream and kth subcarrier for a given modulation only (since it is independent of code rate). If unequal modulation is employed among different spatial streams then the *RawBER* will be evaluated for each spatial stream and afterwards combined in one scalar value (LQM). RawBER is further investigated in Section 5.2.

4.3.5 Channel Capacity Mapping

Channel capacity and cut-off rate are used as a LQM for link level simulations in [FITNESS, 2000]. A single scalar value (LQM) is found by averaging over all the channel capacities of each subcarrier for the current channel realizations to estimate PER. A one dimensional look-up table is used which takes an input the mean of the channel capacity or channel capacity effective SINR and an output as PER. The mean channel capacity of all the subcarriers and spatial streams can be calculated as

$$C_{\text{mean}} = \frac{1}{N_{\text{ss}}\, N_{\text{sd}}} \sum_{j=1}^{N_{\text{ss}}} \sum_{k=1}^{N_{\text{sd}}} \log_2 \left(1 + \mathit{SINR}_j[k]\right) \tag{4.9}$$

where C_{mean} is the average channel capacity, N_{ss} is the number of spatial streams, N_{sd} is the number of data subcarriers and $\mathit{SINR}_j[k]$ is given in Equation (3.32).

A correction factor η can be introduced in the channel capacity mapping for each MCS such that the channel capacity effective SINR (CESM) [WINNER, 2003] can be used to estimate PER for the current channel realization. The channel capacity effective SINR, i.e., $\mathit{SINR}_{\text{eff}}$, is given by

$$\mathit{SINR}_{\text{eff}} = \eta \left(2^{\left(\frac{1}{N_{\text{ss}}\, N_{\text{sd}}} \sum_{j=1}^{N_{\text{ss}}} \sum_{k=1}^{N_{\text{sd}}} \log_2 (1 + \mathit{SINR}_j[k]/\eta) \right)} - 1 \right) \tag{4.10}$$

where η can be optimized as discussed in Equation (4.6), N_{ss} is the number of spatial streams, N_{sd} is the number of data subcarriers and $\mathit{SINR}_j[k]$ is provided by Equation (3.32). Similarly as in the EESM, the PER can be estimated for the computed channel capacity LQM $\mathit{SINR}_{\text{eff}}$ using the one dimensional look-up table. However, the PER estimation accuracy of the CESM is worse than the EESM according to [Brueninghaus et al., 2005], [WINNER, 2003].

4.3.6 Mutual Information Based Mapping (MIBM)

Mutual information is used for system level simulations to estimate PER in [WINNER, 2003], [Ericsson, 2003A], [Brueninghaus et al., 2005] which has shown as a good PER estimator with high accuracy. In [Sayana et al., 2007], mutual information based LQM is suggested as a good metric for the system level simulations for the standard IEEE 802.16e. In a similar way of other LQMs described previously, a look-up table can be used which will take mean mutual information per coded bit or symbol as an input and will estimate corresponding PER for a given MCS and packet length. A single scalar value (LQM) is also found here by averaging over all the mutual information values for each subcarrier and spatial stream. There are basically two methods to obtain the LQM based on MI in this project work. The first method derives the LQM

from the post processing SINR available at each subcarrier and spatial stream. The second method directly computes the LQM from the absolute value of the soft bits (L) entering the decoder. In both methods, the mean MI per coded bit or symbol ($\mathcal{I}_{\text{mean}}^{\text{symbol}}$) of all the symbols or coded bits in a packet is the LQM which is given by

$$\mathcal{I}_{\text{mean}}^{\text{symbol}} = \mathbb{E}\left\{\mathcal{I}^{\text{symbol}}(\cdot)\right\} \ , \tag{4.11}$$

where the definitions of $\mathcal{I}(\cdot)$ are described in Section 5.4.

4.3.7 General Framework of the LQM

A general framework [Brueninghaus et al., 2005] of LQMs can easily be deduced from the 3 chosen metrics for this project work as,

$$\mathcal{F}_{\text{mean}}(\cdot) = \frac{1}{N_{\text{ss}}\, N_{\text{sd}}} \sum_{j=1}^{N_{\text{ss}}} \sum_{k=1}^{N_{\text{sd}}} \mathcal{F}_j[k]\Big(\cdot\Big) \ , \tag{4.12}$$

where $\mathcal{F}$ is a function which depends on the LQM like EESM, RawBER and MIBM ($\mathcal{I}$). Thus,

- for the EESM,

$$\mathcal{F}_j[k]\Big(\cdot\Big) = \exp\left(-\frac{\mathit{SINR}}{\beta}\right) \ . \tag{4.13}$$

- for the RawBER,

$$\mathcal{F}_j[k]\Big(\cdot\Big) = \mathit{RawBER}_M\left(\mathit{SINR}\right) \ , \tag{4.14}$$

  where $\mathit{RawBER}_M\left(\mathit{SINR}\right)$ is a raw (uncoded) bit error rate which depends on the M-ary modulation and SINR. For instance, BPSK modulation has $\mathit{RawBER}_{\text{BPSK}}\left(\mathit{SINR}\right) = Q\left(\sqrt{2\ \mathit{SINR}}\right)$.

- for the first method of the MIBM,

$$\mathcal{F}_j[k]\Big(\cdot\Big) = \mathcal{I}_M^{\text{symbol}}\left(\mathit{SINR}\right) \ , \tag{4.15}$$

  where $\mathcal{I}_M^{\text{symbol}}\left(\mathit{SINR}\right)$ is a mean mutual information per coded bit or symbol which depends on the M-ary modulation and *SINR*.

- for the second method of MIBM,

$$\mathcal{F}_j[k]\Big(\cdot\Big) = \mathbb{E}\left\{f_{\mathcal{I}}\left(|L|\right)\right\} \ , \tag{4.16}$$

  where $|L|$ is the absolute value of the L values or soft bits for the kth subcarier and the jth spatial stream.

4.4 Summary

FLA is chosen rather than SLA because it can dynamically select a suitable MCS value for the current fading channel realization to increase the throughput of a system. LA definition in the IEEE 802.11n standard was introduced in Section 4.2. The different LQMs for the FLA algorithm are introduced. The basic concept behind these LQMs are that they translate a set of CSIs available at the receiver for a fading channel into one or two scalars. These scalars of a current channel state is then used to look-up a pre-computed table or function to estimate a corresponding PER in an AWGN channel for a given MCS and packet length. The three LQMs are chosen for further investigation in this project work: RawBER, EESM and MIBM. The general framework of the these three LQMs is presented in Section 4.3.7.

Fast Link Adaptation Algorithms

5

In this chapter the different link quality metrics and their relation to the fast link adaptation algorithm will be presented. The RawBER based algorithm will be presented first which will give the foundation and structure for the others. Further, the EESM method and three mutal information based methods are presented and discussed. In Section 5.1 the general notation will be introduced to understand the algorithms. The RawBER algorithm is given in Section 5.2. Some of the steps given in the algorithm outline are further elaborated on in Sections 5.2.1 to 5.2.5. The EESM and mutal information methods are described in the Sections 5.3 and 5.4, respectively.

5.1 Receiver Block Diagram and Notations

In this section the focus will be on the block diagram shown in Figure 5.1.

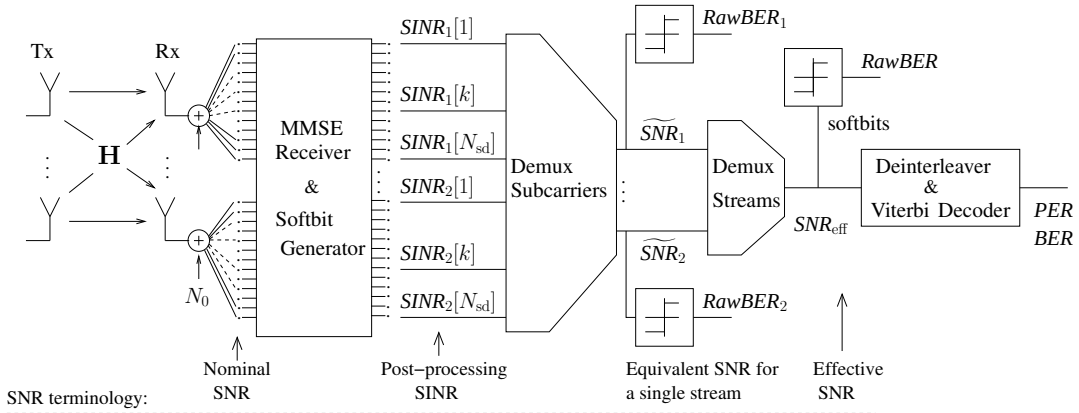

Figure 5.1: *A block diagram of the receiver structure and description of terminologies for the important blocks for the FLA algorithms.*

A signal is transmitted over a channel with the channel matrix $\mathbf{H}$ and noise variance N_0. The associated SNR of the signal is denoted as the nominal SNR or simply

E_s/N_0. After MMSE receiver the associated SINR per symbol is the post-processing $SINR_j[k]$ for the jth stream and kth subcarrier. The generated softbits per subcarrier are demultiplexed into one stream for each spatial stream, and the equivalent SNR for a single stream will be denoted $\widetilde{SNR}_j$. The (uncoded) $RawBER_j$ for each stream is the hard decision of the softbits compared with the transmitted signal, and averaged over all the bits. After demultiplexing the streams, this data stream is associated with the effective SNR_{eff} and *RawBER*. For now, consider $\widetilde{SNR}_j$ and SNR_{eff} as a single scalar SNR after combining multiple inputs with different SINR.

5.2 RawBER Algorithm Outline

In the Figure 5.2, the steps of the RawBER algorithm are shown. To understand the reasoning it is also good to keep in mind the notations of Figure 5.1.

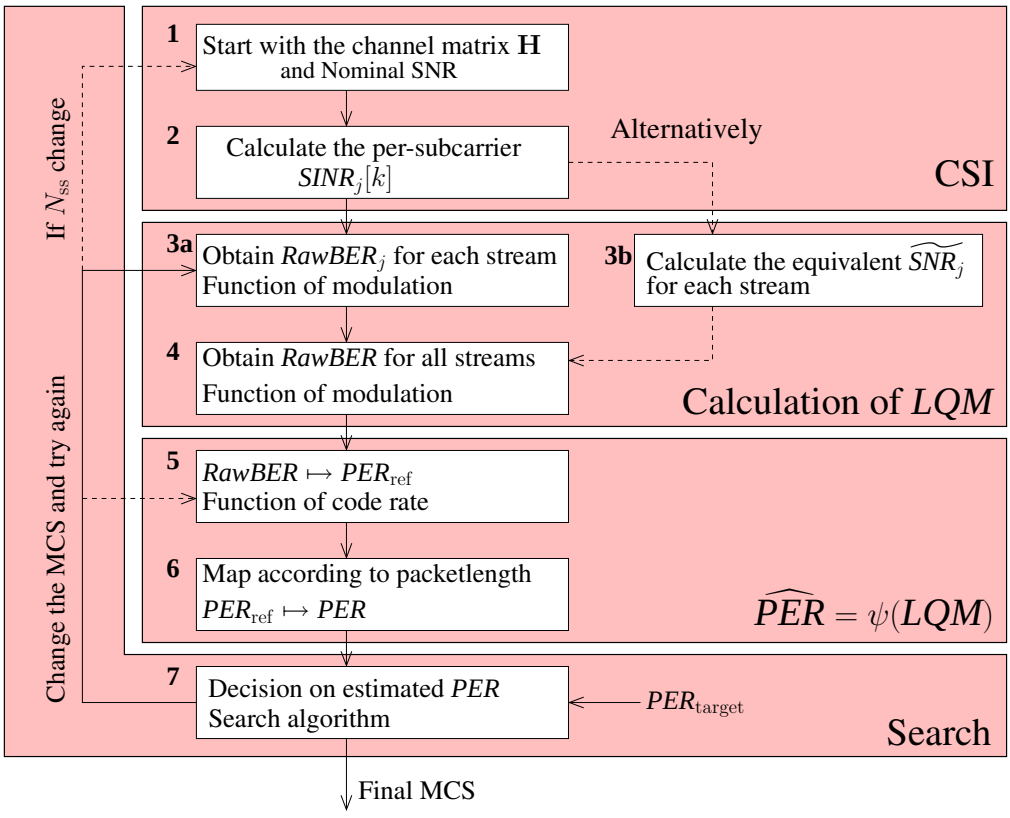

Figure 5.2: *Outline for the RawBER algorithm. The outer filled blocks represent the general steps presented in Figure 4.4.*

The algorithm can be broken down to the following steps.

1 First, the channel matrix $\mathbf{H}[k]$ and nominal SNR are obtained.

2 The post-processing SINRs are calculated for each subcarrier k and spatial stream j as given in Equation (3.32) which is given again for convenience,

$$\mathit{SINR}_j[k] = \frac{1}{\left[\left(\left(\frac{E_s}{N_0}\right)\frac{1}{N_T}\mathbf{H}[k]^H\mathbf{H}[k] + \mathbf{I}_{N_T}\right)^{-1}\right]_{j,j}} - 1\,.$$

3a With the SINR it is possible to estimate the RawBER for each stream. This can be done by calculating the average of the RawBER of all the subcarriers as given in Equation (5.1) for the BPSK case,

$$\begin{aligned}\mathit{RawBER}_j &= \frac{1}{N_{\mathrm{sd}}}\sum_{k=1}^{N_{\mathrm{sd}}}\mathit{RawBER}_j[k] \\ &\approx \frac{1}{N_{\mathrm{sd}}}\sum_{k=1}^{N_{\mathrm{sd}}} Q\left(\sqrt{2\mathit{SINR}_j[k]}\right)\,. \end{aligned} \tag{5.1}$$

As seen in Equation (5.1), the assumption is that the SINR has approximately a Gaussian distribution. The "Gaussian Assumption" will be discussed in Section 5.2.2. Inspired from the EESM method [Ericsson, 2003B], we propose a correction factor, α, such that

$$\mathit{RawBER}_j \approx \left[\frac{1}{N_{\mathrm{sd}}}\sum_{k=1}^{N_{\mathrm{sd}}} Q\left(\sqrt{2\mathit{SINR}_j[k]/\alpha}\right)\right]^{\sqrt{\alpha}} \tag{5.2}$$

and for $\alpha = 1$, Equation (5.2) falls back to Equation (5.1). The variable α can be selected the same way as for β in Equation (4.6).

3b Alternatively, calculate the RawBER from the equivalent SNR, $\widetilde{\mathit{SNR}}_j$

$$\mathit{RawBER}_j = Q\left(\sqrt{2\widetilde{\mathit{SNR}}_j}\right)\,. \tag{5.3}$$

It will discussed in Section 5.2.2 how to obtain $\widetilde{\mathit{SNR}}_j$.

4 Different streams can have different modulation types, (cf. Section B.1), and by combining all the data streams N_{ss} into a single stream the resulting RawBER can be obtained as

$$\mathit{RawBER} = \frac{\sum_{j=1}^{N_{\mathrm{ss}}} b_j\,\mathit{RawBER}_j}{\sum_{j=1}^{N_{\mathrm{ss}}} b_j} \tag{5.4}$$

where b_j is the number of bits per symbol. Example $b_j = 4$ for 16QAM.

5 The input to the Viterbi decoder is associated with the (uncoded) bit error rate *RawBER*. It is possible to estimate the *PER* from the *RawBER* for a packet with a certain length, called PER_{ref}.

6 From PER_{ref}, map this value to *PER* as function of the packet length *PL*. For a convolutional code, a longer packet has a higher *PER* than a shorter packet at fixed SNR.

7 Now, if the estimated *PER* is higher or lower than the desired PER_{target}, change to a lower or higher MCS, respectively, and try again. It is not necessary to step all the way back to step **1** in the FLA algorithm. To take an example, for a change in MCS from 6 to 5 only the code rate changes but the modulation format remains the same. Then it is only necessary to go back to step **5**. When the estimated *PER* is acceptably close to PER_{target}, then select that MCS as the final MCS.

The "Final MCS" is then fed back to the transmitter using the protocol format described in Section 4.2. The different steps are described in details in the subsequent sections. We want to give a short overview here.

[1] For further presentation of the different channel matrix, e.g. beamforming, see Section 5.2.1.

[3a and 3b] Section 5.2.2 discuss numerical results on the "Gaussian Assumption" and approximations of the equivalent SNR.

[5] For the methods of obtaining PER from RawBER, see Section 5.2.3.

[6] Section 5.2.4 will discuss how to obtain *PER* for packets of different lengths.

[7] In Section 5.2.5 the search algorithm is discussed. The search algorithm should find the MCS that maximizes TP while fulfilling the objective of $PER = 1\%$ among all the available MCS using the PER estimation obtained from the steps **1-6**.

5.2.1 Calculation of the Channel Matrix H

In this section we consider how to obtain the channel matrix as seen from the spatial streams and also how to incorporate channel estimation error.

Channel Estimation

For calculation of the channel matrix, $\mathbf{H}[k]$ can under perfect channel knowledge be obtained as a genie from the system. With practical channel estimation an inaccuracy is introduced that can be captured in an error matrix $\mathbf{E}$

$$\hat{\mathbf{H}}[k] = \mathbf{H}[k] + \mathbf{E}[k]\,. \tag{5.5}$$

Let $\mathbf{P} \in \{+1; -1\}^{N_{\mathrm{ss}} \times N_{\mathrm{LTF}}}$ be the orthogonal spreading matrix. When the channel estimations are obtained the system model can be written as

$$\mathbf{y}[k] = \sqrt{\frac{E_s}{N_T}}\mathbf{H}[k]\mathbf{P} + \mathbf{n}[k] \tag{5.6}$$

$$\mathbf{y}[k]\mathbf{P}^{-1} = \sqrt{\frac{E_s}{N_T}}\mathbf{H}[k] + \mathbf{n}[k]\mathbf{P}^{-1} = \widehat{\mathbf{H}}\,. \tag{5.7}$$

The variance matrix of the channel estimates is $\sigma^2_{\mathbf{E}} = N_0\mathbf{I}$. This type of channel estimation simply adds additive noise with variance N_0 or equivalent a loss of $3\,\mathrm{dB}$ in SNR. So, when moving from perfect channel estimation $\mathbf{H}$ to practical channel estimation $\widehat{\mathbf{H}}$ the nominal noise is increased by $3\,\mathrm{dB}$ [Lampe, 2003, p.163]. However, when smoothing is employed this is no longer the case. Simulations have shown that an increase of roughly $2\,\mathrm{dB}$ can be observed when smoothing is applied.

Spatial Expansion

Spatial expansion is used in the mapping from spatial streams to transmit antennas. This is shown in Figure 5.3.

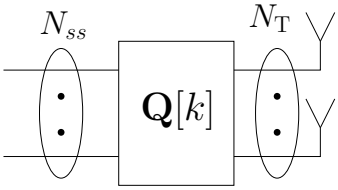

Figure 5.3: *Mapping from N_{ss} streams to N_{T} transmit antennas using the $\mathbf{Q}[k]$ matrix.*

The spatial extension matrix takes the form $\mathbf{Q}[k] = \mathbf{I}_{N_{\mathrm{T}}}$ when $N_{\mathrm{ss}} = N_{\mathrm{T}}$. If $N_{\mathrm{T}} = 2$ and, e.g., MCS 4 with $N_{\mathrm{ss}} = 1$ is utilized, the spatial extension matrix would be

$$\mathbf{Q}[k] = \sqrt{\frac{1}{2}}\begin{bmatrix}1\\1\end{bmatrix} \quad \forall\, k\,. \tag{5.8}$$

If a N_{ss} spatial stream signal is received, what will be the channel matrix and post processing SINRs for a MCS with $N'_{\mathrm{ss}} < N_{\mathrm{ss}}$ spatial streams? Let the known channel

matrix be $\mathbf{H}[k]$ if all dimensions are sounded in the MFB request, $N_{\mathrm{ss}} = N_{\mathrm{T}}$. The corresponding channel equation for $N'_{\mathrm{ss}} < N_{\mathrm{ss}}$ is then

$$\boldsymbol{y}'[k] = \mathbf{H}'[k]\boldsymbol{x}'[k] + \boldsymbol{n}'[k] \tag{5.9}$$

$$= \mathbf{H}[k]\mathrm{diag}(\boldsymbol{\phi}_{\Delta}[k])\mathbf{Q}'[k]\boldsymbol{x}'[k] + \boldsymbol{n}'[k] \tag{5.10}$$

where $H'[k]$ is $N_{\mathrm{R}} \times N'_{\mathrm{ss}}$, $H[k]$ is $N_{\mathrm{R}} \times N_{\mathrm{ss}}$, $\mathrm{diag}(\boldsymbol{\phi}_{\Delta}[k])$ is $N_{\mathrm{ss}} \times N_{\mathrm{ss}}$, $\boldsymbol{x}'[k]$ is $N_{\mathrm{ss}} \times 1$ and $\mathbf{Q}'[k]$ is $N_{\mathrm{T}} \times N'_{\mathrm{ss}}$. Note that we assume $N_{\mathrm{ss}} = N_{\mathrm{T}}$. The vector $\boldsymbol{\phi}_{\Delta}[k]$ is the corresponding change in the cyclic shift when changing from N_{ss} to N'_{ss} spatial streams

$$\boldsymbol{\phi}_{\Delta}[k] = \begin{bmatrix} \exp\left(j\frac{2\pi k\Delta_{\mathrm{CS},1}}{64}\right) \\ \vdots \\ \exp\left(j\frac{2\pi k\Delta_{\mathrm{CS},N_{\mathrm{ss}}}}{64}\right) \end{bmatrix} \tag{5.11}$$

with $\Delta_{\mathrm{CS},s}$ the coefficients for the change of cyclic shift for the sth stream and j is here the imaginary unit.

Beamforming

Beamforming is a technique to improve the reception by orthogonalizing the channel. Beamforming modifies the channel as seen from the FLA algorithm. So, in order to do a proper estimation when beamforming is active, the channel matrix considered should be the modified channel matrix.

For beamforming, consider the SVD decomposition of the channel matrix $\mathbf{H}[k]$,

$$\mathbf{H}[k] = \mathbf{U}[k]\mathbf{\Sigma}[k]\mathbf{V}[k]^H \tag{5.12}$$

with $\mathbf{U}[k]^H\mathbf{U}[k] = \mathbf{I}$ and $\mathbf{V}[k]^H\mathbf{V}[k] = \mathbf{I}$. If now the transmitted symbol vector $\boldsymbol{x}[k]$ is premultiplied with $\mathbf{V}[k]$, by setting $\mathbf{Q}[k] = \mathbf{V}[k]$, then we obtain

$$\boldsymbol{y}[k] = \sqrt{\frac{E_s}{N_T}}\mathbf{H}[k]\mathbf{V}[k]\boldsymbol{x}[k] + \boldsymbol{n}[k] = \mathbf{U}[k]\mathbf{\Sigma}[k]\boldsymbol{x}[k] + \boldsymbol{n}[k]\,. \tag{5.13}$$

So, the channel matrix under beamforming is $\mathbf{H}_B[k] = \mathbf{U}[k]\mathbf{\Sigma}[k]$. The benefit of beamforming is the simple orthogonal structure of $\mathbf{H}_B[k]$ because $\mathbf{H}_B[k]^H\mathbf{H}_B[k] = \mathbf{\Sigma}^2[k]$. This allows for simple and optimal receivers [Gresset, 2006].

5.2.2 Gaussian Assumption and Equivalent SNR Approximation

In Section 3.4.4 the MMSE output was discussed as being equivalent to a Gaussian channel. Here the Gaussian assumption will be further evaluated with examples of

numerical results. The equivalent SNR approximation is evaluated at the end of this section and all the results are discussed.

The "Gaussian Assumption" is an assumption that the interference and Gaussian noise can be modelled as having a single Gaussian distribution. For the purpose of the RawBER link quality metric, only the tail is interesting to give an accurate estimate of the RawBER. So, to be more precise, if the tail of interference and Gaussian noise can be well modelled as the tail of a single Gaussian, then

$$\mathit{RawBER}_{\text{measured}} \approx \mathit{RawBER}_{\text{estimated}} = Q\left(\sqrt{\mathit{SINR}}\right) \tag{5.14}$$

for QPSK. So, if $\mathit{RawBER}_{\text{measured}}$, measured just before the input to the decoder is approximately equal to $\mathit{RawBER}_{\text{estimated}}$, the "Gaussian Assumption" will be valid for the purpose of using RawBER as a link quality metric. Consider the concept shown in Figure 5.4(a) having a of $\mathit{RawBER}_{\text{estimated}}$ versus $\mathit{RawBER}_{\text{measured}}$. Each measurement (*) represents a single channel realization and the diagonal line represents equality in Equation (5.14) or pure Gaussian noise averaged over infinite number of symbols.

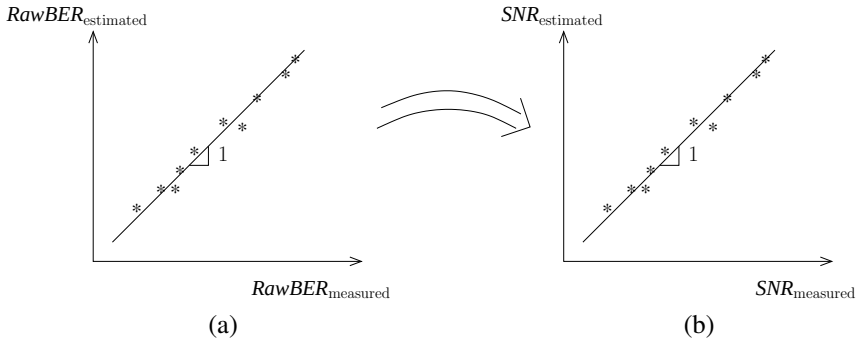

Figure 5.4: *Evaluation of the Gaussian assumption in (a) RawBER domain or (b) SNR domain. The diagonal line represents ideal estimation.*

To understand the outcome well, the numerical results are however plotted $\mathit{SNR}_{\text{estimated}}$ versus $\mathit{SNR}_{\text{measured}}$ because we have a better understanding and interpretation of SNR than of RawBER, see Figure 5.4(b). The variable $\mathit{SNR}_{\text{estimated}}$ is obtained by the inverse error function for QPSK, as

$$\mathit{SNR}_{\text{estimated}} = \left[Q^{-1}\left(\mathit{RawBER}_{\text{estimated}}\right)\right]^2 . \tag{5.15}$$

Plotting the results in the SNR domain require a one-to-one mapping from RawBER domain like the one provided in Equation (5.15). Some of the results are given in Figure 5.5 for nominal SNR in a practical range. To allow comparison, all figures have the same grid spacing of $2\,\mathrm{dB}$.

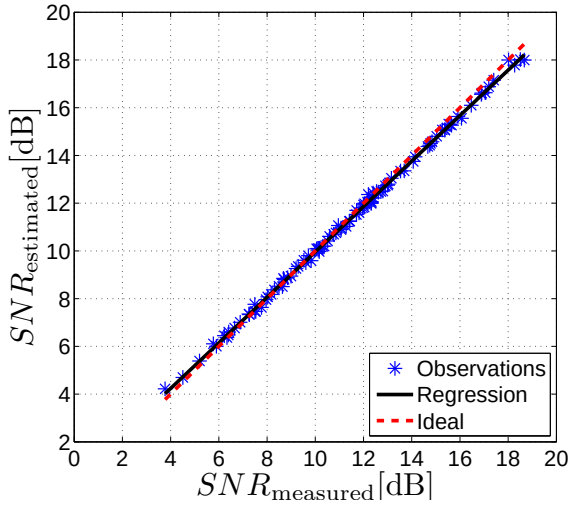

(a) *Perfect channel estimation,* 1×1*, channel B, MCS* 3*,* 16*QAM, SNR* $=$ $20\,\text{dB}$.

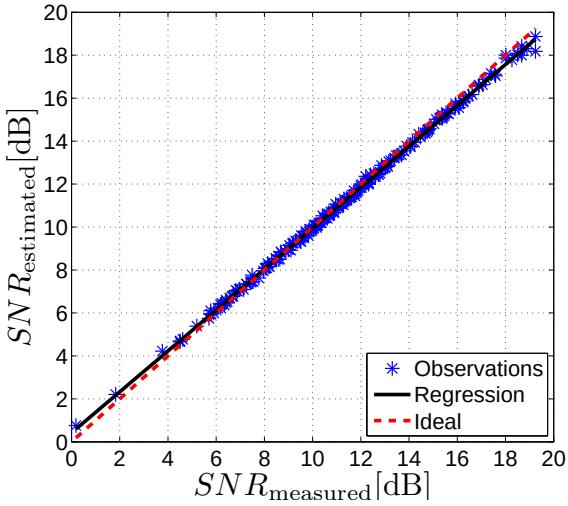

(b) *Perfect channel estimation,* 1×1*, channel B, MCS* 11*,* 16*QAM, SNR* $=$ $24\,\text{dB}$.

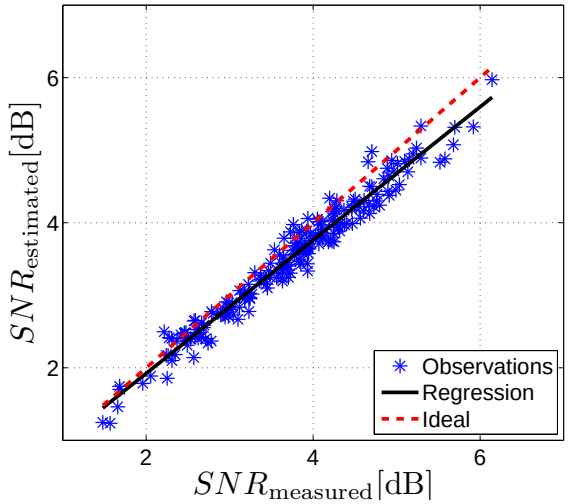

(c) *Perfect channel estimation,* 1×1*, channel E, MCS* 8*, BPSK, SNR* $=$ $12\,\text{dB}$.

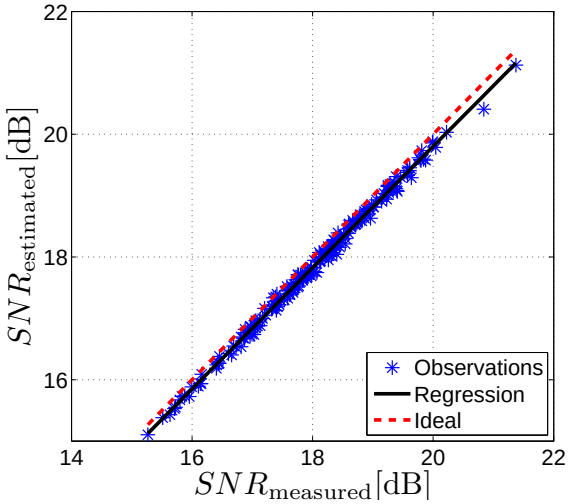

(d) *Perfect channel estimation,* 1×1*, channel E, MCS* 13*,* 64*QAM, SNR* $=$ $28\,\text{dB}$.

5.5(a) This plot shows that under a SISO system there is no interference and each sub-carrier can simply be considered as a scaled AWGN channel. The "Gaussian Assumption" is then, of course, valid.

5.5(b) The measured and the estimated SNR seem to match very closely for this MIMO case. So, the interference and noise in a MIMO system seem to be accurately modelled as Gaussian because the fluctuations in the estimation are about the same as for the SISO system in 5.5(a).

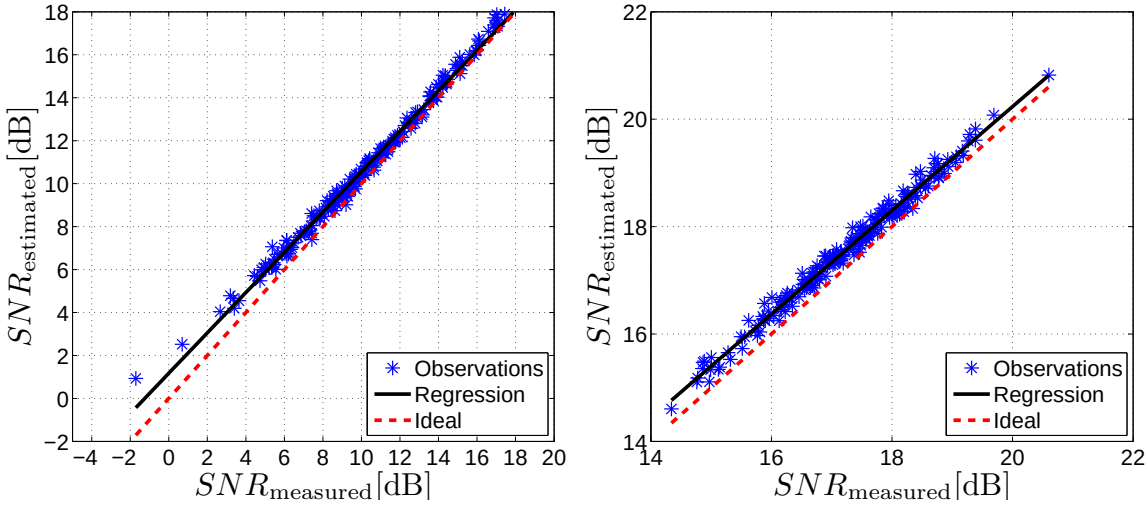

(e) *Practical channel estimation,* 1×1*, channel B, MCS* 11*,* 16*QAM, SNR* $=$ $24\,\text{dB}$.

(f) *Practical channel estimation,* 1×1*, channel E, MCS* 13*,* 64*QAM, SNR* $=$ $28\,\text{dB}$.

Figure 5.5: *Various plots of the observations for evaluation of the Gaussian assumption. Each observation represents a single channel realization.*

5.5(c)(d) These are results for channel model E. They show that the "Gaussian Assumption" is valid under different channel models. For the BPSK case in (c) larger estimation errors are observed, up to $0.5\,\text{dB}$. This is because the interference has a stronger discrete component for BPSK modulation than for higher order modulations. A simple Gaussian model is not accurate anymore.

5.5(e & f) The two plots show the result when channel estimation with smoothing is employed. Compared to Figure 5.5 (b) and (d) the estimation is worse and a small biased is observed in subplot (f). In subplot (e) the regression approaches the ideal estimation asymptotically for high SNR.

Equivalent SNR Approximation

The idea with the equivalent SNR approximation is to reduce the computational burden for calculating RawBER_j. To compute RawBER_j as given in the Equation (5.16) it requires N_{sd} terms of Q-functions or look-up tables

$$\mathit{RawBER}_j = \frac{1}{N_{\text{sd}}} \sum_{k=1}^{N_{\text{sd}}} Q\left(\sqrt{2\mathit{SINR}_j[k]}\right) . \tag{5.16}$$

Two approximations of Equation (5.16) were suggested in [Peng et al., 2007] such that only a single Q-function or look-up table is used.

$$\mathit{RawBER}_j = Q\left(\sqrt{2\widetilde{\mathit{SNR}}_j}\right) \quad \text{with} \tag{5.17}$$

$$\widetilde{\mathit{SNR}}_j \approx \frac{1}{2}(\overline{\mathit{SINR}_j} + \check{\mathit{SINR}}_j) \tag{5.18}$$

$$\approx \frac{2}{N_{\mathrm{sd}}} \sum_{k:\mathit{SINR}_j[k]<\overline{\mathit{SINR}_j}} \mathit{SINR}_j[k] \tag{5.19}$$

with $\overline{\mathit{SINR}_j} = {}^1/_{N_{\mathrm{sd}}} \sum_k \mathit{SINR}_j[k]$ and $\check{\mathit{SINR}}_j = \min_k\{\mathit{SINR}_j[k]\}$ over all subcarriers. The results of the approximation in Equation (5.18) is given in Figure 5.6 for channel B and channel E.

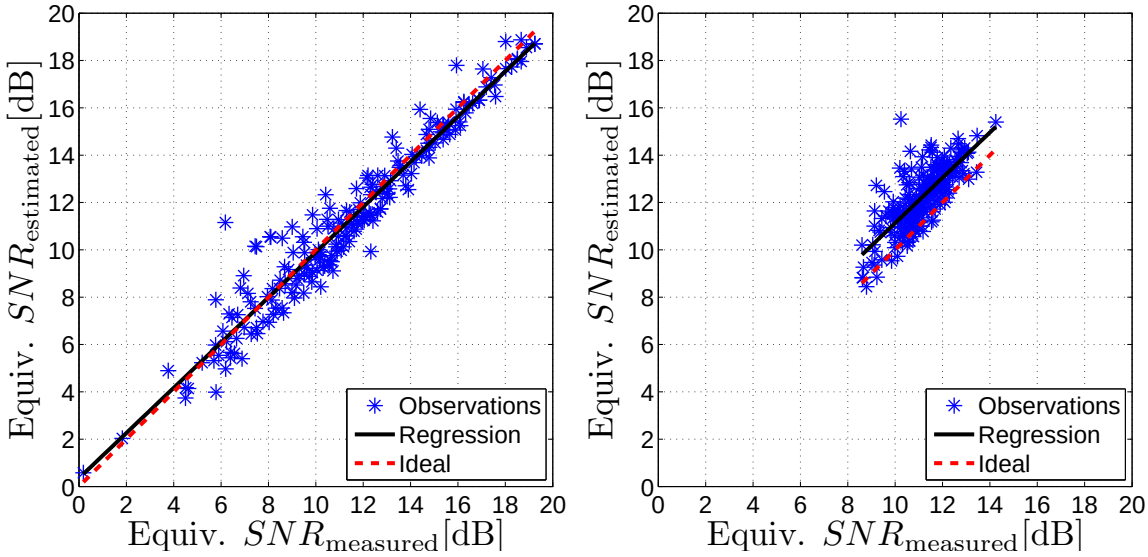

(a) *Perfect channel estimation,* 1×1*, channel B, MCS* 11*,* 16*QAM, SNR* $=$ $24\,\mathrm{dB}$.

(b) *Perfect channel estimation,* 1×1*, channel E, MCS* 11*,* 16*QAM, SNR* $=$ $20\,\mathrm{dB}$.

Figure 5.6: *Plot of the observations plot for the approximation of the equivalent SNR,* $\widetilde{\mathit{SNR}}_j$*. Each observation represents a single channel realization.*

The observations in Figure 5.6(a) are more scattered than those in Figure 5.5(b). For channel E, Figure 5.6(b), the estimation is biased. Let us discuss these results.

From the Figures 5.6(a) and (b) we can see that some channel realizations are estimated quite poorly. The estimation error is up to $4.5\,\mathrm{dB}$. A span of $4.5\,\mathrm{dB}$ in SNR results in PER variations of around 5 decades (cf. Figure B.3). We consider this as a significant estimation error. The channel realizations which are poorly estimated and lay below the ideal line, results in a too pessimistic MCS selection with a resulting lower TP but with a low PER. The channel realizations which is poorly estimated and lay above the ideal line, results in a too optimistic MCS selection with a resulting

higher TP but also with a high PER (a lower TP might be generated if the PER is too high). We are however constraint to target a $PER = 1\%$. So if the subgroup of the too optimistic selected MCS has a too high PER, these packet errors could easily dominate the entire overall PER. The selection of MCS should then be selected pessimistic for the rest of the time because almost no more packet errors are allowed if an overall PER of 1% is to be met. A pessimistic selection algorithm will generate a lower TP. There is also a time aspect in these considerations. If a channel realization is poorly estimated, then it will probably be poorly estimated within a time window corresponding to the coherence time. A too optimistic MCS selection could lead to a fatal link adaption in this time window and almost all packets could be lost.

If $\overline{SINR_j} = \ddot{SINR}_j$ being the median of the SINRs across the subcarriers, then Equation (5.19) is exactly the same as the instantaneous SINR in Equation (4.2). A linear sum of SINR. It was observed that instantaneous SINR is an inaccurate metric [Simoens et al., 2005] (cf. Section 4.3.1). It is not clear how often $\overline{SINR_j} = \ddot{SINR}_j$, but it gives an indication that RawBER estimation using the equivalent SINR is not a good approximation. The calculation of equivalent SNR assumes a certain distribution among the SNR of the subcarriers. This distribution changes with different channel types when the delay spread changes. That may be the reason why the estimation in the Figure 5.6(a) is unbiased but biased in the Figure 5.6(b). We conclude that the approximations in (5.18) and (5.19) are not accurate enough for RawBER estimation. However, the "Gaussian Assumption" is accurate enough for the purpose of calculating $RawBER_j$ when using Equation (5.14).

5.2.3 Mapping from RawBER to PER

In the previous section the Gaussian assumption was verified and $RawBER_j[k]$ for a single subcarrier can then be obtained using well known formulas (see Section B.1 for the expressions for the different modulation schemes). The *RawBER* from combining the different streams is obtained from Equation (5.4). If the *RawBER* at the input to the decoder is known, the associated estimated *PER* for the output can be obtained by a mapping as in Figure 5.7. Firstly, bounds was investigated to avoid simulations but it was not possible to obtain bounds that was tight enough as shown in Appendix B.4.

To take an example in Figure 5.7. Let $RawBER = 0.05$ for 16QAM then the estimated *PER* will be 1% when selecting $R_c = 1/2$. The curves in Figure 5.7 are obtained by simulations in the AWGN channel. An important notion here is that the curves, e.g., rate $1/2$, are not overlapping. If they were overlapping, it would imply that

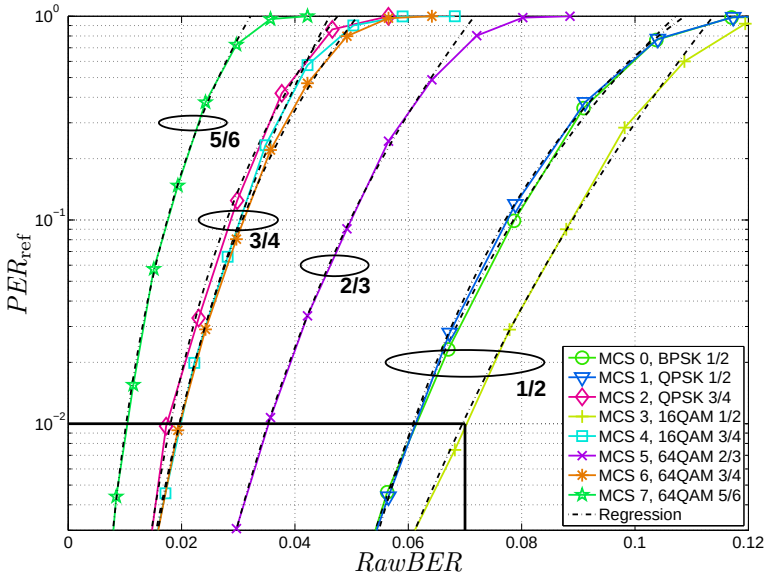

Figure 5.7: *Relation between RawBER and* PER_{ref}*. MaxLog mapper, full trace back Viterbi decoder, info packet length* $PL = 1024\,\mathrm{Bytes}$ *and* $20\,\mathrm{MHz}$ *interleaver used for simulation. MCSs with same code rate are grouped together.*

regardless of the modulation, the same *RawBER* will yield the same *PER*. This is true for hard-decision decoding but not for soft-decision decoding which is employed in these simulations. For soft-decision decoding, the coding gains for higher order modulations are larger than for BPSK and QPSK [Prasad et al., 2000, p.64]. The reason for this is as follows. In Figure 5.8(a) it can be seen that a single input value, $\mathrm{Re}\{\hat{x}\}$ or $\mathrm{Im}\{\hat{x}\}$ results in two soft output values for c_1 and c_2. The reliabilities, $|L|$, for the softbits are shown in Figure 5.8(b) which shows that the reliability for both bits never equals 0. Further, in the center region (around 01 and 11), if one bit gets less reliable the other gets more reliable because of the diagonal crossing curves. These positive effects of higher order Gray mapped constellations can not occur for BPSK and QPSK where a single input value results in a single output value.

5.2.4 Estimation of PER for Different Packet Lengths

PER is in general a function of the packet length when using convolutional code. For the same *BER*, a longer packet will have a higher *PER* [Costello et al., 1999]. Let us consider Figure 5.9 to assess how much the packet length can influence *PER*. The simulations shows an *SNR* difference of approximately $2\,\mathrm{dB}$ to obtain the same *PER* between packet length of $16\,\mathrm{Bytes}$ and $16384\,\mathrm{Bytes}$. Hence we need an adaptation to accurately estimate PER for different packet lengths.

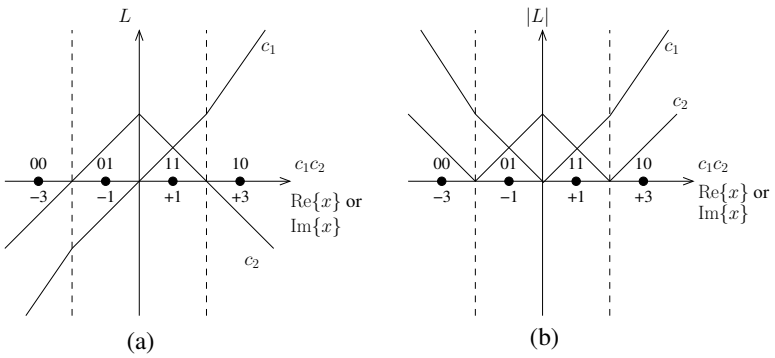

Figure 5.8: *Mappings of received signal (*$\mathrm{Re}\{x\}$ *or* $\mathrm{Im}\{x\}$*) to softbit value (L) for* 16*QAM (*4*PAM). The mapping in the left hand Figure (a) and the corresponding reliability* $|L|$ *in the right hand Figure (b).*

5.2.4.1 Packet Length Prediction

A problem for the receiver is to know the packet length of the next packet to be sent from the transmitter. The length for the next packet sent from the transmitter is not signaled between the receiver and transmitter (cf. the Section 4.2) [IEEE802.11n]. Therefore, the FLA algorithm which resides in the receiver can only make a guess on the next packet length sent from the transmitter side. The packet length is determined by different parameters [Bansal, 2007].

- Different applications produce different packet length. A video packet is around $1.5\,\mathrm{kBytes}$ and voice around $100\,\mathrm{Bytes}$.
- In IEEE 802.11n packet aggregation is used to collect multiple packets to a single packet to improve the TP at the MAC layer.
- The fragmentation threshold for a single packet.
- The remaining length of the transmit opportunity TXOP determines how long the last packet can be.
- The MAC layer performs (slow) link adaptation when the desired PER is not met. The adaption algorithm would first lower the MCS or increase power and as a last option reduce the packet length. This will under a proper FLA scheme happen infrequently because it performs link adaptation itself.

Hence, the packet length is almost random from packet to packet [Bansal, 2007]. Under these circumstances it appears feasible not to assume anything. We will simply expect that the length of the next packet will be the same as for the previous packet because no other solution to this problem seems plausible.

5.2.4.2 PER Correction for Different Packet Lengths

To estimate *PER* for different packet lengths, a number of different approaches could be considered. To take an example, consider that all the bit errors are independent and then calculate *PER* as,

$$\widehat{PER} = 1 - \underbrace{\underbrace{(1-BER)^{PL}}_{\text{All } PL \text{ bits are correct}}}_{\text{Not all } PL \text{ bits are correct}} \tag{5.20}$$

with *PL* as the packet length in info bits. However, independent bit errors does not seem to be a good assumption because the error probabilities are not disjoint [Proakis, 2001, p.487]. This is because the different paths in the trellis are overlapping. Some authors utilizes the first error event instead of BER in Equation (5.20) [Costello et al., 1999]. Instead, assume two different packets with packet lengths PL_1 and PL_2 transmitted over the same channel. Using Equation 5.20 we obtain

$$\widehat{PER}_1 = 1 - (1-BER_1)^{PL_1} \quad \text{and} \quad \widehat{PER}_2 = 1 - (1-BER_2)^{PL_2}\,. \tag{5.21}$$

Now, combining the two equations with $BER_1 = BER_2$ which holds if the same modulation and coding is used

$$\widehat{PER}_2 = 1 - (1-\widehat{PER}_1)^{PL_1/PL_2}\,. \tag{5.22}$$

This means that if $\widehat{PER}_1$ and the corresponding packet length PL_1 are known beforehand, $\widehat{PER}_2$ can be obtained. So, simulations are conducted for a reference $PER_{\text{ref}} = PER_1$ and reference packet length $PL_{\text{ref}} = PL_1$, and the PER for a packet with a different length can simply be computed by

$$\widehat{PER} = 1 - (1-PER_{\text{ref}})^{PL/PL_{\text{ref}}}\,. \tag{5.23}$$

Figure 5.9 shows the accuracy of Equation (5.23). Four different packet lengths are simulated in the AWGN channel for MCS 0. The PER curve with packet length $PL = 1024$ is selected as the reference curve PER_{ref}. Figure 5.9 shows that the Equation (5.23) has a good accuracy except when mapping to a very low packet length, *PL*. The accuracy for these mappings will only be good for lower PER. But the accuracy is still good in the decision region around PER = 1%. For Figure 5.9 only packet lengths up to $16384\,\text{Bytes}$ were simulated even though packets can have lengths of up to $65535\,\text{Bytes}$ [IEEE802.11n, sec.21.1]. Within resonably time, it was practically not possible to obtain sufficient statistics with that packet length.

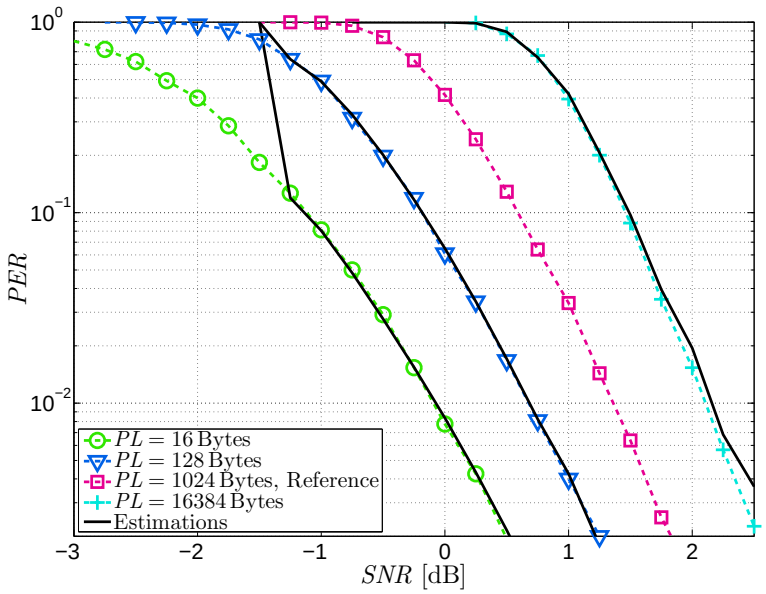

Figure 5.9: *PER for packets of different packet lengths PL for MCS 0, BPSK* $R_\mathrm{c} = 1/2$*. MaxLog mapper, full trace back Viterbi decoder and* $20\,\mathrm{MHz}$ *interleaver used for simulation.*

5.2.5 Search Algorithm

By considering MCS 0 to 7, one could get the idea that MCS 0 always yields a lower PER for the same SNR than MCS 1, MCS 1 produces lower PER than MCS 2 and etc. (cf. the Figure B.3). If this is the case, it is possible to consider a directional search among the available MCS as optimal. This is because

$$MCS\,x > MCS\,y \Leftrightarrow PER(MCS\,x) > PER(MCS\,y) \Leftrightarrow TP_{\max}(MCS\,x) > TP_{\max}(MCS\,y) \tag{5.24}$$

for x, y being available MCS values. Equation (5.24) is fulfilled for the available MCS in the AWGN channel but does *not* always hold for fading channels. If some subcarriers are in deep fade it is more important to have a high Hamming distance rather than a high Euclidean distance in the constellation [Prasad et al., 2000, p.68]. To take an example, 16QAM $R_\mathrm{c} = 1/2$ with the modulation and coding product $MCP = 4{\times}1/2 = 2$ can, for some channel realizations, generate a lower PER for the same SNR than QPSK $R_\mathrm{c} = 3/4$ with $MCP = 1.5$. Consider Figure 5.10 to elaborate on this problem. For a single fading channel realization when averaged over different noise realizations, MCS 3 can have a lower PER than MCS 2 for fixed SNR.

The search algorithm should identify the property described in Figure 5.10. Hence, if the search should select the MCS with the highest MCP, it should never search from the lowest MCS but always from the top. So, three search schemes are presented and discussed. See also the Figure 5.11 for schematic examples of the algorithms.

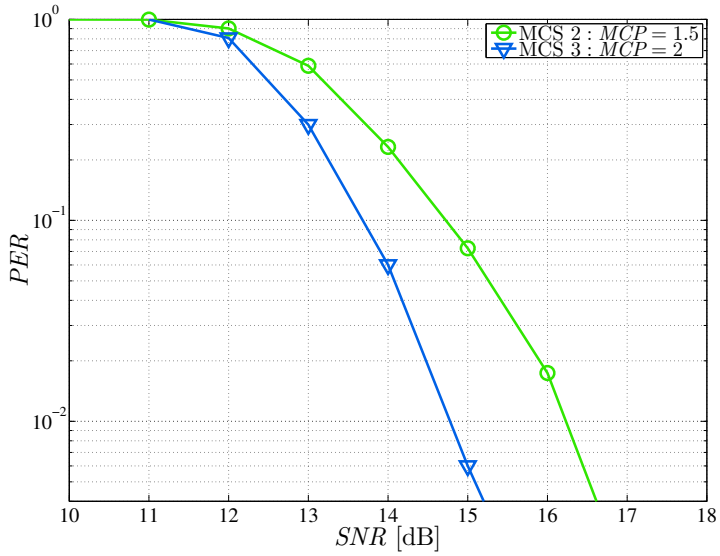

Figure 5.10: *Evaluation of MCS 2 and 3 for a single channel realization of channel type B. MCS 3 with MCP = 2 has a lower PER for the same SNR than MCS 2 with MCP = 1.5.*

- **Total Search –** The expected PERs for all available MCS are calculated and the MCS with the highest MCP that fulfills $PER(MCS) < PER_{\text{threshold}}$ is selected as the final MCS. The Total Search is also known as the exhaustive search. This method has the highest computational burden of the three search methods presented here but will be the optimal search scheme with these constraints.

- **Search from top –** The expected PER is started evaluated from the MCS with the highest MCP and it is checked whether $PER(MCS) < PER_{\text{threshold}}$ is fulfilled. If not, it will check the MCS with the second highest MCP and so on until $PER(MCS) < PER_{\text{threshold}}$ is fulfilled or the lowest MCP has reached. For the worst case scenario this method has the same computational burden as "Total Search". This method has a lower computational burden than "Total Search" but is still optimal.

- **Search from last –** The expected PER is evaluated from the MCS which the FLA algorithm suggested as the final MCS at the last request. The search is then conducted either upwards or downwards until the MCS with the highest MCP has $PER(MCS) < PER_{\text{threshold}}$. This search method will not identify the problem in the Figure 5.10 when the search is conducted upwards. But, if the feedback interval between transmitter STA and receiver STA is comparable to the coherence time, the channel is approximately in the same state. The new final MCS should then be close to the last final MCS and the search could be conducted with a low computational burden. This method will be sub-optimal.

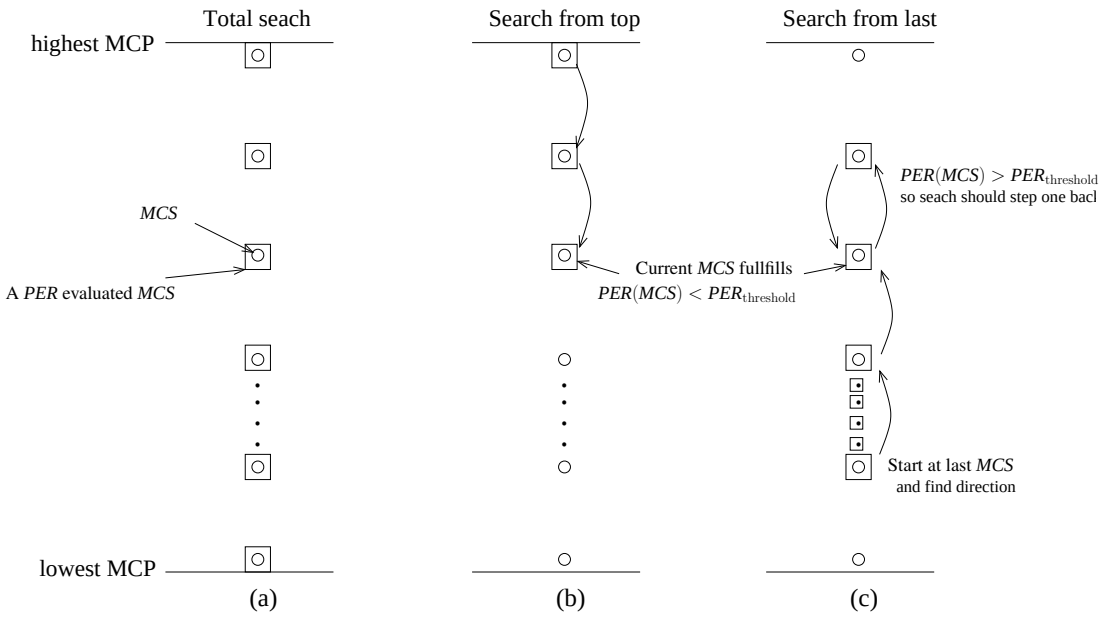

Figure 5.11: *The three different search schemes suggested: (a) The Total search, (b) Search from top and (c) Search from last.*

All the different search methods are conducted with respect to MCP. The available MCSs are in MCP ordered set given in the Tables 5.1 and 5.2. It can be seen in Table 5.2 that some MCS has the same MCP, i.e., $MCS = 4, 10, 33$ has all $MCP = 3$. When more than one MCS share the same MCP, all the MCS with the same MCP are evaluated before it is decided in which direction the search should be conducted or whether the search is finished. This is to avoid the situations where MCS 10 has a lower PER than MCS 4 and if the search was conducted from the top this particular information would never have been identified. So, all MCS having the same MCP are treated equally and evaluated at the same step of the search algorithm. Finally, the one with the lowest PER among the group with the same MCS is selected. This is only the case for the "Search from top"- and the "Search from last"-algorithms because "Total Search" checks all MCSs anyway.

Table 5.1: *MCP ordered set for $N_{\mathrm{T}} = 1$ transmit antenna.*

MCPIndex	0	1	2	3	4	5	6	7
MCS	0	1	2	3	4	5	6	7
MCP	0.5	1	1.5	2	3	4	4.5	5

Table 5.2: *MCP ordered set for $N_{\mathrm{T}} = 2$ transmit antennas.*

MCPIndex	0	1	2	3	4	5	6	7	8	9	10
MCS	0	1	8	2	3	9	4	10	33	5	11
MCP	0.5	1	1	1.5	2	2	3	3	3	4	4
$\rightarrow$	11	12	13	14	15	16	17	18	19	20	21
	34	6	36	7	35	12	37	38	13	14	15
	4	4.5	4.5	5	5	6	6	7.5	8	9	10

5.2.6 Summary

A simple structure of the receiver was discussed to give the definitions of the terminologies used. The outline for the RawBER based algorithm is presented which also gives the general structure for the other methods presented in the Sections 5.3 and 5.4. The RawBER method uses the uncoded bit error rate the input to the decoder as a LQM. Some settings will modify the channel matrix as observed from the data streams, and this is included in the SINR calculation. The Gaussian Assumption was verified but the low-complexity computation of the equivalent SNR was not accurate enough and will not be used. The link between RawBER and PER is a look-up function (regression) generated by simulations in the AWGN channel. The PER is a function of the packet length. For the receiver it is not possible to know the length of the next packet. The FLA algorithm simply assumes that the packet length for the next transmission is the same as the packet length for the previous transmission. We show an accurate method of obtaining the PER for packets of different packet lengths. Three different MCS search methods are given and they will be evaluated in Section 6.4.

5.3 Exponential Effective SNR Mapping (EESM)

As it is introduced before, the EESM translates the instantaneous set of CSIs, i.e., post processing SINRs available for all subcarriers ($\{\mathit{SINR}[1],\ \cdots,\ \mathit{SINR}[N_{\mathrm{sd}}]\}$), into a single scalar LQM which is known as $\mathit{SNR}_{\mathrm{eff}}$. Mathematically, the concept of LQM based on $\mathit{SNR}_{\mathrm{eff}}$ is given below again for convenience.

$$\mathit{PER}_{\mathrm{AWGN}}(\mathit{SNR}_{\mathrm{eff}}) \ \approx\ \mathit{PER}_{\mathrm{FadingChannel}}\left(\left\{\underbrace{\mathit{SINR}[1],\ \cdots,\ \mathit{SINR}[N_{\mathrm{sd}}]}_{\mathit{CSI}}\right\}\right)\ , \quad (5.25)$$

where N_{sd} is the number of data subcarriers, $\mathit{PER}_{\mathrm{FadingChannel}}\left(\{\mathit{CSI}\}\right)$ is the PER of the fading channel and $\mathit{PER}_{\mathrm{AWGN}}\left(\mathit{SNR}_{\mathrm{eff}}\right)$ is the corresponding PER in an AWGN

channel for SNR_{eff}. In other words, the scalar LQM (SNR_{eff}) is obtained for the set of SINRs, i.e., $\{SINR[1],\ SINR[2],\ \cdots,\ SINR[N_{\text{sd}}]\}$, in the fading channel that will render the same PER in an AWGN channel.

The EESM is derived based on the Union-Chernoff bound of error probabilities. The union bound of symbol error probability is given by [Proakis, 2001]

$$P_{\text{s}} \leq \sum_{d=d_{\min}}^{\infty} \alpha_d \, PEP(d, SNR) \ , \tag{5.26}$$

where SNR is SNR per symbol, $d_{\min}$ is the minimum distance of the binary code, α_d is the number of codewords with Hamming weight d and $PEP(d, SNR)$ is the pair wise error probability for a given Hamming distance d and SNR.

For BPSK transmission under an AWGN channel, PEP is equal to [Proakis, 2001]

$$PEP_{\text{BPSK}}\,(d, SNR) = Q\left(\sqrt{2\,d\,SNR}\right) \ . \tag{5.27}$$

The Chernoff bound of $Q\left(\sqrt{2\,d\,SNR}\right)$ is given by

$$Q\left(\sqrt{(2\,d\,SNR)}\right) \leq \exp\left(-d\,SNR\right) \ . \tag{5.28}$$

So, continuing from Equation (5.27)

$$PEP_{\text{BPSK}}\,(d, SNR) \leq \exp\left(-d\,SNR\right) \ . \tag{5.29}$$

Similarly for QPSK, PEP is given by

$$PEP_{\text{QPSK}}\,(d, SNR) = Q\left(\sqrt{d\,SNR}\right) \tag{5.30}$$

$$\leq \exp\left(-\frac{d\,SNR}{2}\right) \ . \tag{5.31}$$

For 16QAM and 64QAM, the closed form solution is given by a sum of Q functions [Yoon et al., 2000] (cf. Appendix B.1). However, if Gray mapping is employed, then the PEP approximation for 16QAM and 64QAM can be given by a single Q function [Yoon et al., 2000] which can be generalized as,

$$PEP_{\text{M}}\,(d, SNR) \approx a\ Q\left(\sqrt{\left(\frac{d\,SNR}{b}\right)}\right) \tag{5.32}$$

$$\leq a\ \exp\left(-\frac{d\,SNR}{b}\right) \ , \tag{5.33}$$

where a and b are dependent on the M-ary modulation and the approximation is accurate for high SNR.

Without loss of generality, the SISO-OFDM system model is considered for the derivation of SNR_{eff}. Since the MMSE output is considered as the output of an equivalent Gaussian channel, then the probability of at least one pairwise error for N_{sd} Gaussian channels is

$$PEP_{\text{M}}\left(d, \left\{SNR[1],\ \cdots,\ SNR[N_{\text{sd}}]\right\}\right) = 1 - \prod_{k=1}^{N_{\text{sd}}}\left(1 - PEP_{\text{M}}\left(d, SNR[k]\right)\right) \tag{5.34}$$

$$\leq 1 - \prod_{k=1}^{N_{\text{sd}}}\left(1 - a\ \exp\left(-\frac{d\,SNR[k]}{b}\right)\right) \tag{5.35}$$

$$\leq 1 - \left[1 - \sum_{k=1}^{N_{\text{sd}}}\left(a\ \exp\left(-\frac{d\,SNR[k]}{b}\right)\right)\right] \tag{5.36}$$

$$= \sum_{k=1}^{N_{\text{sd}}}\left(a\ \exp\left(-\frac{d\,SNR[k]}{b}\right)\right) \tag{5.37}$$

When going from Equation (5.35) to (5.36), higher orders of exponentials are discarded.

Now, the aim is to find a scalar LQM SNR_{eff}, such that it fulfills the condition provided in Equation (5.25). So, taking mean of Equation (5.37) such that the single scalar SNR_{eff} can map the set of N_{sd} SINRs as given below

$$PEP_{\text{M}}\left(d, SNR_{\text{eff}}\right) \approx \left(\frac{1}{N_{\text{sd}}}\right) PEP_{\text{M}}\left(d, \left\{SNR[1],\ SNR[2],\ \cdots,\ SNR[N_{\text{sd}}]\right\}\right) \tag{5.38}$$

$$\Leftrightarrow\ PEP_{\text{M}}\left(d, SNR_{\text{eff}}\right) \approx \left(\frac{1}{N_{\text{sd}}}\right) \sum_{k=1}^{N_{\text{sd}}}\ a\ \exp\left(-\frac{d\,SNR[k]}{b}\right) \tag{5.39}$$

$$a\ \exp\left(-\frac{d\,SNR_{\text{eff}}}{b}\right) = \left(\frac{1}{N_{\text{sd}}}\right) \sum_{k=1}^{N_{\text{sd}}}\ a\ \exp\left(-\frac{d\,SNR[k]}{b}\right) \tag{5.40}$$

$$\left(\frac{-d}{b}\right) SNR_{\text{eff}} = \log\left(\frac{1}{N_{\text{sd}}} \sum_{k=1}^{N_{\text{sd}}} \exp\left(-\frac{d\,SNR[k]}{b}\right)\right) \tag{5.41}$$

$$SNR_{\text{eff}} = -\left(\frac{b}{d}\right) \log\left(\frac{1}{N_{\text{sd}}} \sum_{k=1}^{N_{\text{sd}}} \exp\left(-\frac{SNR[k]}{(b/d)}\right)\right) \tag{5.42}$$

$$SNR_{\text{eff}} = -\beta \log\left(\frac{1}{N_{\text{sd}}} \sum_{k=1}^{N_{\text{sd}}} \exp\left(-\frac{SNR[k]}{\beta}\right)\right)\ , \tag{5.43}$$

where β has to be numerically optimized. The reason is that the derivation of SNR_{eff} starts with Chernoff upper bound which is not a tight bound for low SNR regime

[Biglieri and Divsalar, 2005] and other approximations are also used. So, a suitable β is not found to be equal to b/d after optimizing numerically. Thus, β is a correction factor which minimizes the mismatch between the actual PER and the estimated PER. Furthermore, a suitable β depends on the modulation and coding scheme, as b and d depend on the modulation and code rate, respectively.

Similarly, the general formula for the $SINR_{\text{eff}}$ in the context of MIMO-OFDM is given by [Simoens et al., 2005]

$$SINR_{\text{eff}} = -\beta \, \log\left(\frac{1}{N_{\text{ss}}\, N_{\text{sd}}} \sum_{j=1}^{N_{\text{ss}}} \sum_{k=1}^{N_{\text{sd}}} \exp\left(-\frac{SINR_j[k]}{\beta}\right)\right) \, , \tag{5.44}$$

where $SINR_j[k]$ is given in Equation (3.32), N_{ss} is the number of spatial streams and N_{sd} is the number of data subcarriers. The parameter β can be optimized to fit the model for the PER estimation accuracy using Equation (4.6) for each MCS. The optimal β value shall be independent of channel models [Blankenship et al., 2004], [Ericsson, 2003B].

It is worth to accentuate here that the EESM's Equation (C.4) can also be derived from the RawBER method using single Q-function especially for 16QAM and 64QAM since BPSK and QPSK are exactly given by single Q function. Let us simply consider BPSK modulation, then

$$RawBER = Q(\sqrt{2SNR}) \, . \tag{5.45}$$

Now, if we consider the approximation of Q function provided in [Peng et al., 2007] which is given as

$$Q(\sqrt{x}) \approx p \, \exp\left(-\frac{x}{q}\right) \, , \tag{5.46}$$

where $p = 0.23$ and $q = 1.75$, then the mean RawBER (cf. Equation (4.8)) for BPSK modulation in SISO can be given again here to show the relation of EESM and RawBER, i.e.,

$$RawBER_{\text{mean}} = \left(\frac{1}{N_{\text{sd}}}\right) \sum_{k=1}^{N_{\text{sd}}} Q\left(\sqrt{2\, SNR_j[k]}\right) \tag{5.47}$$

$$p \, \exp\left(-\frac{2\, SNR_{\text{eff}}}{q}\right) \approx \left(\frac{1}{N_{\text{sd}}}\right) \sum_{k=1}^{N_{\text{sd}}} p \, \exp\left(-\frac{2\, SNR_j[k]}{q}\right) \, . \tag{5.48}$$

Thus , following the above EESM derivation, Equation (5.48) will end up with Equation (5.43).

Implementation Recipe for the EESM

The following steps are used for the implementation of the EESM method. It is assumed that suitable β values are pre-computed for each MCS. Figure 5.12 shows the performance curves of PER versus SNR in an AWGN channel for each MCS. Furthermore, it shows the regression (look-up function) which is used to map the SNR_{eff} or $SINR_{\text{eff}} = SNR$ to the corresponding PER in step **4**.

1 Obtain the channel matrix per subcarrier ($\mathbf{H}[k]$) and the noise variance (N_0).

2 The post-processing $SINR_j[k]$ is calculated using Equation (3.32).

3 $SINR_{\text{eff}}$ is calculated using Equation (C.4).

4 The computed $SINR_{\text{eff}}$ is mapped to the corresponding reference PER, i.e., PER_{ref}, for the current MCS in the MCS search loop.

5 The estimated *PER* is corrected for the current packet *PL* by Equation (5.23).

6 MCS search (cf. Section 5.2.5) can be performed by repeating steps **2** to **5** until a MCS renders the highest MCP with PER less than a selection threshold.

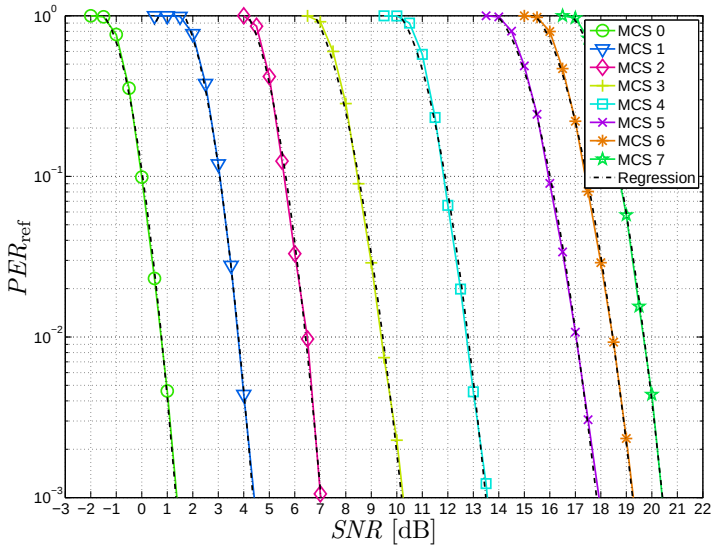

Figure 5.12: *Performance curves of PER_{ref} versus SNR in AWGN channel for MCS 0 to 7. MaxLog soft demapper, full trace back Viterbi decoder, information packet length $PL = 1024$ Bytes and 20 MHz interleaver are used for the simulations. The regressions are second order log-linear which are used for mapping from SNR_{eff} to PER_{ref}.*

5.3.1 Summary

The derivation of the EESM is started with the Union-Chernoff bound and thereafter with other approximations which have led to introduce β as a correction factor for each MCS (cf. general Equation (C.4)). A suitable β can numerically be fine tuned for each MCS (cf. Section 4.6) to minimize the mismatch between the actual PER and the estimated PER. The PER estimation accuracy of the EESM and its performance for throughput versus SNR are assessed and compared with the other LQMs in Chapter 6.

5.4 Mutual Information Based Mapping (MIBM)

The two basic methods of mutual information based mapping (MIBM) were discussed in the Section 4.3.6. The first method depends on the post processing SINRs and the second method depends on the absolute value of the soft bits (LLRs). The concept of MI based LQM is similar to the LQM of RawBER and EESM. The MI based LQM translates the instantaneous set of CSIs, i.e., post processing SINRs or absolute values of LLRs, into a single scalar LQM. As given previously, the general concept of LQM based on MI can be given by

$$PER_{\mathrm{AWGN}}(LQM) \;\approx\; PER_{\mathrm{FadingChannel}}\left(\left\{CSI\right\}\right) \;, \tag{5.49}$$

where $PER_{\mathrm{FadingChannel}}\left(\left\{CSI\right\}\right)$ is the PER of the current fading channel and $PER_{\mathrm{AWGN}}(LQM)$ is the corresponding PER in an AWGN channel. In other words, the scalar LQM is computed for the set of CSIs of the fading channel which will render the same PER in an AWGN channel. MIBM is based on the mutual information per coded bit which is the the mutual information between a coded bit at the input of the symbol mapper (modulator) and its corresponding LLR at the output of the MaxLog demapper (demodulator) [Sayana et al., 2007].

The concept of MI under consideration is shown in Figures 5.13(a) and 5.13(b) [Sayana et al., 2007] which considers an equivalent channel by combining the symbol mapper, channel, MIMO receiver and soft bit (MaxLog) demapper between encoder and decoder. If the codeword length is very large in a BICM, the bit interleaver breaks the memory of the modulator such that the system shown in Figure 5.13(b) can be represented by an equivalent parallel bit channel model [Caire et al., 1998] which is shown in Figure 5.13(c).

It is worth to mention that if there is an asymmetric bit location in the signal constellation, then each bit of the symbol will experience a different bit channel [Sayana et al., 2007]. So, it can be construed that each bit of the symbol may have

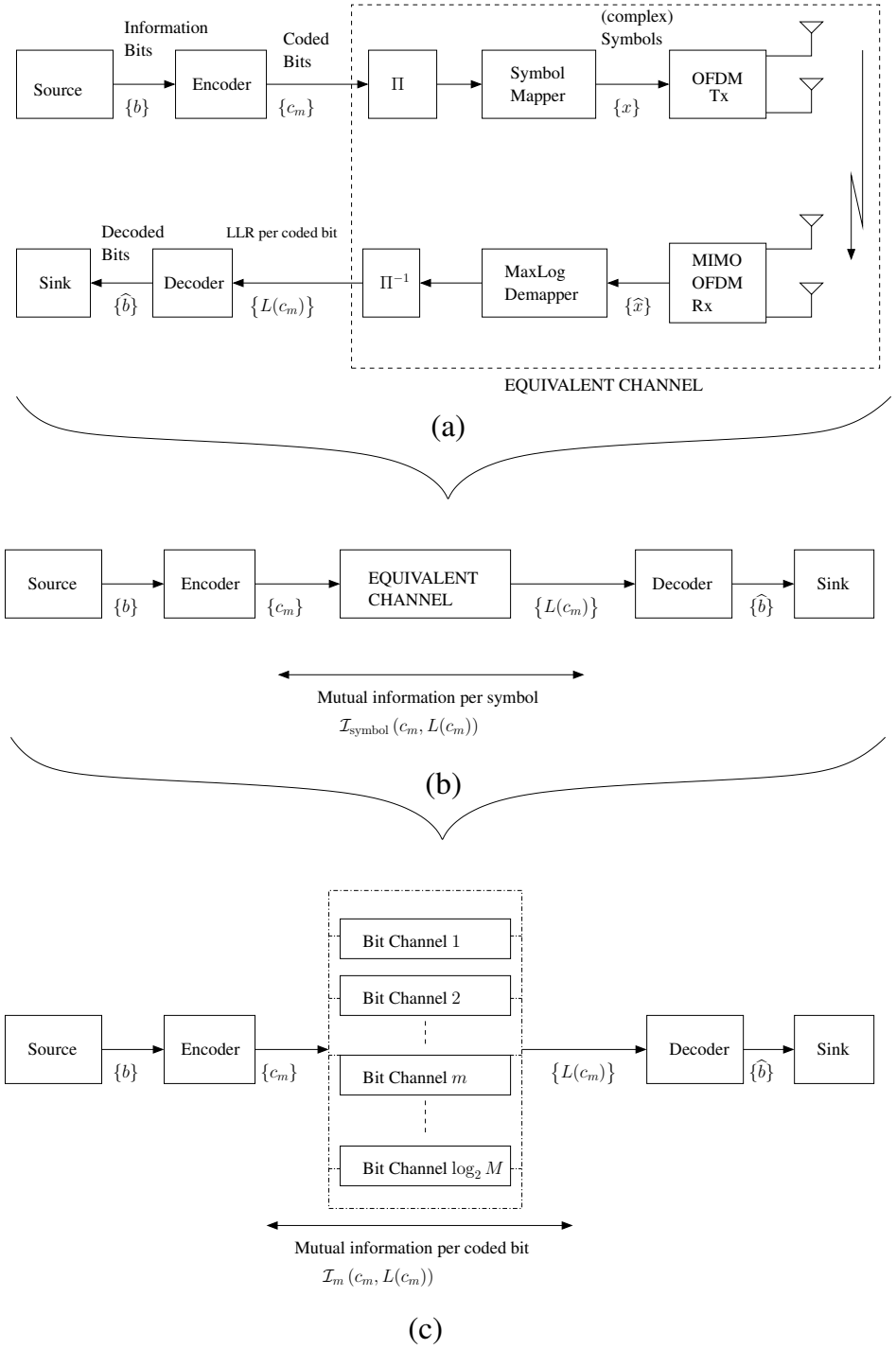

Figure 5.13: *A block diagram of MIMO-OFDM system which represents the concept of MIBM with an equivalent parallel bit channel model for one symbol having $log_2 M$ bits.*

different statistical property. The bits in a symbol are assumed to be equiprobable. So, the mean mutual information per coded bit or symbol can be written as

$$\mathcal{I}^{\text{symbol}} = \left(\frac{1}{\log_2 M}\right) \sum_{m=1}^{\log_2 M} \mathcal{I}_m \left(c_m, L(c_m)\right) \tag{5.50}$$

where, $L(c_m)$ is given in Equation (3.39) and M is the order of M-ary signal constellation. Furthermore, MI per coded bit is given as [Brink, 2001] [Sayana et al., 2007]

$$\mathcal{I}_m\left(c_m, L(c_m)\right) = \frac{1}{2}\sum_{c_m=\{0,1\}}\int_{-\infty}^{+\infty} p_{\mathrm{LLR}}(z|c_m) \cdot \log_2\left(\frac{2\,p_{\mathrm{LLR}}(z|c_m)}{p_{\mathrm{LLR}}(z|c_m=0)+p_{\mathrm{LLR}}(z|c_m=1)}\right)dz\,, \tag{5.51}$$

where z is a LLR integration variable and $p_{\mathrm{LLR}}(z|c_m)$ is the conditional PDF of LLR which will be discussed later in this Section.

The LLR of each coded bit is given in Equation (3.42) which is reconsidered here for convenience,

$$L\left(c_m\right) = \log\left(\frac{\sum\limits_{s\in\mathcal{S}_1^m}\exp\left(-\frac{|\widehat{x}-s|^2}{\widetilde{N}_0}\right)}{\sum\limits_{s\in\mathcal{S}_0^m}\exp\left(-\frac{|\widehat{x}-s|^2}{\widetilde{N}_0}\right)}\right)\,,$$

where $\widehat{x}$ is the MMSE output which is considered equivalent to Gaussian channel (cf. Section 3.5), so $\widetilde{N}_0 = 1/\mathit{SINR}$ is the post processing noise variance.

Since Gray mapping is employed, then the real and imaginary part can be decoded independently. Now, if the symbol x was modulated by BPSK $(\log_2 M = 1)$, i.e., bit $c_1 = 1$ was transmitted as $x = +1$ and bit $c_1 = 0$ was transmitted as $x = -1$, then using Equation (3.42),

$$L_{\mathrm{BPSK}}\left(c_1\right) = \log\left(\frac{\exp\left(-\frac{\left|\mathrm{Re}\{\widehat{x}\}-(+1)\right|^2}{2\left(\widetilde{N}_0/2\right)}\right)}{\exp\left(-\frac{\left|\mathrm{Re}\{\widehat{x}\}-(-1)\right|^2}{2\left(\widetilde{N}_0/2\right)}\right)}\right) \tag{5.52}$$

$$= \frac{2}{\left(\widetilde{N}_0/2\right)}\,\mathrm{Re}\{\widehat{x}\}\,. \tag{5.53}$$

Similarly, the L_{QPSK} can be given as [Seethaler et al., 2004]

$$L_{\mathrm{QPSK}}\left(c_m\right) = \begin{cases} \dfrac{2\sqrt{2}}{\left(\widetilde{N}_0/2\right)}\,\mathrm{Re}\{\widehat{x}\} & m=1\,, \\ \dfrac{2\sqrt{2}}{\left(\widetilde{N}_0/2\right)}\,\mathrm{Im}\{\widehat{x}\} & m=2\,. \end{cases} \tag{5.54}$$

The LLR per (coded) bit is Gaussian distributed such that the mean of the PDF of LLR μ_{LLR} is half of the variance of the PDF of LLR σ^2_{LLR} [Brink, 2001], i.e.,

$$\mu_{\mathrm{LLR}} = \frac{\sigma^2_{\mathrm{LLR}}}{2} \; . \tag{5.55}$$

The conditional PDF of LLR is given as [Brink, 2001]

$$p_{\mathrm{LLR}}(z|c_m) = \frac{1}{\sqrt{2\pi\sigma^2_{\mathrm{LLR}}}} \exp\left(- \frac{|z - \mu_{\mathrm{LLR}} c_m|^2}{2\sigma^2_{\mathrm{LLR}}} \right) \; . \tag{5.56}$$

For instance, in case of BPSK the mean is $\mu_{\mathrm{LLR}} = 2 \Big/ \left(\widetilde{N}_0/2 \right)$ (conditioned on $x = \pm 1$) and $\sigma^2_{\mathrm{LLR}} = 4 \Big/ \left(\widetilde{N}_0/2 \right)$ which fulfills the above condition given in Equation (5.55). So, using Equation (5.51), the MI per coded bit for BPSK can be simplified as [Brink, 2001]

$$\mathcal{I}_1 \left(c_1, L(c_1) \right) = 1 - \int_{-\infty}^{+\infty} \frac{1}{\sqrt{2\pi\sigma^2_{\mathrm{LLR}}}} \exp\left(- \frac{|z - \sigma^2_{\mathrm{LLR}}/2|^2}{2\sigma^2_{\mathrm{LLR}}} \right) \cdot \log_2 \left(1 + \exp(-z) \right) \, dz \tag{5.57}$$

$$= \mathcal{I}^{\mathrm{symbol}} \left(\mathrm{BPSK} \right) \triangleq J \left(\sigma_{\mathrm{LLR}} \right) = J \left(4 \Big/ \left(\widetilde{N}_0/2 \right) \right) = J \left(\sqrt{8 \, \mathit{SINR}} \right) \; , \tag{5.58}$$

where $\widetilde{N}_0 = 1/\mathit{SINR}$ and the approximation of function $J(\cdot)$ is given by [Ericsson, 2003A]

$$J(x) \approx \begin{cases} a_1 x^3 + b_1 x^2 + c_1 x, & \text{for } 0 < x < 1.6363 \\ 1 - \exp a_2 x^3 + b_2 x^2 + c_2 x + d_2, & \text{for } 1.6363 <= x < \infty \; , \end{cases} \tag{5.59}$$

and the coefficients of the $J(\cdot)$ function are given as

$a_1 = -0.0421061$ $b_1 = 0.209252$ $c_1 = -0.00640081$

$a_2 = 0.00181491$ $b_2 = -0.142675$ $c_2 = -0.0822054$ $d_2 = 0.0549608$.

Similarly, for QPSK the MI per coded bit is given as [Sayana et al., 2007]

$$\mathcal{I}_m \left(c_m, L(c_m) \right) = J \left(\sqrt{4 \, \mathit{SINR}} \right) \quad \forall \, m = 1, 2 \; . \tag{5.60}$$

So, using Equation (5.50), the mean MI per coded bit or symbol for QPSK is

$$\mathcal{I}^{\mathrm{symbol}} \left(\mathrm{QPSK} \right) = J \left(\sqrt{4 \, \mathit{SINR}} \right) \; . \tag{5.61}$$

For higher modulations 16QAM and 64QAM, the MI per coded bit $\mathcal{I}_m \left(c_m, L(c_m) \right)$ do not have closed form solutions. However, the mean MI per coded bit or symbol for

Table 5.3: *General formula: Mutual Information per symbol for BPSK, QPSK,* 16*QAM and* 64*QAM.*

Modulation	$\mathcal{I}_j^{\text{symbol}}[k]$
BPSK	$= J\left(\sqrt{8\,\mathit{SINR}_j[k]}\right)$
QPSK	$= J\left(\sqrt{4\,\mathit{SINR}_j[k]}\right)$
16QAM	$\approx \frac{1}{2}J\left(a_3\sqrt{\mathit{SINR}_j[k]}\right) + \frac{1}{4}J\left(b_3\sqrt{\mathit{SINR}_j[k]}\right) + \frac{1}{4}J\left(c_3\sqrt{\mathit{SINR}_j[k]}\right)$
64QAM	$\approx \frac{1}{3}J\left(a_4\sqrt{\mathit{SINR}_j[k]}\right) + \frac{1}{3}J\left(b_4\sqrt{\mathit{SINR}_j[k]}\right) + \frac{1}{3}J\left(c_4\sqrt{\mathit{SINR}_j[k]}\right)$
$\forall\ j = 1, 2, \cdots, N_{ss};\ k = 1, 2, \cdots, N_{\text{sd}}$ where, N_{ss} is the number of spatial streams, N_{sd} is the number of data subcarriers, $\mathit{SINR}_j[k]$ is given in Equation (3.32), $\{a_3,\ b_3,\ c_3\}$ and $\{a_4,\ b_4,\ c_4\}$ are provided in Equation (5.62).	

16QAM and 64QAM are found in [Sayana et al., 2007] which are given in Table 5.3 along with the results for BPSK and QPSK.

The coefficients given in [Sayana et al., 2007] for 16QAM and 64QAM did not match well with the performance of MI versus SNR in our simulator. The reason for disparity in coefficients is that they have done numerical integration to obtain approximate MI for a LogAPP demapper whereas we have obtained the MI directly using the absolute values of the LLRs for a MaxLog demapper. The numerical integrations to obtain MI are very cumbersome and sometimes not very accurate [Land et al., 2004]. The description to obtain MI for MaxLog demapper from the absolute values of LLRs will be discussed later in this Section. A non-linear least squares fit is conducted to obtain the following coefficients which match better with the MI for the MaxLog demapper,

$$\begin{aligned} a_3 &= 0.8818 \quad b_3 = 1.6764 \quad c_3 = 0.9316 \\ a_4 &= 1.1233 \quad b_4 = 0.4381 \quad c_4 = 0.4765 \quad . \end{aligned} \tag{5.62}$$

The MI for one symbol, i.e., $\mathcal{I}^{\text{symbol}}$, has been shown up to now. In general, the mean of MI per symbol of all the data subcarriers and spatial streams can be given as,

$$\mathcal{I}_{\text{mean}}^{\text{symbol}} = \frac{1}{N_{\text{ss}} N_{\text{sd}}} \sum_{j=1}^{N_{\text{ss}}} \sum_{k=1}^{N_{\text{sd}}} \mathcal{I}_j^{\text{symbol}}[k]\left(\mathit{SINR}_j[k]\right)\ , \tag{5.63}$$

where $\mathcal{I}_j^{\text{symbol}}[k]$ is given in Table 5.3 for the given modulation. It is worth to mention that the calculation of $\mathcal{I}_{\text{mean}}^{\text{symbol}}$ is independent of coding rate.

We have described how to find $\mathcal{I}_j^{\text{symbol}}[k]$ by the Equations provided in Table 5.3 which depend on the post processing SINR. The accurate MI per symbol $\mathcal{I}_j^{\text{symbol}}[k]$ can be computed online using the absolute values of the LLRs, if a LogAPP demapper is employed [Land et al., 2004]. In practical systems, MaxLog demapper is generally employed rather than LogAPP demapper because of its low complexity as discussed in Section 3.5. For BPSK and QPSK, the LLRs of LogAPP and MaxLog demapper are exactly same; however, for 16QAM and 64QAM the LLR of MaxLog demapper is same as LogAPP demapper for high SNR regime which is shown in Figure 5.14. The loss in MI for 64QAM compared to 16QAM is bit higher for low SNR regime.

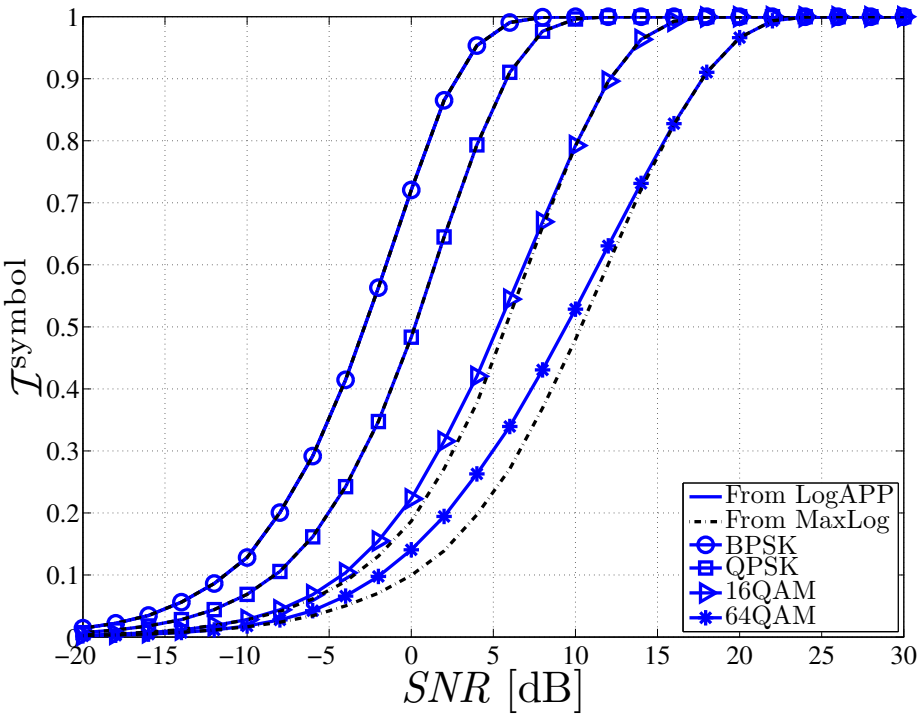

Figure 5.14: *Comparison of MI obtained from MaxLog and LogAPP demapper for BPSK, QPSK, 16QAM and 64QAM. MI obtained from both of them are same for high SNR regime, however for low SNR regime there is some loss.*

However, the direct computation of MI is still considered because of its simplicity even though there is some loss for the low SNR regime which is given as

$$\begin{aligned}\mathcal{I}_j^{\text{symbol}}[k] &= \mathbb{E}\left\{ f_{\mathcal{I}}\left(\left| \boldsymbol{L}_j[k](c_m) \right| \right) \right\} \\ &= \left(\frac{1}{\log_2 M} \right) \sum_{m=1}^{\log_2 M} f_{\mathcal{I}}\left(\left| \boldsymbol{L}_j[k](c_m) \right| \right), \end{aligned} \tag{5.64}$$

where $\boldsymbol{L}_j[k](c_m)$ is a vector of LLRs of mth coded bit of all the OFDM symbols for the kth subcarrier and jth spatial stream. The function $f_{\mathcal{I}}(\cdot)$ is given by [Land et al., 2004],

$$f_{\mathcal{I}}(x) = \left(\frac{1}{1+\exp(+x)}\right)\log_2\left(\frac{2}{1+\exp(+x)}\right) + \\ + \left(\frac{1}{1+\exp(-x)}\right)\log_2\left(\frac{2}{1+\exp(-x)}\right), \tag{5.65}$$

for $x \geq 0$.

Similar to Equation (5.63), in general, the mean MI of all the coded bits in all the OFDM symbols, the data subcarriers and spatial streams is given by

$$\mathcal{I}_{\text{mean}}^{\text{symbol}} = \left(\frac{1}{N_{\text{sd}}N_{\text{ss}}N_{\text{symb}}\log_2 M}\right)\sum_{j=1}^{N_{\text{ss}}}\sum_{k=1}^{N_{\text{sd}}}\sum_{m=1}^{\log_2 M}\sum_{n=1}^{N_{\text{symb}}} f_{\mathcal{I}}\left(\left|L_j^n[k](c_m)\right|\right), \tag{5.66}$$

where N_{sd} is the number of data subcarriers, N_{ss} is the number of spatial streams, N_{symb} is the number of OFDM symbols, $\log_2 M$ is the number of bits in the M-ary modulated symbol, the function $f_{\mathcal{I}}(\cdot)$ is given in Equation (5.65) and $L_j^n[k](c_m)$ is the LLR of the mth coded bit for the nth OFDM symbol, kth subcarrier and jth spatial stream

Equation (5.66) can be intimidating but it shows the concept. However, this Equation to represent the mean of all the softbits can be shown in a simple form for the implementation purpose as

$$\mathcal{I}_{\text{mean}}^{\text{symbol}} = \left(\frac{1}{PL_{\text{coded}}}\right)\sum_{p=1}^{PL_{\text{coded}}} f_{\mathcal{I}}\left(\left|L_p\right|\right), \tag{5.67}$$

where PL_{coded} is the number of bits in a coded packet having length PL and L_p is the LLR of the pth coded bit in the packet.

Up to now, we have only discussed mutual information as a general concept. Now, we will consider mutual information as a link quality metric (LQM). At this point, the three LQMs based on MI given below will be discussed in the following sections.

- Mean mutual information per coded bit mapping (MMIBM)
- Mutual information effective SNR mapping (MIESM)
- Mean mutual information reliability mapping (MMIRM)

5.4.1 Mean Mutual Information per Coded Bit Mapping (MMIBM)

Mean Mutual Information per coded Bit Mapping is an LQM based on the post processing SINRs. In this method, PER can be estimated directly from the mean MI domain using a look-up function. Figure 5.15 shows the relation between the mean MI per coded bit and PER for the basic MCS set in an AWGN channel. A suitable MCS search is conducted using the following steps which are similar to the RawBER method.

Implementation Recipe for the MMIBM

1 Obtain the channel matrix per subcarrier ($\mathbf{H}[k]$) and the noise variance (N_0).

2 The post-processing $SINR_j[k]$ is calculated using Equation (3.32) for all the data subcarriers and spatial streams.

3 The mean MI per coded bit $\mathcal{I}_{\text{mean}}^{\text{symbol}}$ is computed using Equation (5.63) for the current modulation in the MCS search. The MI per symbol $\mathcal{I}_j^{\text{symbol}}[k]$ is provided in Table 5.3 for the considered modulation.

4 The computed $\mathcal{I}_{\text{mean}}^{\text{symbol}}$ is mapped to a corresponding reference PER, i.e., PER_{ref}, for the current modulation and coding scheme (MCS) in the MCS search loop using a look-up function (regression) shown in Figure 5.15.

5 The estimated *PER* is corrected for the current packet having length *PL* using Equation (5.23).

6 MCS search (cf. Section 5.2.5) is performed by repeating steps **3** to **5** until the current MCS renders PER less than or equal to the threshold of the target PER, e.g., 1%.

5.4.2 Mutual Information Effective SNR Mapping (MIESM)

Similar to EESM, an effective SNR (SNR_{eff}) can also be calculated from the mean of MI per symbol of all the data subcarriers and spatial streams. The effective SNR (SNR_{eff}) based on MI can be a link quality metric (LQM) to estimate *PER* of the current channel state. It can be seen in Table 5.3, that the MI for 16QAM and 64QAM are

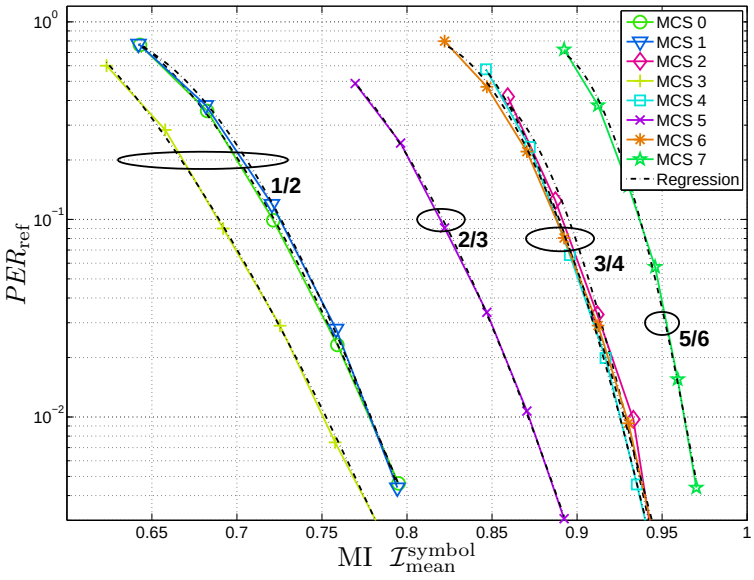

Figure 5.15: *Performance curves of* PER_{ref} *versus MI* $\left(\mathcal{I}_{\text{mean}}^{\text{symbol}}\right)$ *in an AWGN channel for the basic MCS set, i.e., MCS* 0 *to* 7*. Different modulations with same code rate are grouped together, e.g., MCS* 2*,* 4 *and* 6 *which have the code rate* $3/4$*. MaxLog soft demapper, full trace back Viterbi decoder, information packet length PL* $=$ 1024 *Bytes and* 20 *MHz interleaver are used for the simulations. The regressions are second order log-linear which are used for mapping from* $\mathcal{I}_{\text{mean}}^{\text{symbol}}$ *to* PER_{ref}*.*

given by the sum of $J(\cdot)$ functions. In MIESM, a single $J(\cdot)$ is used for all the modulations and coding schemes (MCS) with a correction factor γ which can numerically be optimized for each MCS similar to β for EESM (cf. Equations 4.6). The effective SNR (SNR_{eff}) utilizes the $J^{-1}(\cdot)$ function which is found in [Ericsson, 2003A]. The effective SNR (SNR_{eff}) based on MI for a given MCS is [Ericsson, 2003A],

$$SNR_{\text{eff}} = \gamma \left[J^{-1}\left(\frac{1}{N_{\text{ss}} N_{\text{sd}}} \sum_{j=1}^{N_{\text{ss}}} \sum_{k=1}^{N_{\text{sd}}} J\left(\sqrt{\frac{SINR_j[k]}{\gamma}} \right) \right) \right]^2 , \tag{5.68}$$

where γ depends on MCS, $SINR_j[k]$ is given in Equation (3.32), N_{ss} is the number of spatial streams, N_{sd} is the number of data subcarriers, $J(\cdot)$ is given in Equation (5.59) and $J^{-1}(y)$ is given by

$$J^{-1}(y) \approx \begin{cases} a_5 y^2 + b_5 y + c_5 \sqrt{y}, & \text{for } 0 < y < 0.3646 \\ a_6 log\left(b_6 (y-1)\right) + c_6 y, & \text{for } 0.3646 \leq y \leq 1\,. \end{cases} \tag{5.69}$$

The coefficients of $J^{-1}(y)$ are given as,

$$\begin{aligned} a_5 &= 1.09542 \quad & b_5 &= 0.214217 \quad & c_5 &= 2.33727 \\ a_6 &= -0.706692 \quad & b_6 &= -0.386013 \quad & c_6 &= 1.75017\,. \end{aligned}$$

Implementation Recipe for the MIESM

It is assumed that suitable γ values for each MCS are available before PER estimation. A look-up function is required too having performance data of PER versus SNR in an AWGN channel for all the basic MCS set (cf. Figure 5.12). However, the look-up function for the MIESM is same as the EESM because both of them computes effective SNR.

1 Obtain the channel matrix per subcarrier ($\mathbf{H}[k]$) and the noise variance (N_0).

2 The post-processing $SINR_j[k]$ is calculated using Equation (3.32) for all the data subcarriers and spatial streams.

3 Calculate the effective SNR (SNR_{eff}) using Equation (C.6) for the current MCS in the MCS search loop.

4 Map the effective SNR to a corresponding reference PER, i.e., PER_{ref}, using look-up function (regression) shown in Figure 5.12.

5 The estimated *PER* is corrected for the current packet having length *PL* using Equation (5.23).

6 MCS search (cf. Section 5.2.5) can be performed by repeating steps **3** to **5** until the current MCS renders PER less than or equal to the threshold of the target PER, e.g., 1%.

5.4.3 Mean Mutual Information Reliability Mapping (MMIRM)

The LQMs RawBER, EESM, MMIBM and MIESM depend on the post processing SINRs, however MMIRM depends only on the soft bits generated by the demapper.

The MCS search of MMIRM is bit different than the other methods. A packet which is modulated and coded with a particular MCS value is used for sounding the channel such that FLA can recommend the transmitter a suitable MCS. Well, MMIRM computes the link quality metric, i.e., the mean MI per coded bit, using Equation (5.67) for the received packet. Thereafter, the corresponding PER_{ref} is estimated from the computed mean MI per coded bit using the look-up function of MMIBM for the received MCS of the packet. However, it is necessary to obtain the estimated PERs of other MCSs depending on the search method to find a suitable MCS which will render

PER below the threshold of the target PER. Since MI is dependent on the modulation but independent of the code rate, then the PER of the considered modulation but different code rates can directly be obtained using the look-up function of MMIBM. For an example, if MCS 4 is used in the received packet then it will still be easy to obtain an estimated PER for MCS 3, because both are 16QAM. However, it is not straightforward to calculate mean MI of other modulations because only the softbits for the used modulation are known. Now, what shall the MCS search do? Furthermore, the softbits can not be generated for other modulations at the receiver side unless the receiver simulates the packet transmission for other modulations which is infeasible in practice. Therefore, the easiest way to estimate the mean MI of other modulation is by assuming that the effective SNR of the current channel realization is independent of modulation and coding. This means that there is a unique SNR, which describes the PER for all the MCS. This is true for the AWGN channel where the PER is completely determined by the SNR for a given system. However, the assumption of a unique effective SNR independent of modulation and coding does not always hold true for a fading channel. An extreme counter example for this assumption is provided in Figure 5.10. Here we show that for a particular fading channel realization, MCS 3 has a lower PER than MCS 2 for fixed SNR. But we can not find a unique SNR which describes this property in the AWGN. We need at least two SNRs. However, we will still suggest the following method to obtain the MI for other modulations such that the PER for other modulations can be estimated when conducting the MCS search.

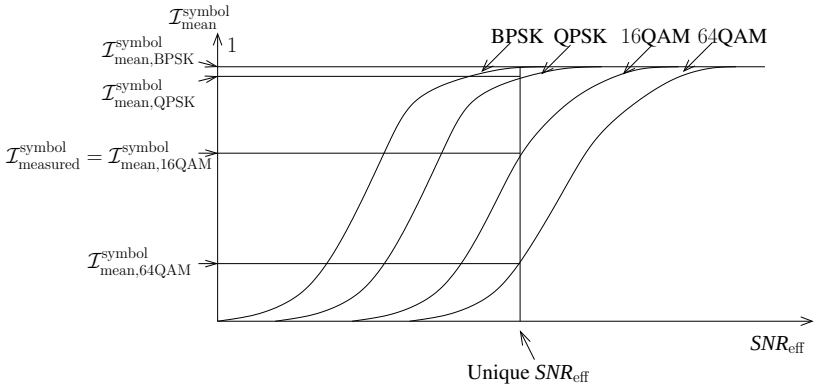

Figure 5.16: *Description of how to obtain the MI for other modulation schemes when* 16*QAM was used for generating the softbits.*

Consider Figure 5.16 when the channel was sounded using MCS 4, i.e., 16QAM. The mean MI $\mathcal{I}^{\text{symbol}}_{\text{measured}}$ is computed using Equation (5.67) for the received packet. We then assume that the SNR_{eff} is same for that particular channel independent of modulation and coding. An effective SNR is found using inverse mapping of MI versus

SNR_{eff}. After the computation of SNR_{eff}, the mean MI is found for the other modulations required to perform MCS search as shown in Figure 5.16. In this way we can perform a search among the available MCS.

Another issue of this method is how to estimate the mean MI when we are observing a two spatial stream signal but need to estimate the corresponding mean MI for a single stream. If one stream is mapped to two antennas (cf. Figure 5.3) all the symbols are copied to both transmit antennas and the energy is divided equally. Two (ideally) independent observations of the same symbol is then observed. We suggest to use the following approach, which is obtained heuristically

$$\mathcal{I}_{mean}^{symbol} = (1 - \mathcal{I}_{mean,1}^{symbol})\mathcal{I}_{mean,2}^{symbol} + \mathcal{I}_{mean,1}^{symbol} \tag{5.70}$$

where $\mathcal{I}_{mean,j}^{symbol}$ denotes the mean MI per coded bit of the jth spatial stream.

Implementation Recipe for the MMIRM

1 Calculate the mean MI, $\mathcal{I}_{\text{mean}}^{\text{symbol}}$ using Equation (5.66).

2 Use the method presented in Figure 5.16 to obtain the expected MI for the modulation under consideration in the MCS search loop.

3 Map the mean MI to a reference PER, PER_{ref} using the look-up function (regression) in Figure 5.15.

4 The estimated *PER* is corrected for the current packet having length *PL* using Equation (5.23).

5 MCS search (cf. Section 5.2.5) can be performed by repeating steps **2** to **4** until the current MCS renders PER less than or equal to the threshold of the target PER, e.g., 1%.

5.4.4 Summary

Three mutual information based LQMs are presented which are known as the MMIBM, MIESM and MMIRM (it is named in our work). The MMIBM and MIESM algorithms depend on the post processing SINR whereas the MMIRM depends on the reliability of the soft bits.

In MMIBM, the LQM is the mean MI per coded bit which is directly used to estimate the corresponding PER in an AWGN channel for a given MCS and packet length.

In MIESM, the effective SNR is computed from the mean MI per coded bit to estimate corresponding PER which has a correction factor γ like EESM too. Similar to the EESM method, a suitable γ value has numerically to be found for each MCS.

In MMIRM, the LQM is also the mean MI per coded bit similar to MMIBM, however this LQM does not depend on the post-processing SINR. It depends on the absolute values of the LLRs or soft bits which are available after the LogMax demapper. The MCS search of MMIRM is conducted in a different way by assuming that the effective SNR of the channel is independent of the MCS which is explained in Section 5.4.3.

The numerical results of these three LQMs with the RawBER and the EESM are presented in the following Chapter 6.

6 Numerical Results

In this chapter, the performance of the FLA algorithm for the five investigated LQMs (RawBER, EESM, MMIBM, MIESM and MMIRM) are presented and assessed by numerical results. Firstly, the accuracy of the packet error rate estimation is discussed in Section 6.1. Optimal performance curves are presented in Section 6.2. Then throughput and PER for the different methods are evaluated in Section 6.3 under ideal assumptions and the different search methods are evaluated in Section 6.4. In Section 6.5 we address the performance with practical channel estimation and other impairment. In Section 6.6, the TP performance of the FLA algorithms are evaluated with respect to feedback delay.

6.1 PER Estimation Accuracy

As discussed earlier, an FLA algorithm mainly comprises an LQM which estimates the PER and a MCS search mechanism. It is therefore very interesting to know the accuracy of the PER estimation and the distribution of the estimation error. The estimation error is evaluated by measuring the actual PER and comparing it with the estimated PER. Each of the measured PERs is obtained by averaging over the different noise realizations for a fixed MCS, channel realization and nominal SNR.

Figure 6.1 shows the estimated PERs versus measured PERs in an AWGN channel for MCS 0. From this Figure, it can be comprehended that the mapping functions of all the considered LQMs are quite accurate with very low MSEs. The mean squared error is calculated as

$$MSE = \frac{1}{N_{\text{measured}}} \sum_{i=1}^{N_{\text{measured}}} \left| \log_{10}(PER^{i}_{\text{measured}}) - \log_{10}(PER^{i}_{\text{estimated}}) \right|^2 \qquad (6.1)$$

where N_{measured} is the number of measurements considered. Similar performance has been observed for all the basic MCSs, however they are not presented in this section for brevity. This also shows that all the LQMs yield perfect knowledge of the PER in

the AWGN channel. In the AWGN channel, if the MCS and one of these measures: RawBER, SNR, MI and PER are known, it is possible to obtain the values of the rest of the measures because they form a unique one to one mapping among themselves.

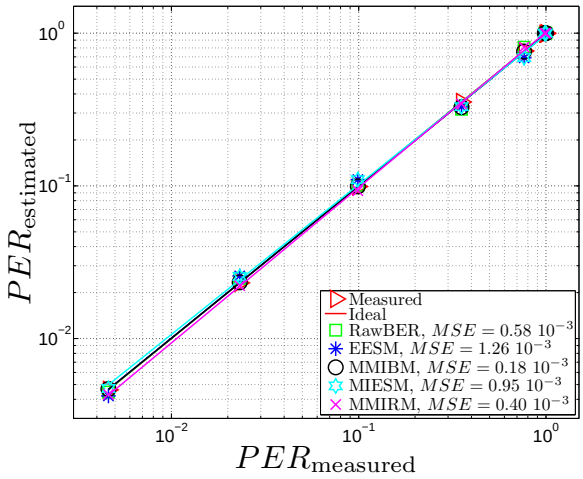

Figure 6.1: *Estimated PERs versus measured PERs in an AWGN channel for MCS 0.*

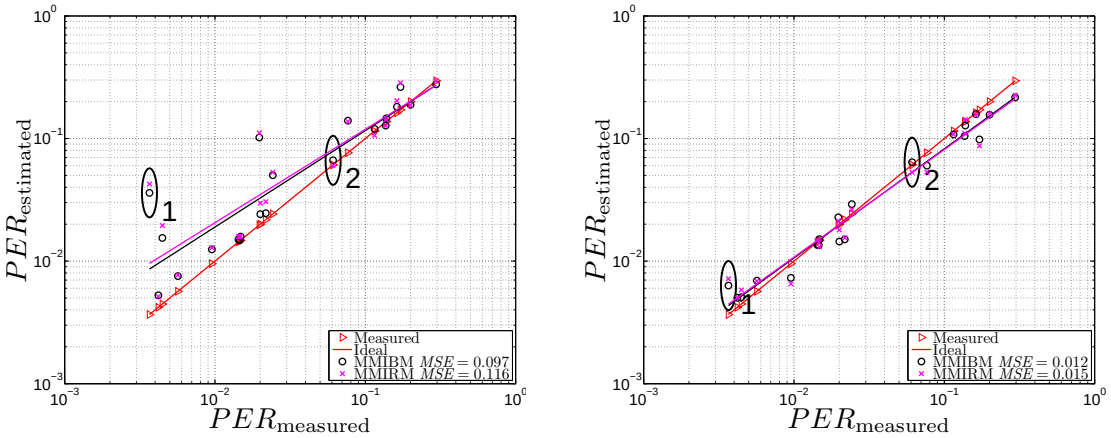

(a) **(b)**

Figure 6.2: *PER estimations (a) without correction factors and (b) with correction factors for the MMIBM and MMIRM with MCS 0, channel B and bandwidth* 20 MHz. *Perfect channel is available at the Rx.*

Figure 6.2(a) shows the PER estimation of MMIBM and MMIRM for MCS 0 under perfect channel knowledge, channel model B. In this Figure, two channel realizations are encircled and numbered as 1 and 2. The PER estimation error for channel realization number 1 is approximately 1 decade whereas PER estimation error for channel realization number 2 is very low. If we ponder over Figure 6.3, which shows the variation of post processing SINRs and corresponding MIs for each subcarrier, then it can

be observed that the variance of the SINRs and MIs are quite high for channel realization 1. It can also be seen in this figure that the maximum amplitude difference in SNR is around $\max\{SINR[k]\} - \min\{SINR[k]\} = +6 - (-11.5) = 17.5\,\mathrm{dB}$. On the other hand, when we consider over the same Figure 6.3 at the channel realization 2 then the variance of SINRs and MIs are quite low. Similar behaviours are observed for all the basic MCS set for the considered channel realizations. However, they are not presented here for succinct discussion. Therefore, to cope with this problem of high dynamics for the computation of LQMs, MMIBM and MMIRM, we propose a correction term for both of them inspired from [Bjerke et al., 2005].

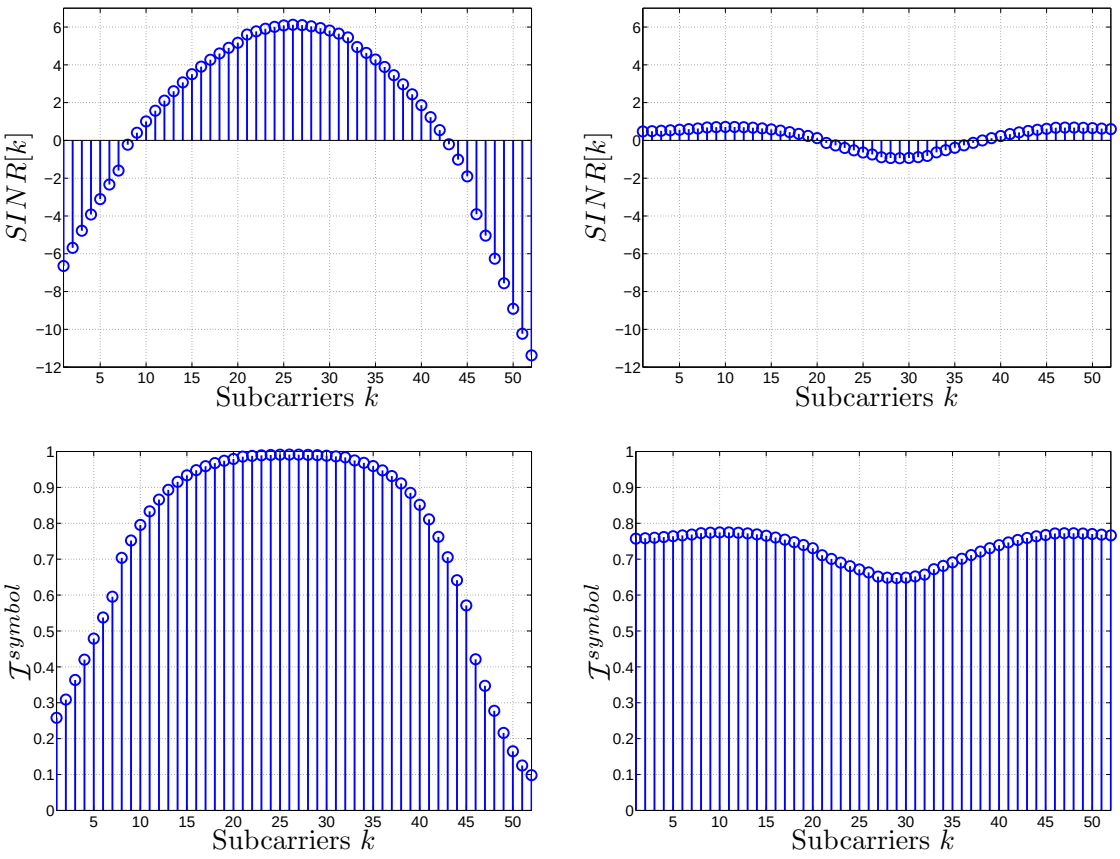

(Channel realization 1) **(Channel realization 2)**

Figure 6.3: *Variation of the post processing SINRs and the corresponding MIs over all the subcarriers for the given channel realizations. Channel model B,* 20 MHz.

The LQM of MMIBM including the λ corrector factor is given by

$$\mathcal{I}_{\text{eff}}^{\text{symbol}} = \underbrace{\frac{1}{N_{\text{ss}} N_{\text{sd}}} \sum_{j=1}^{N_{\text{ss}}} \sum_{k=1}^{N_{\text{sd}}} \mathcal{I}_j^{\text{symbol}}[k]\,(SINR_j[k])}_{=\text{ Equation (5.63)}} + \lambda \underbrace{\left[\frac{1}{N_{\text{ss}}} \sum_{j=1}^{N_{\text{ss}}} var_k \left\{\mathcal{I}_j^{\text{symbol}}[k]\right\}\right]}_{\text{correction term}}, \tag{6.2}$$

and the λ is a correction factor which has to be optimized for each MCS similar to β for the EESM. Similarly, the LQM of MMIRM including the κ correction factor is given by

$$\mathcal{I}_{\text{eff}}^{\text{symbol}} = \underbrace{\left(\frac{1}{PL_{\text{coded}}}\right) \sum_{p=1}^{PL_{\text{coded}}} f_{\mathcal{I}}\Big(\big|L_p\big|\Big)}_{=\text{ Equation (5.67)}} + \kappa \left[\frac{1}{N_{\text{ss}}} \sum_{j=1}^{N_{\text{ss}}} var_k \left\{\mathcal{I}_j^{\text{symbol}}[k]\right\}\right] , \quad (6.3)$$

where $\mathcal{I}_j^{\text{symbol}}[k]$ is given in Equation (5.64) but it is given again for brevity

$$\mathcal{I}_j^{\text{symbol}}[k] = \left(\frac{1}{\log_2 M}\right) \sum_{m=1}^{\log_2 M} f_{\mathcal{I}}\Big(\big|\boldsymbol{L}_j[k](c_m)\big|\Big) .$$

and κ has to be optimized for each MCS too. After the addition of a suitable correction term for MCS 0 in both the MMIBM and MMIRM, it can be seen in Figure 6.2(b) that the mean squared errors (MSEs) are lower for both of them than without the correction factor given in Figure 6.2(a). The reason for adding the variance term is not directly linked to the variance. If a relative small number of subcarriers are in deep fade and the other subcarriers are reliable, then the convolutional code can easily decode these errors. At least, the decoding performance using just the mean MI as an indicator is not enough. Other work in [Yan et al., 2007] [Jones et al., 2002] use MI as a PER indicator and have not included any kind of correction factor but they do not consider fading channels with high SINR dynamics as the IEEE channel models have. A max-min SINR dynamic as high as $32\,\text{dB}$ was observed for a single channel realization (channel B, $20\,\text{MHz}$). The issue of high dynamics in a channel is also addressed in [3GPP2, 2003].

Figure 6.4(a), (b), (c) and (d) show the PER estimations versus actual measured PERs for MCS $7, 2, 10$ and 11 with perfect estimation for channel model B, $20\,\text{MHz}$. In Figure 6.4 we can see that the estimation points are scattered around the measured points or the red coloured diagonal line representing ideal estimation. In Figure 6.4(a), all the regressions of the 5 LQMs are following the red coloured diagonal line. However, this is not the case for RawBER and MMIRM when considering Figure 6.4(b). From the MSEs provided in Figure 6.4, we can also see that EESM, MMIBM and MIESM have approximately equal estimation accuracy with MMIRM slightly less accurate. Moreover, the PER estimates of RawBER are not that accurate. We also observe higher estimation error in 2×2 system shown in Figure 6.4(c) and (d) than in 1×1 system shown in (a) and (b).

Figure 6.5 shows the distribution of the estimation errors when averaged over all the MCS 0 to 15. The evaluation of the estimation errors is performed on the same data set as for the training of the correction factors of all the LQMs.

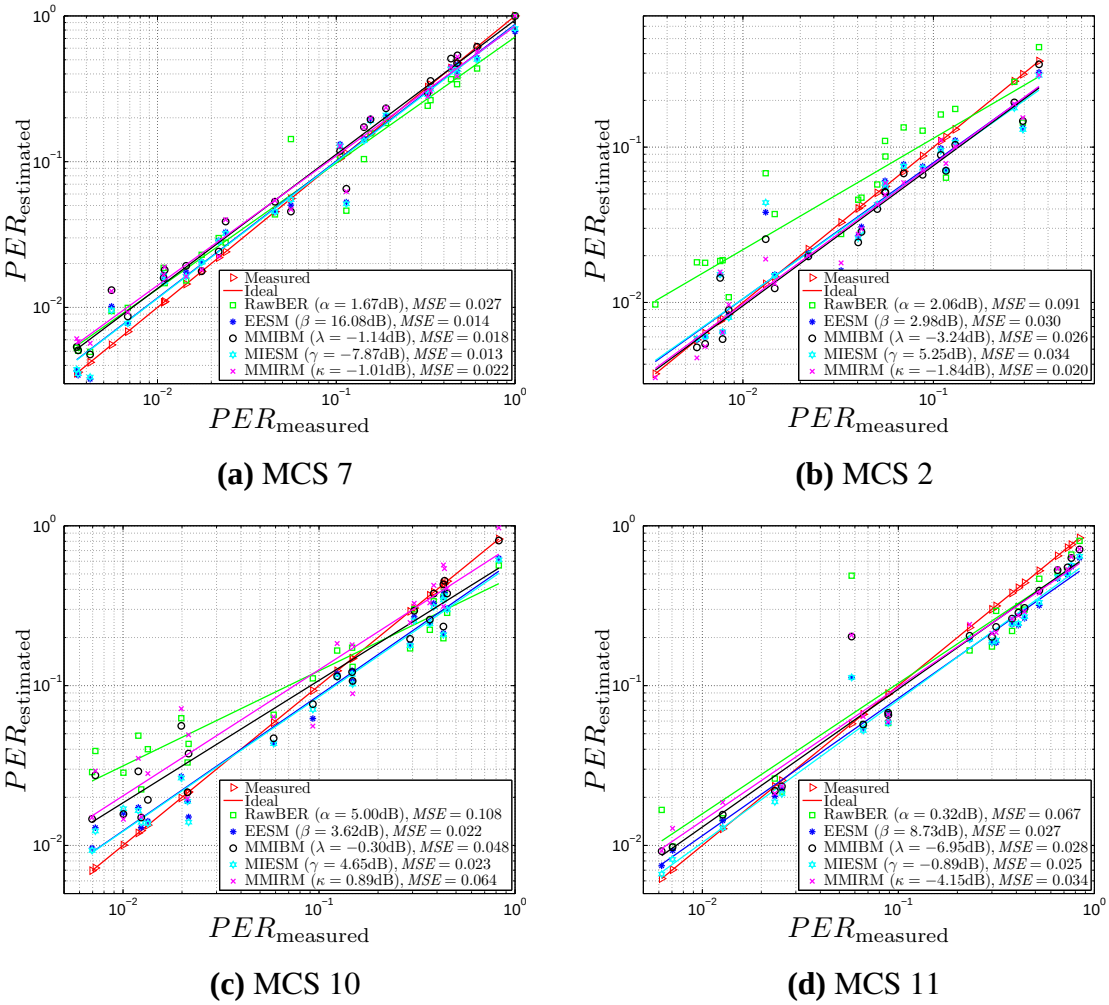

(a) MCS 7 **(b)** MCS 2

(c) MCS 10 **(d)** MCS 11

Figure 6.4: *PER estimations for the different LQMs for (a) MCS* 7*, (b) MCS* 2*, (c) MCS* 10*, (d) MCS* 11 *with perfect estimation and channel model B,* 20 MHz*. The red diagonal line represents ideal estimation. The other colored lines represent the regression of the respective LQM's PER estimation. At least 50 packet errors are considered for all the measured points.* $N_{\text{measured}} = 25\,(MCS\ 7), 23\,(MCS\ 2), 23\,(MCS\ 10), 20\,(MCS\ 11)$*. MSE evaluation is performed on the same data set as the optimization.*

It is already indicated in Figure 6.4 that the methods EESM, MMIBM, MIESM and MMIRM have almost the same estimation accuracy when observing the distribution of estimation errors in Figure 6.5. The methods RawBER and MMIRM have however a longer tail towards the left hand side, i.e., "Overshoot estimation". For MMIRM, an estimation error up to one and a half decade is observed. It is apprehended that the RawBER and EESM are almost the same methods in Section 5.3, however the PER estimation accuracy of the EESM is better than the RawBER. The reason can be that the optimization variable β is working better for EESM in PER versus SNR domain than the α for PER versus RawBER domain. The MMIBM and MMIRM both are

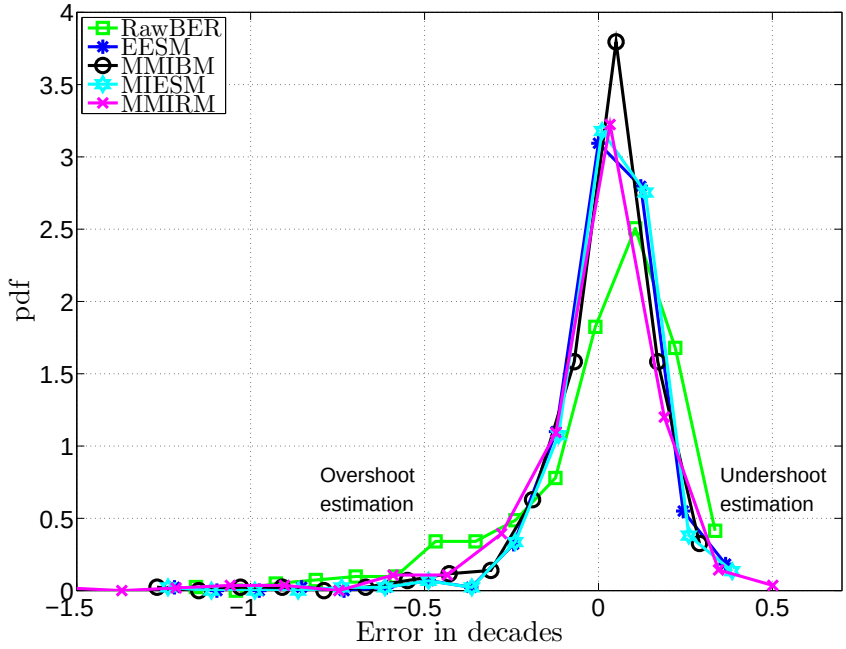

Figure 6.5: *Distribution of estimation error for measurements of MCS* 0 *to* 15*. Packet error distribution is evaluated on the same data set as the optimization of the correction factors.*

based on MI per coded bit, however the PER estimation accuracy of MMIBM is better than the MMIRM under perfect channel conditions. The reason behind this can be that MMIBM considers the average statistics while MMIRM depends on the limited statistics of a single packet received having length of $1024\,\mathrm{Bytes}$.

For perfect conditions, it can be concluded that the EESM, MMIBM and MIESM are superior to RawBER and MMIRM when it comes to PER estimation.

6.2 Throughput Bounds and Evaluation of Performance

In this section, different concepts will be explained for evaluating the performance of the fast link adaptation algorithms. First the fixed MCS and related concepts are discussed followed by the bounds for any FLA algorithm and the bound for the particular FLA algorithm of interest.

6.2.1 Fixed MCS, Envelope and PER Constraint Envelope

To describe the concepts of fixed MCS, envelope and PER constraint envelope, consider the example in the Figure 6.6.

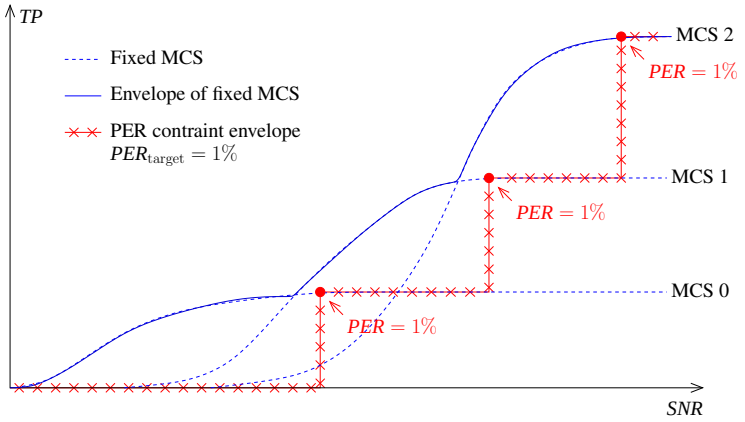

Figure 6.6: *A description of TP curves and their terminology.*

Fixed MCS is without the usage of link adaptation. The same MCS is always used regardless of measured PER and the current channel state. This curve is almost sigmoidal (S-shape) because of the following definition of TP. Header and media access timing is not included in this definition. Further, if just one bit in the packet is wrong, the entire packet is discarded [Bansal, 2007]. The service provided is a packet-based service. This effect is included in the definition of throughput *TP* in Equation (6.4) because only the bits in the successful packets are used to calculate the throughput,

$$TP = \frac{\text{Number of info bits in successful transmitted packets}}{\text{Time utilized for the packets}} \qquad [\text{bits/sec}] \tag{6.4}$$

or equivalent

$$TP(MCS, PER) = (1 - PER)TP_{\max}(MCS) \qquad [\text{bits/sec}]\,, \tag{6.5}$$

where $TP_{\max}(\text{MCS})$ denotes the maximum achievable TP given in Table B.1. When *PER* decreases, *TP* increases.

The fixed MCS envelope in Figure 6.6 is the upper envelope of all the fixed MCSs. The fixed MCS envelope will have a quite high PER.

The PER constraint envelope is the fixed MCS envelope with the constraint $PER \leq PER_{\text{target}}$. That is, the observed *PER* should be below a certain threshold. Slow link adaptation adapts to ensure a certain PER by shifting MCS slowly considering long term statistics. So, this will be equivalent to shift between the fixed MCS. For comparison, we will consider the throughput for the PER constraint envelope to be equal to the ideal throughput for slow link adaptation.

6.2.2 Algorithm Upper Bound

An idea from [Freudenthaler et al., 2007] is used to evaluate the performance of the FLA algorithms. We will refer to this method as the "Freudenthaler scheme". The flowchart of the idea is shown in Figure 6.7.

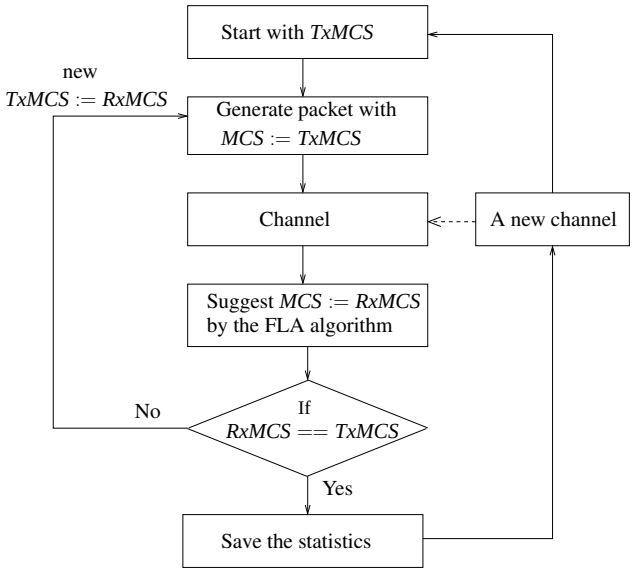

Figure 6.7: *Flowchart for the Freudenthaler scheme.*

An MCS is selected on the transmitter side, called *TxMCS*. A packet is formed with the particular MCS and sent across a channel. On the receiver side the FLA algorithm is executed which suggests an MCS value for the current channel, called *RxMCS*. If $TxMCS \neq RxMCS$, the MCS did not match with the channel condition according to the FLA algorithm and the transmitter should try to send a new packet with $TxMCS := RxMCS$. If $TxMCS = RxMCS$ then, according to the selection algorithm, the optimal MCS was selected for that particular channel. The statistics PER and TP for the particular transmission are saved for the evaluation. A new channel is selected and the algorithm starts from the top again.

If perfect channel estimation is employed then the algorithm will run 2 loops. This is because the channel matrix and noise variance are same under both loops and the selection algorithm will then select exactly the same MCS *RxMCS* in the second run. Under non-perfect channel estimation, the channel matrix is estimated and it will change with the particular noise realization. So, more than 2 runs can be expected. The benefits of the Freudenthaler scheme are:

- It ensures that for the considered statistics, the MCS used on the channel is equal to the MCS the FLA algorithm will select.

- The MCS is used with no delay.
- No MFB delay and errors on the side channel. The transmitter always receives the MCS suggestion from the receiver.

So, the performance under the Freudenthaler scheme is an upper bound for the algorithm under evaluation. The only degrading performance is the inaccuracy of the PER estimation. The inaccuracy can then be studied separately from other issues such as delay and side channel errors.

6.2.3 Performance Upper Bound

A performance upper bound is used such that it is possible to compare the performance under the Freudenthaler scheme with the performance that can be achievable. This gives an indication of how much more it should be possible to gain. The first idea was to include a theoretical bound [Goldsmith et al., 1997], but the practical performance was far from the theoretically bound and hence not useful for comparison. So, a practical upper bound is considered. One way to obtain a practical upper bound is to evaluate the PER for all MCS, SNR and channel realizations [Simoens et al., 2005]. The upper bound can then be constructed using the genie knowledge of the PER. This upper bound is then an upper bound for any link adaptation scheme which uses a PER estimation algorithm. A perfect PER estimation algorithm will reach this upper bound. This bound has a high computational burden because reliable (perfect) PER must be simulated for all MCSs, SNRs and channel realizations under consideration. Let N_{MCS}, N_{SNR}, N_{CR} be the number of MCSs, SNRs and channel realizations. Let N_{PT} be the number of packet transmissions to obtain a reliable PER for a particular MCS, SNR and channel realization. The method in [Simoens et al., 2005] has the complexity

$$\mathcal{O} = N_{\mathrm{MCS}} \times N_{\mathrm{SNR}} \times N_{\mathrm{CR}} \times N_{\mathrm{PT}} \,. \tag{6.6}$$

We propose an upper bound which can be obtained with lower complexity. In fact, it will have the complexity,

$$\mathcal{O} = N_{\mathrm{MCS}} \times N_{\mathrm{SNR}} \times N_{\mathrm{CR}} \,. \tag{6.7}$$

The reduced cost in complexity comes with the cost of a less tight bound. The upper bound proposed will be an upper bound of any link adaptation algorithm and not an upper bound for any link adaptation algorithm constraint that uses a PER estimation algorithm. Even with perfect PER estimation it will not be possible to reach the upper bound. However, the upper bound proposed will still prove to be useful. The upper bound is obtained with the algorithm depicted in Figure 6.8.

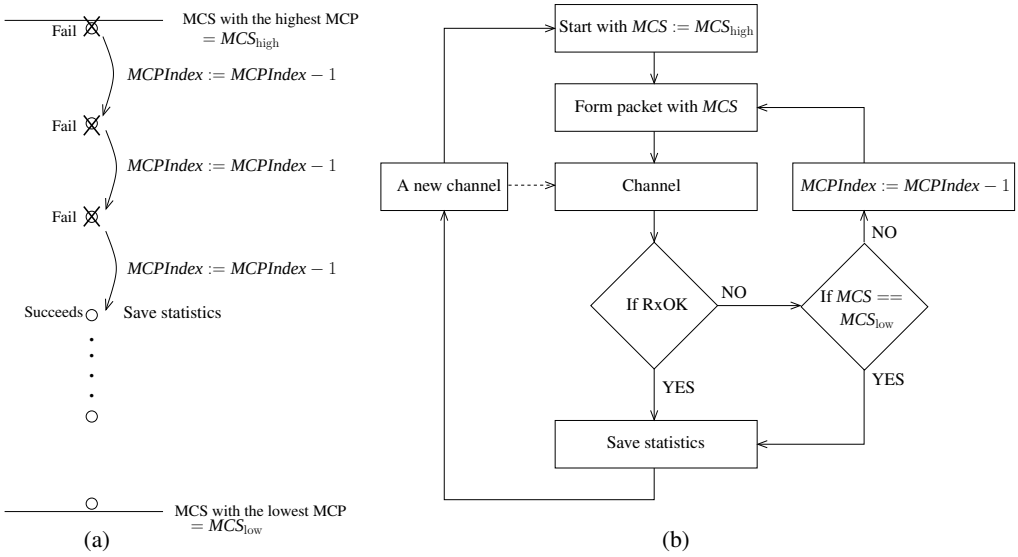

Figure 6.8: *(a) Description and (b) flowchart for the evaluation of the practical upper bound. See Tables 5.1 and 5.2 for the relation between MCPIndex and MCS.*

Start from the MCS value with the highest MCP as in Figure 6.8 (a), e.g., 64QAM with rate $5/6$. Form a packet with that MCS and send it across the channel. If the transmission fails, step one MCS down and try again. This loop continues with the same channel realization until the packet is received successfully. The statistics, such as PER and TP for the packet is saved. It may happen that the MCS bound MCS_{low} has reached, and then the transmission statistics is saved regardless the packet transmission failure. When the statistics is saved as shown in Figure 6.8 (b), a new channel realization is selected and the algorithm starts from the top again with MCS_{high}. The only time a packet error will occur in the statistics is when the lowest MCS fails. This means that the PER for the upper bound should be equal to the PER for the lowest fixed MCS. Besides fixing the channel realization, the noise realization is also fixed. However, the coded packet length changes when MCS changes, so the length of the noise vector does no longer fit and only the first part of the noise vector is used.

The upper bound algorithm always utilizes the MCS with the highest MCP which supports the particular channel and nominal SNR. Hence, this method will maximize the throughput. Furthermore, the method will minimize PER because it always select an MCS that does not fail. The exception is when MCS 0 with BPSK $R_{\mathrm{c}} = 1/2$ fails but this is the most robust transmission scheme available. To conclude, the method in Figure 6.8 maximizes the throughput and minimizes the PER and this method will therefore produce the upper bound of the performance for any link adaptation algorithm. To be accurate, the upper bound will be a upper bound of TP but a lower bound of PER.

One idea could also be to evaluate the packet by stepping up from MCS_{low}, opposite the scheme shown in Figure 6.8. This method has a flaw because it may happen, say that MCS 2 fails but MCS 3 could have succeeded. It is discussed in the Section 5.2.5 that for some channel realizations it is more important to have a high Hamming distance rather than a high Euclidean distance in the constellation [Prasad et al., 2000, p.68]. So, MCS 3 can have a lower PER than MCS 2 for some fading channel realizations. Hence, the method by evaluating from MCS_{low} and upwards is not optimal.

For simulation, all the settings in the upper bound and Freudenthaler scheme are fixed. The fixed settings such as the channel type, packet length and channel estimation are same to ensure correct comparison between the upper bound and the results of the Freudenthaler scheme.

The question is how tight the upper bound can be expected to be; How close can the performance under the Freudenthaler scheme approach the upper bound? Firstly, the performance is simulated using the same settings and the bound should then be quite tight. The difference is in the trials. Consider an example where MCS 6 will result in a PER of 90% for a particular channel and nominal SNR. The FLA algorithm should not select this MCS because it has statistically too high PER but the algorithm should go for a lower MCS. However, there is still 10% chance that it may succeed. Whether the packet will fail or succeed can only be discovered by a trial. This is exactly what the upper bound methods explore by performing trial transmission for each MCS and only record the statistics if the transmission is successful. One could say that the trials are free for the upper bound algorithm. The FLA algorithm is opposite in this sense, because it only considers the estimated statistical property and all trials have a price. It is possible to win in the lotto but statistically it may not be attractive enough to participate without free trials. If the method with the genie knowledge of the PER was used [Simoens et al., 2005], we would have avoided the problem with the trials and the bound would have been tighter. But again, it will have a much higher complexity.

6.3 Throughput and PER with Ideal Conditions

The TP and PER versus SNR are shown in this section for all the 5 LQM methods whose PER estimation errors were discussed in the Section 6.1. Figure 6.9(a) shows the TP of the fixed MCS, fixed MCS envelope, the PER constraint envelope, the upper bound and the TP using firstly RawBER as the LQM for FLA. The channel model B with $20\,\text{MHz}$ bandwidth has the lowest frequency diversity and no spatial diversity because the SISO case is considered. So, from Figure 6.9(b) it can be observed that even if MCS 0 is always send, a PER of 1% can first be achieved at $SNR = 22\,\text{dB}$.

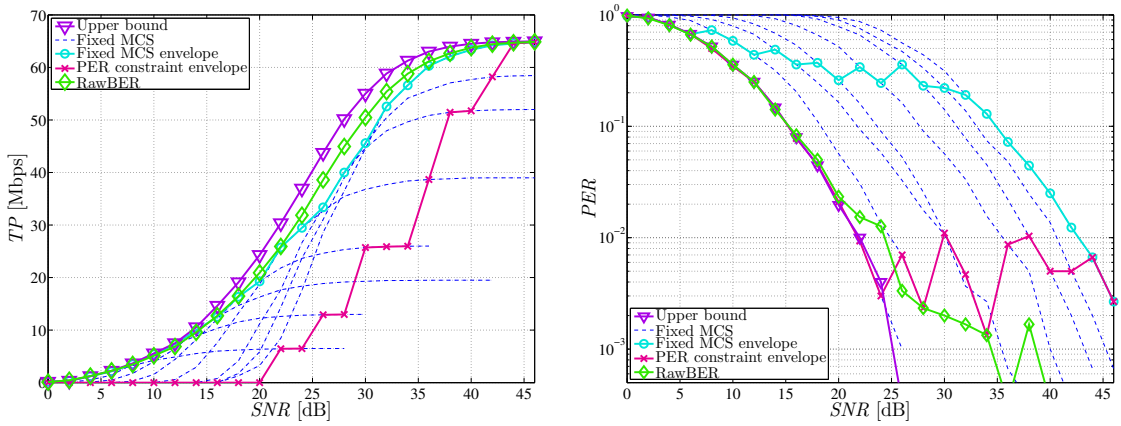

Figure 6.9: *Evaluation of the (a) TP and (b) PER with perfect channel knowledge at the Rx. Channel model B with bandwidth* $20\,\mathrm{MHz}$*,* $1{\times}1$*, target PER* 1%*. The RawBER method is evaluated using the Freudenthaler scheme and MCS search "Total Search".*

If Figure 6.9(b) is pondered over, it can be observed how the upper bound follows the fixed MCS 0 as expected. We also observe that the PER using the RawBER FLA algorithm follows the upper bound up to around $SNR = 20\,\mathrm{dB}$ and then approaches $PER = 1\%$ slower than the upper bound. Ideally, it would have followed the upper bound and thereafter the line of $PER = 1\%$. For clarification, the upper bound of TP performance is a lower bound of PER.

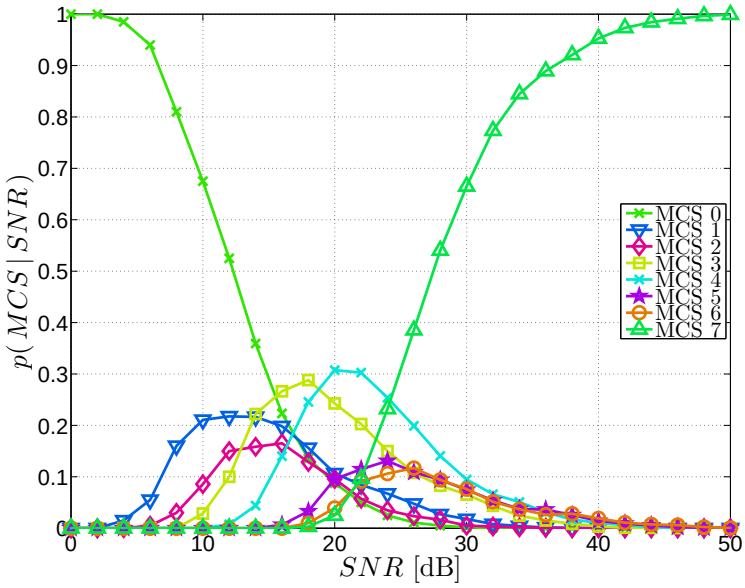

Figure 6.10: *The probability for a MCS to be selected given a certain SNR for the RawBER method, channel model B,* $20\,\mathrm{MHz}$*,* $1{\times}1$*.*

The gain of using FLA algorithm when comparing to the PER constraint envelope is up to 300% in TP for *SNR* $22\,\mathrm{dB}$ with almost the same PER. It is clear that the gain is largest in the mid SNR regime. Here the FLA algorithm has different MCSs to choose. The upper bound, FLA algorithm and MCS 0 to 7 merge at low and high SNR because the selection algorithm is bounded by the available MCSs. The loss from the upper bound to the FLA algorithm is maximum 17% in TP or $\sim 1.5\,\mathrm{dB}$ in SNR. However, the bound is not reachable as the upper bound explores trials (cf. Section 6.2.3).

Figure 6.10 shows how the MCSs are selected over the SNR range. At low SNR only MCS 0 is selected and as the SNR increases the different MCS starts to be selected. It is observed that even at a high nominal SNR the FLA algorithm still selects a low MCS. This generates a tail of the MCS selection on the right hand side. This effect is observed because of the fading process where the link quality sometimes can drop drastically and the FLA algorithm then selects a low MCS accordingly.

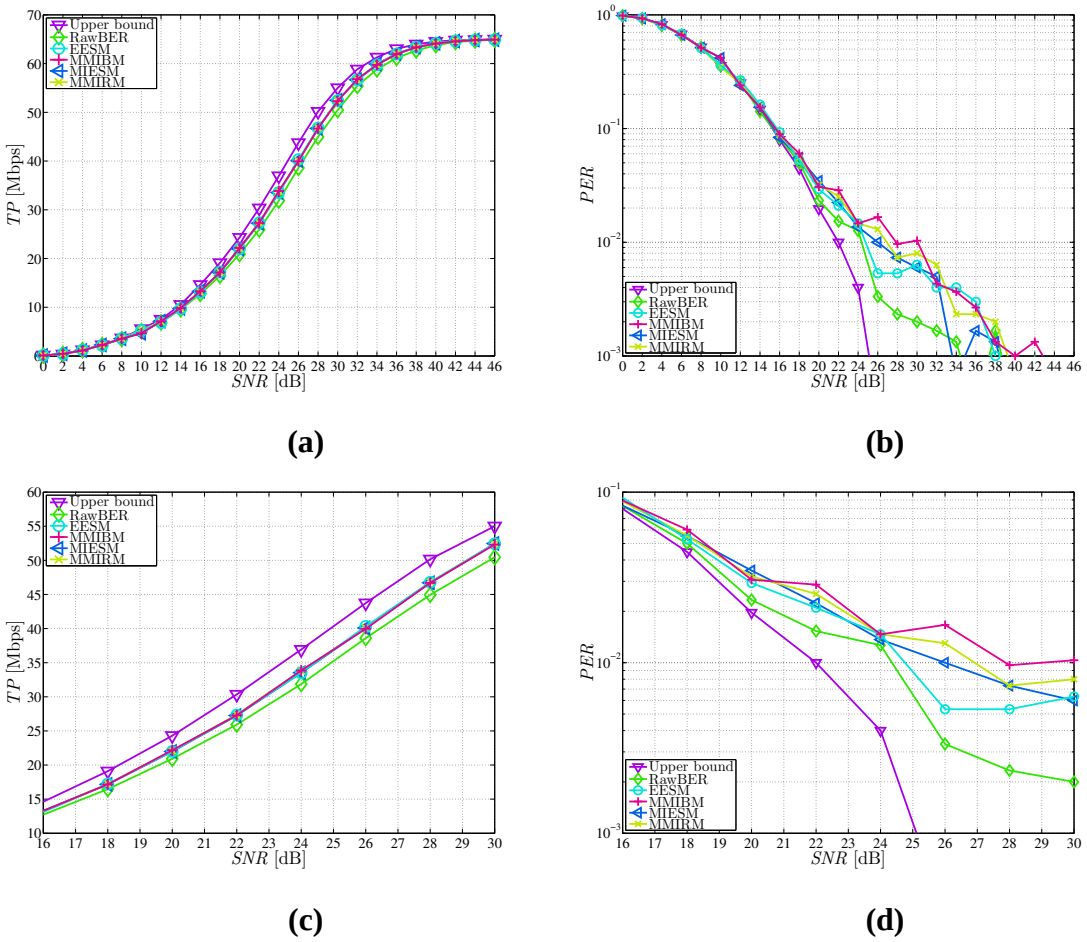

Figure 6.11: *Evaluation of the (a)(c) TP and (b)(d) PER with perfect channel knowledge at the Rx. The figures (c) and (d) are zoomed versions of (a) and (b). Channel model B with bandwidth* $20\,\mathrm{MHz}$*,* 1×1*, target PER* 1%*. All LQMs are evaluated using the Freudenthaler scheme and MCS search "Total Search".*

In Figure 6.11 we can see the TP and PER for all the considered LQMs and the upper bound. In Section 6.1, we have concluded that the RawBER is a less accurate method than the other methods under ideal conditions. Furthermore, we can see that this is also the case for the TP performance where RawBER generate the lowest TP with approximately the same PER. The accuracy of the EESM, MIESM, MMIBM and MMIRM are approximately the same, and the TP and PER performances are also approximately the same. The reason why the four methods with good estimation accuracy do not improve the TP and lower the PER more, is because the difference in the accuracy is too small to improve the FLA algorithm. In the SISO system, there are 8 MCSs to choose from and they are spread over a wide SNR range. So, the PER estimation for the different MCS are often separated by several decades and might not even be close to the selection threshold. Even an error of one decade might result in the selection of the same MCS as if perfect PER estimation was available. The TP will be same, if the same MCS is selected. From Figure 6.11(c) we can see that the algorithm using the EESM, MIESM, MMIBM and MMIRM are approximately $1\,\mathrm{dB}$ from the upper bound and the loss in TP is maximum 10%. The increase in TP relative to the PER constriant envelope is 320% at $SNR = 22\,\mathrm{dB}$.

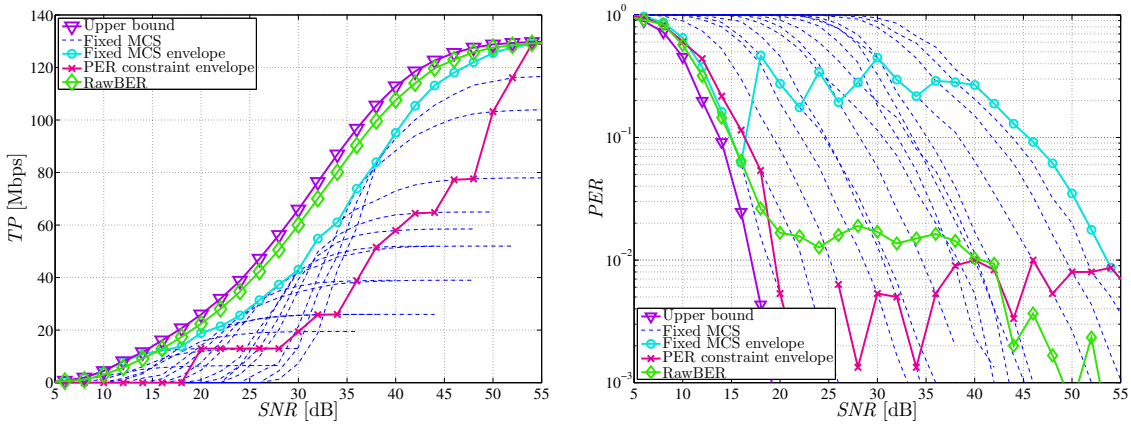

Figure 6.12: *Evaluation of the (a) TP and (b) PER with perfect channel knowledge at the Rx. Channel model B with bandwidth* $20\,\mathrm{MHz}$*,* $2{\times}2$*, target PER* 1%*. The RawBER method is evaluated using the Freudenthaler scheme and MCS search "Total Search".*

Figure 6.12 shows the TP and PER evaluation for a $2{\times}2$ system with the fixed MCS curves. It is interesting to see how much the RawBER based FLA algorithm is lifted from the fixed MCS envelope, and follows the upper bound in Figure 6.12(b) and settles to a relative stable PER between 1% and 2%. Figure 6.13 shows the evaluation for all LQM. The maximum difference in SNR between the upper bound and the

RawBER, EESM, MIESM and MMIBM is around 1.25 dB whereas in the 1×1 system shown in Figure 6.11(a), the difference is around 1 dB. Furthermore, in the 2×2 system the PER curves of all the LQMs are a bit farther from the upper bound than for the 1×1 system in Figure 6.11. We also observe that MMIRM is not providing as high throughput as the other methods. Analysis of the MCS selection indicates that Equation (5.70) is the problem, which is used for calculating the MI for a single stream when a signal of two streams is received. The loss in TP is significant and a replacement for Equation (5.70) must be identified, if MMIRM is to be considered for the MIMO systems. For reference, the MCS selection probability is given for the 2×2 system with MIESM in Appendix, Figure D.1.

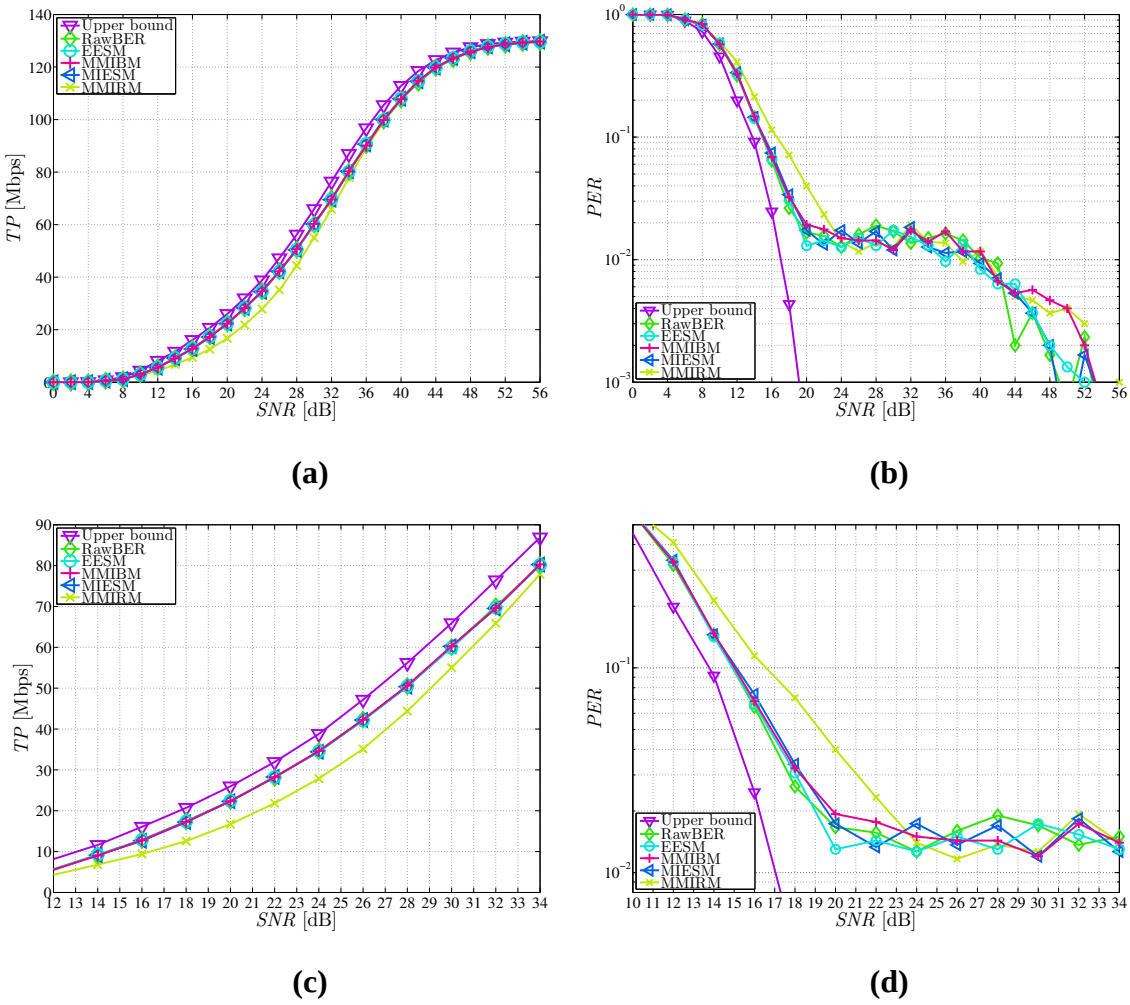

Figure 6.13: *Evaluation of the (a)(c) TP and (b)(d) PER with perfect channel knowledge at the Rx. The figures (c) and (d) are zoomed versions of (a) and (b). Channel model B with bandwidth* 20 MHz*,* 2×2*, target PER* 1%*. All LQMs are evaluated using the Freudenthaler scheme and MCS search "Total Search".*

6.3.1 Throughput and PER for Different Channel Models

The different correction factors should be independent of channel models to ensure a stable FLA algorithm. The correction factor is found to be slightly dependent on the channel model after performing the optimization of the correction factors for individual channel models of B and E. This could however also indicate that the number of measurement points is too small to obtain accurate optimization factors. It will be preferred, if only one set of optimization variables is used such that the modem does not have to identify the kind of channel environment it operates in. So, we perform a joint optimization of measurement from both channel B and E to obtain correction factors representing a trade-off of accuracy between the considered channel models. We then execute the FLA algorithm with a set of correction factors which is optimized for the particular channel model and compare it with the performance for the set of correction factors that is jointly optimized for channel model B and E. Figure 6.14 shows the results of this test. From Figure 6.14, we conclude that it is not possible to observe any degradation in the performance when considering the joint optimized correction factors "ChB&E" compared to the optimized correction factors "ChB".

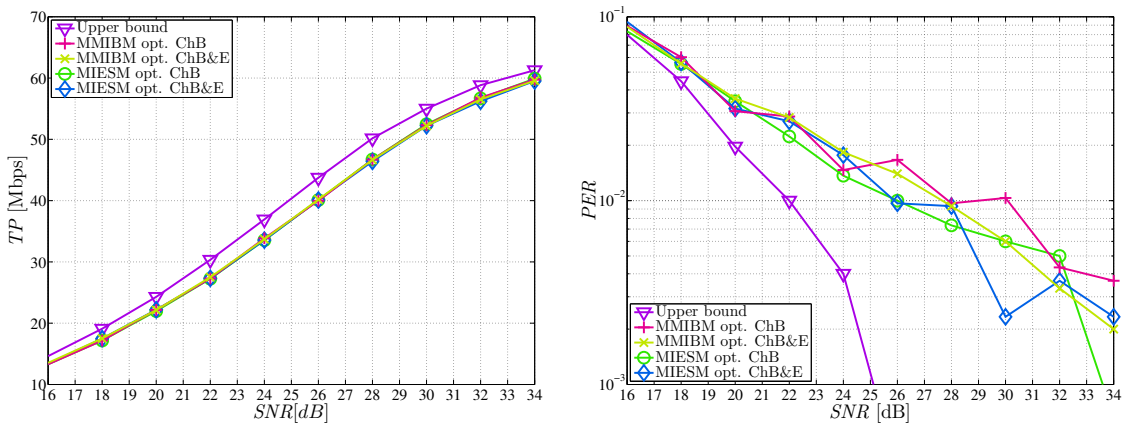

Figure 6.14: *Evaluation of the (a) TP and (b) PER with perfect channel knowledge at the Rx. Channel model B with bandwidth* $20\,\mathrm{MHz}$*,* $\bowtie$*, target PER* 1%*. Both LQMs are evaluated using the Freudenthaler scheme and MCS search "Total Search". The indicator "ChB" means that the coefficients,* λ *and* γ *for MMIBM and MIESM respectively, are optimized for this particular channel mode while "ChB&E" utilizes joint optimized variables for both channel B and E.*

Figure 6.15 shows the TP and PER for channel model E, if the same joint optimized correction factors are utilized as in Figure 6.14. The loss compared to the upper bound is at most 15% in TP or $\sim 1.5\,\mathrm{dB}$ in SNR. The PER does not achieve 1% because channel E is more frequency selective and thereby it is harder to estimate the PER

accurately. So, the uncertainity for selecting an MCS given a channel is larger as when compared to channel model B, and this is the reason for the increased gap to the upper bound and having higher PER.

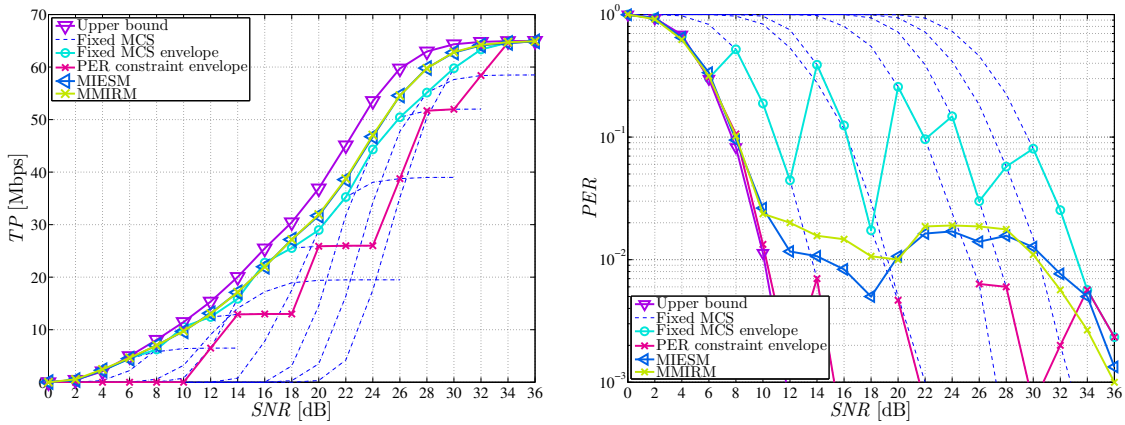

(a) **(b)**

Figure 6.15: *Evaluation of the (a) TP and (b) PER with perfect channel knowledge at the Rx. Channel model E with bandwidth* 20 MHz*,* 1×1*, target PER* 1%*. Both LQMs are evaluated using the Freudenthaler scheme and MCS search "Total Search". The coefficients for the LQMs are joint optimized variables.*

The difference in TP of the FLA and the PER constraint envelope curve is much lower under channel E shown in Figure 6.15 than under channel B shown in Figure 6.11. The frequency diversity is higher in channel E; therefore the "channel quality" will be more stable (cf. Figure 2.10). For systems with higher diversity, the gain of using an FLA algorithm is less pronounced. One could say that the FLA algorithm exploits the lack of diversity. Clearly, fast link adaptation has no meaning in an AWGN channel with infinite diversity.

Figure 6.16 shows the selection of MCSs along the SNR. Compared to Figure 6.10 for channel B, we observe that at a fixed SNR in the mid SNR regime, the FLA algorithm selects a wider range of MCS for channel B compared to channel E because the channel quality simply varies the most in channel model B.

6.4 Search Methods

In Section 5.2.5 three different search schemes were presented which we will evaluate here for a 2×2 system.

From Figure 6.17 we can see that "Total Search" and "Search from top" both yield the same performance. This is because both methods are optimal and the same MCS

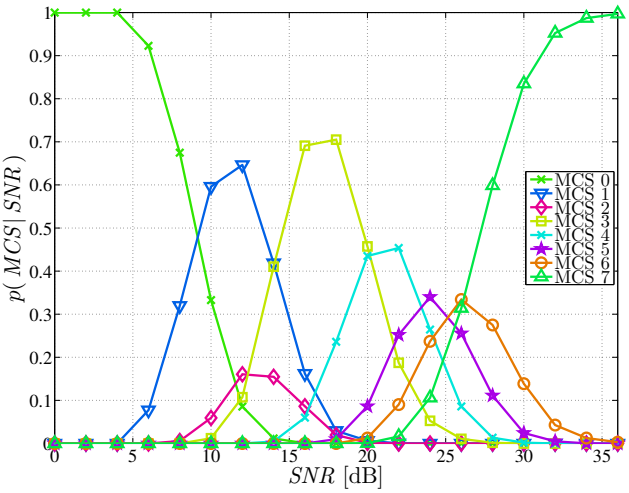

Figure 6.16: *The probability for a MCS to be selected given a certain SNR for the MIESM method, channel model E,* $20\,\mathrm{MHz},\ 1{\times}1$.

is selected for the same channel (cf. Section 6.4). However, "Search from top" has a lower computational burden and will only in the worst case has the same computational burden as "Total search". The worst case will be if MCS 0 is selected. The method "Search from last" is sub optimal and it is observed in Figure 6.17 that there is a TP loss up to 4.5% at $28\,\mathrm{dB}$. This is interpreted as a significat loss introduced only by the search method. So, we conclude that the sub optimal "Search from last" should only be used if the time requirement for the MCS search can not be met with the optimal method "Search from top".

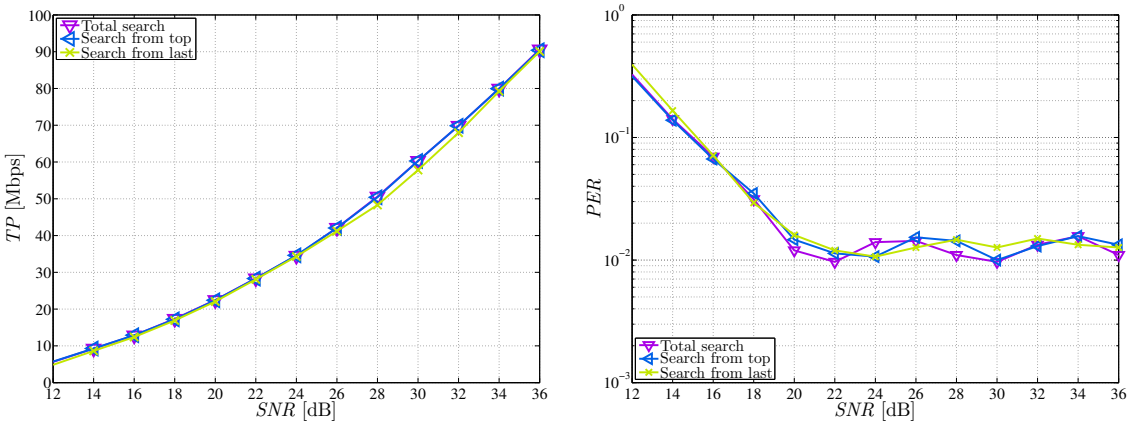

(a) **(b)**

Figure 6.17: *Evaluation of the (a) TP and (b) PER with perfect channel knowledge at the Rx. Channel model B with bandwidth* $20\,\mathrm{MHz}$, $1{\times}1$, *target PER* 1%. *Evaluated using a practical evaluation scheme with a MCS request and a data transmission. LQM is EESM.*

6.5 Throughput and PER with Non Ideal Conditions

For non ideal conditions we consider channel and noise variance estimation error. The channel estimation is given in Equation (5.7); the noise variance estimation error is modelled as having a Gaussian distribution with variance $\sigma^2_{\Delta N_0} = 1/8\,\mathrm{dB}$ and uncorrelated between each packet transmission. Figure 6.18 shows the simulations with these settings.

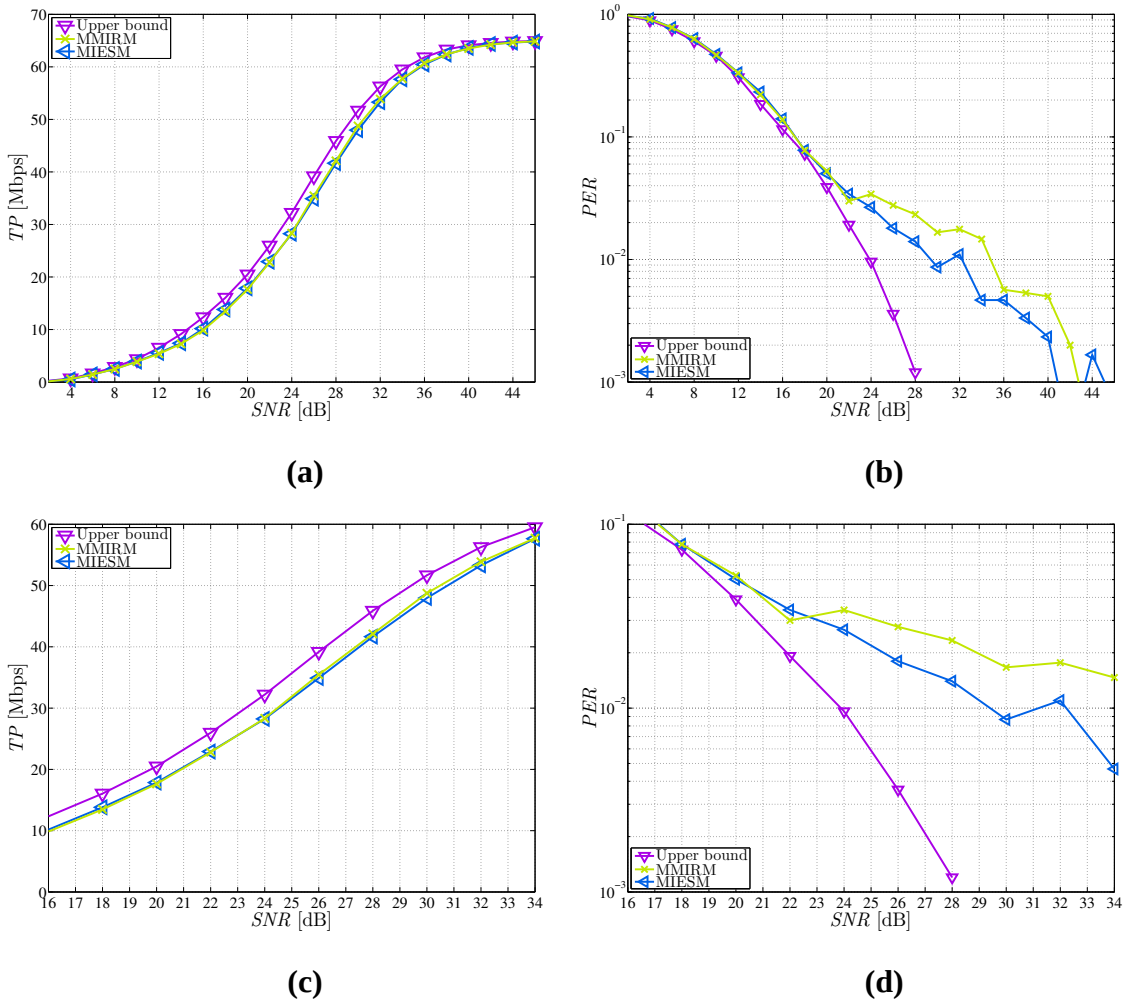

Figure 6.18: *Evaluation of the (a) TP and (b) PER with practical channel estimation at the Rx. Channel model B with bandwidth* $20\,\mathrm{MHz}$*,* $1{\times}1$*, target PER* 1%*. The LQMs, MMIRM and MIESM, are evaluated using a practical evaluation scheme with a MCS request and a data transmission, and MCS search is "Total Search".*

In Figure 6.18 it is observed that the PER for MMIRM is higher than for MIESM but MMIRM has a slightly higher TP. In terms of overall performance, both methods are almost same for the settings used in Figure 6.18. We were expecting that MMIRM would outperform the other LQMs when considering practical estimations because it

utilizes the soft bits which directly determines the PER. However, MMIRM estimates the PER for the MFB request and will assume the same effect of practical estimation errors for the data transmission. But, the effects of the impairments are uncorrelated between the MFB request and the data transmission in these simulations. The assumption of the (almost) same estimation error will hence not be true and this extra information which MMIRM models are then of no use in this setup.

Even if it is possible to improve MMIRM and making it superior to MIESM, we observe that the improvements in TP and PER can only be minor. The distance to the throughput upper bound is no more than $1.50\,\mathrm{dB}$ and for perfect channel knowledge it is $1\,\mathrm{dB}$. So, the expected gain can only be in the order of $\sim 0.5\,\mathrm{dB}$. The possible improvement in PER is also small because MIESM is following the bound quite tight. So, for the settings used in Figure 6.18, the possible gain of improving MMIRM is limited tightly by the small gap between MIESM and the upper bound.

6.6 MCS Feedback Delay

The performance of the FLA is evaluated with respect to MCS feedback (MFB) delays. An MFB delay is the amount of time for an estimated MCS at the receiver to be available at the transmitter. Figure 6.19(a) shows the throughput versus delay characteristics for a $1{\times}1$ and $2{\times}2$ systems at both *SNR* $20\ \mathrm{dB}$ and $30\ \mathrm{dB}$. Figure 6.19(c) shows the performance of the same *TP* with higher resolution up to $10\ \mathrm{ms}$ delay. For the evaluation of the impact of MCS feedback delay on the performance, MIESM is chosen as a candidate for the LQM because it is one of the best LQMs which has low estimation error. Figure 6.19(b) shows the corresponding *PER* versus delay characteristics for both systems under consideration and Figure 6.19(d) shows the performance of the *PER* with higher resolution up to $10\ \mathrm{ms}$ delay.

A common characteristic can be seen in these figures that there are two regimes in *TP* and *PER* vs. MFB delay plots: non-linear and saturation regimes [Larry et al., 1992]. The non-linear regime can be considered in Figure 6.19(a) up to feedback delay of $40\ \mathrm{ms}$, where the loss of *TP* for a given system and SNR is significant from $0\ \mathrm{ms}$ to $40\ \mathrm{ms}$ delay. Similarly the non-linear regime can also be considered in Figure 6.19(b) up to $40\ \mathrm{ms}$ delay, where the *PER* increases by approximately one decade. The saturation regime can be considered in both figures when the feedback delay exceeds $40\ \mathrm{ms}$ where the corresponding *TP* and *PER* are almost constant with respect to delay. It can also be construed from these figures that the loss of *TP* for the first $2\ \mathrm{ms}$ delay is subtle, i.e., $\sim 1.5\ \%$ in both systems. After the first $2\ \mathrm{ms}$ delay, *TP* loss rate increases by a factor of approximately $1.5 - 2$ with every $2\ \mathrm{ms}$ MFB delay. Similarly, the corresponding

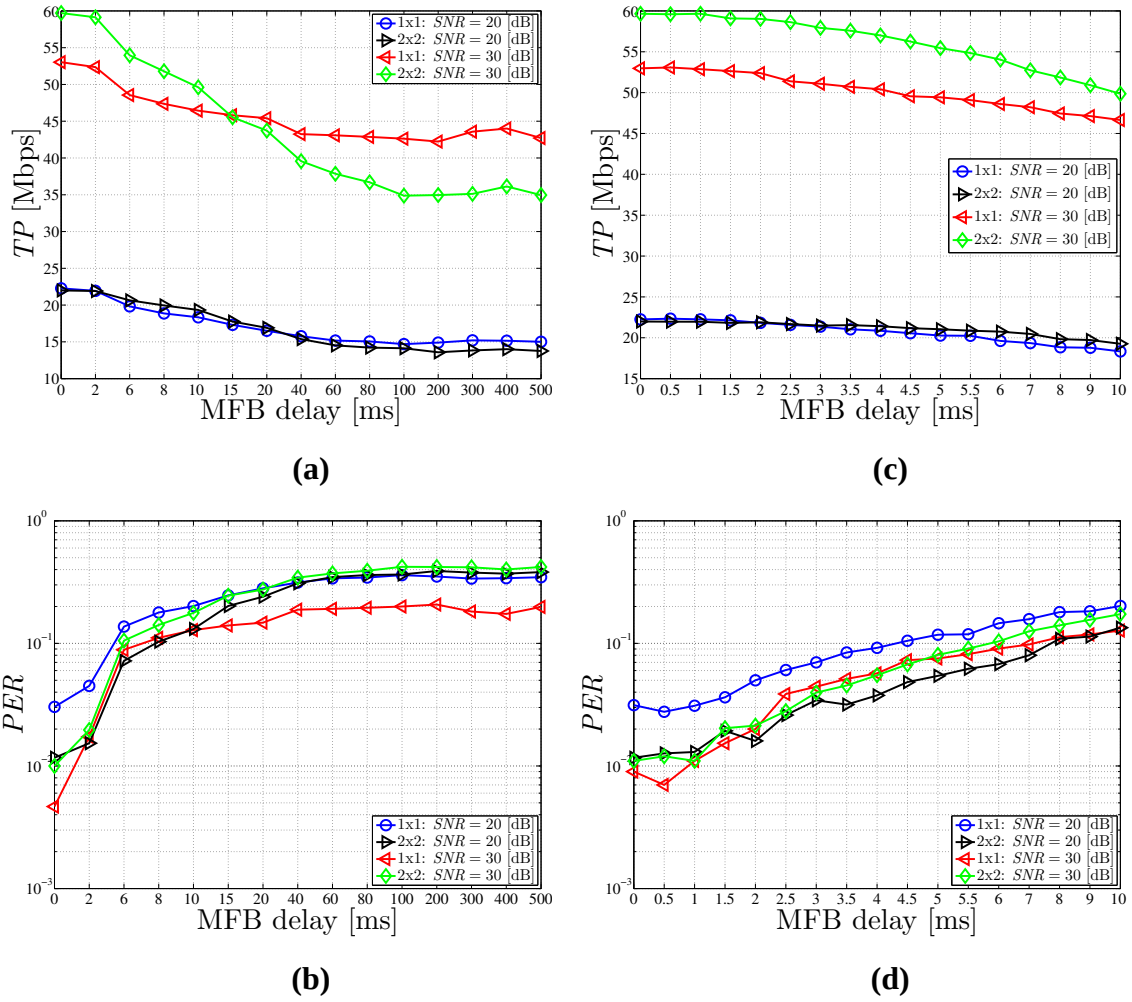

Figure 6.19: *Evaluation of the ((a) and (c)) TP, and ((b) and (d)) PER vs. MFB delay in the FLA with perfect channel knowledge at the Rx. The performances are evaluated at SNRs* 20 dB *and* 30 dB *for MFB delays up to ((a) and (c))* 500 ms *and with higher resolution up to ((b) and (d))* 10 ms*. Channel model B with bandwidth* 20 MHz*, LQM: MIESM and MCS search: "Total Search".*

PER also increases by a factor of approximately $1.5 - 2$ with every 2 ms MFB delay up to 10 ms delay. Furthermore, from these figures, it can be seen that for the first 2 ms delay, the rate of *TP* loss is trivial but the *PER* has almost doubled for a given system and SNR. So, to keep the PER at the desired target PER, the PER threshold can be lowered by an outer loop which depends on the long term statistics. At *SNR* 20 dB, the *TP* losses in both 1×1 and 2×2 systems are around 29 % from 0 ms to 40 ms delay. However, at *SNR* 30 dB, the loss rate of *TP* in the 2×2 system is higher than in the 1×1 system because the FLA in 1×1 system at this SNR chooses mostly the maximum available MCS 7 (cf. Figure 6.10) whereas the FLA in 2×2 system has more number of MCSs to choose for the adaptation. Thus, it can be said that the performance of

the FLA is mostly affected by the MFB delay in the mid SNR regime where FLA has more freedom to choose different MCSs.

The performance of the FLA is also evaluated with respect to various velocities of the scatterers and MFB delays. Figure 6.20(a) and (b) show the *TP* and *PER* versus MFB delay with different velocities of the scatterers. As it is discussed in the IEEE channel models' Section 2.3.3, that the coherence time decreases with the increasing velocity of scatterers. Thus, due to the decreasing coherence time, it can be seen in Figure 6.20(a) and (b) that the rate of *TP* loss and the corresponding *PER* increase with increasing velocity of scatterers. Furthermore, consider a *TP* achieved in Figure 6.20(a), for instance, 17 Mbps when the velocity of the scatterers is 2.0 km/h at the MFB delay 10 ms. Now, if the velocity of the scatterers is doubled to 4.0 km/h, then the same $TP = 17$ Mbps will be achieved around half of the MFB delay of 10 ms, that is at 5 ms. In Figure 6.20(b), the *PER*, for instance, is 6×10^{-2} at the MFB delay 1.5 ms when the velocity of the scatterers is 2.0 km/h. Now, the *PER* will approximately get twice to 1.2×10^{-1}, by doubling the velocity of the scatterers to 4.0 km/h. The behaviour of the TP and PER with the different velocities of the scatterers are prominent in the range of MFB delays $1 - 10$ ms.

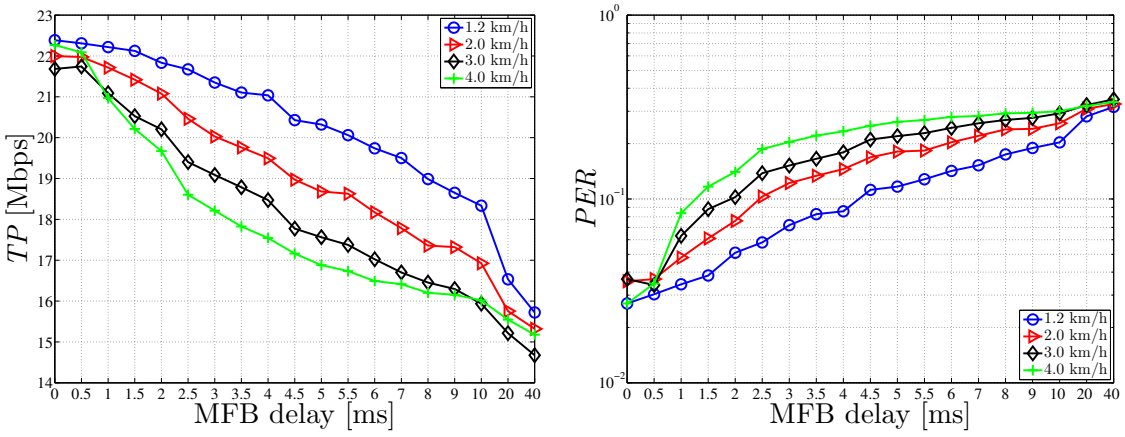

(a) **(b)**

Figure 6.20: *Evaluation of the TP and PER versus MFB delay with four different velocities of the scatterers of channel model B and perfect channel knowledge at the Rx. However, in the standard [TGn IEEE802.11], velocity of the scatterers is only* 1.2 km/h. *The performance is evaluated for* 1×1 *system at SNR* 20 dB*, for channel bandwidth* 20 MHz*, LQM: MIESM and MCS search: "Total Search".*

The expected delay is hard to obtain as the delay is unconstrained. The access mechanisms in IEEE 802.11x like DIFS (distributed inter frame space) and SIFS (short inter frame space) are having timings in the order of μs. So, we may expect an imme-

diate and unsolicited response for an MCS feedback, loosely talking, in the order of $1-2$ ms and 2 ms$-$implementation dependent, respectively. Since it is hard to estimate the MFB delay in general, we suggest to have an outer loop, i.e., SLA on FLA to maintain the PER at the desired target PER by adapting the threshold of PER.

6.7 Summary

In this chapter, the performance of the FLA algorithm were presented and assessed by the numerical results. The PER estimation accuracy was evaluated and a correction term for MMIBM and MMIRM were given to improve the accuracy for channel realizations with high dynamics among the subcarriers. It was concluded that EESM, MMIBM and MIESM have approximately the same estimation accuracy with MMIRM slightly less accurate, and RawBER is the least accurate method. It was shown how to obtain the bounds for the FLA algorithm of interest and how a bound for any FLA algorithm could be acquired.

The TP and PER were evaluated for 1×1 and 2×2 systems. For channel model B a gain of up to 320% can be observed. This high gain is however only possible in the mid SNR regime and for setups with low diversity because the FLA algorithm exploits lack of diversity.

The suitable correction factors of all the five LQMs which are dependent on MCS, are also turned to be bit dependent on the channel models. However, the correction factors optimized jointly having a training set from both channel models B and E, rendered acceptable performances of TP and the corresponding PER for all the methods. So, it should then be possible to consider only one set of suitable correction factors which can be used for all the channel models.

The search method “Search from top” should be used as it renders the same performance as “Total search” with less or equal computational burden. The sub optimal method “Search from last” should only be used if the time requirement for the MCS search can not be met with “Search from top”.

It was anticipated that the method MMIRM would be a superior method when considering practical channel estimation and other impairments. However MMIRM and MIESM had the same performance in the SISO system. It was discussed than even though MMIRM models the estimation errors of the receiver, this new information will have no value if the estimation errors are uncorrelated between the MFB request and the data transmission. For the settings investigated, the possible gain of improving MMIRM will be minor because the methods evaluated was already close to the upper bound.

The TP and PER performances were evaluated with respect to MFB delay and different velocities of the scatterers of channel model B under ideal conditions. The TP and PER versus MFB delay for a given velocity of the scatterers can be divided into two regions, a non-linear and a saturation region. In the non-linear region, the TP loss rate and PER increase non-linearly with the increasing MFB delay while in the saturation region, the TP loss rate and PER remain almost stagnant. It is also observed that if the velocity of scatterers is decreased to half of its value, then approximately the same TP can be achieved by doubling the MFB delay. The PER approximately doubles by doubling the velocity for a given MFB delay.

7 Conclusions

The IEEE 802.11n standard offers roughly ten times higher throughput than the IEEE 802.11a/g standard such that an application like video streaming can be supported. Since the wireless channel is slowly time varying, fast link adaptation can be employed to increase throughput. However, FLA is not mandatory in the IEEE 802.11n standard.

The realm of this project work was to investigate various FLA algorithms for the IEEE 802.11n standard which select dynamically a suitable MCS for the current wireless channel realization. The FLA algorithm selects a suitable MCS for the current channel realization which renders high throughput while maintaining a certain target PER like 1%. The suitable MCS is recommended to the transmitter via the LA protocol defined in the standard IEEE 802.11n.

The IEEE channel models are briefly described which are slowly time varying and frequency selective fading channels. In the IEEE 802.11n standard, MIMO BICM-OFDM concepts are implemented. The basic fundamentals of MIMO and OFDM were introduced. MIMO provides array and diversity gain. OFDM decouples the frequency selective fading channel into parallel flat fading channels. BICM is employed to improve the performance in fading channels. The linear MMSE MIMO receiver's output is considered equivalent to a Gaussian channel which in general holds well for the low SNR regime. The Gaussian assumption were validated and adduced by the numerical results for the practical SNR ranges used in IEEE 802.11n.

In this project work, several LQMs were discussed for the purpose of an FLA algorithm. The FLA algorithm mainly consists of an LQM and MCS search mechanism. For detailed investigations the three link quality metrics, i.e., RawBER, EESM and MIBM were selected and implemented in MATLAB. MIBM is a common concept which depends on mutual information and is further divided into three LQMs known as MMIBM, MIESM and MMIRM. Thus, there are a total of five LQMs whose performances are assessed in this work. The RawBER, EESM, MMIBM and MIESM utilize the computed post processing SINRs. The method we propose, MMIRM, depends

on the absolute values of the soft bits generated by a MaxLog (LogAPP) demapper. The main objective of these LQMs are to map a set of CSIs for a fading channel into one scalar metric. This single scalar of a current channel state is then mapped by a pre-computed function to estimate a corresponding PER in an AWGN channel for a considered MCS in an MCS search. A search is performed until the MCS is found having the highest MCP and a PER below a certain threshold.

Numerical results for the five LQMs were assessed. To improve the PER estimation accuracy for MMIBM and MMIRM, we have proposed a correction term based on the variance motivated by [Bjerke et al., 2005]. After the correction term to both of them, EESM, MIESM and MMIBM yield almost the same PER estimation accuracy; MMIRM is slightly less accurate and RawBER is the least accurate LQM. To obtain these correction factors of all the five LQMs, a least squares fit is performed in the logarithmic PER domain. The correction factors shall depend only on MCS but ideally independent of channel models. PER measurements statistics are not reliable enough to make a solid conclusion on the correction factors independent of channel type. However, simulations have shown that the correction factors optimized using the training set of measurement points from both channel B and E, can be used for channel B without noticeable change in the performance. Thus, we assume that one set of optimized correction factors can be used for all IEEE channel models.

The optimal performance of the FLA algorithm is assessed using a scheme called "Freudanthaler"[Freudenthaler et al., 2007] by us which ensures that only the inaccuracy of the PER estimation is observed. Moreover, we present a simple and useful upper bound of any FLA algorithm which can only be obtained by simulations. This useful upper bound has lower complexity than in [Simoens et al., 2005] however it is less tight and practically unreachable.

The throughput curve for the FLA algorithms using the best LQMs are at most $1\ \mathrm{dB}$ and $1.25\ \mathrm{dB}$ from the throughput curve of the upper bound in 1×1 and 2×2 systems, respectively. If we compare the FLA algorithm with the PER constraint envelope, the FLA can gain up to 320% throughput while maintaining almost the same PER. The FLA algorithm exploits the system which has very low diversity. So, the gain of the FLA is higher in channel B than channel E because channel E has higher frequency diversity and hence a more stable channel "link quality". Furthermore, the gain is most pronounced in the mid SNR regime.

Under ideal conditions and in SISO system, the TP and PER performances of the EESM, MIESM, MMIBM and MMIRM are approximately same but better than the RawBER method as expected. In 2×2 system, the performance of the EESM, MIESM, MMIBM and RawBER are same but better than the performance of MMIRM. The

method MMIRM falls behind because it does not handle the one spatial stream case accurately when estimating an MCS from a two spatial stream signal.

The search methods “Total Search” and “Search from top” produces the same throughput but the latter one has a lower computational burden. The “Search from last” is a sub-optimal method and shall only be employed when the time constraints of the modem design requires a time efficient search method.

Under non-ideal conditions, SISO system, MMIRM and MIESM perform equally well. It was discussed that the modelling of the estimation errors in the MMIRM method has no value if the estimation errors are uncorrelated between the MFB request and the data transmission. For the settings used, any improvements of MMIRM would only have a minor effect because both MMIRM and MIESM were close to the performance bound.

For a practical two node system, the FLA in a receiver estimates an MCS depending on the current channel state which is fedback to the transmitter. When the MCS feedback delay increases, the TP loss rate and PER of the system will initially increase non-linearly up to the $40\ \mathrm{ms}$ feedback delay and thereafter the TP and PER are almost stagnant. So, the TP and PER versus MFB delay characteristic curves can be divided into two regimes, a non-linear and a saturation regime. It is also observed that when the coherence time of a channel decreases, the TP loss and PER increase for a given MFB delay.

Bibliography

[3GPP2, 2003] L. T. 3GPP2. Reverse Link Hybrid ARQ: Link Error Prediction Methodology Based on Convex Metric. Standardization Document, 3rd generation partnership project 2 3GPP2, 2003.

[Bansal, 2007] A. Bansal. Personal communications on MAC issues, Wipro, 2007.

[Biglieri and Divsalar, 2005] E. Biglieri and D. Divsalar. Upper Bounds to Error Probabilities of Coded Systems over AWGN and Fading Channels. Global Telecommunications Conference, GLOBECOM 2000, Vol. 3, pp. 1605 – 1610, Nov. 27 - Dec. 1 2000.

[Bjerke et al., 2005] B. A. Bjerke, J. Ketchum, R. Walton and S. Nanda. Packet Error Probability Prediction for System Level Simulations of MIMO-OFDM Based 802.11n WLANs. Qualcomm, Inc, 2005.

[Blankenship et al., 2004] Y. Blankenship, P. Sartori, B. Classon, V. Desai and K. Baum. Link error prediction methods for multicarrier systems. Vehicular Technology Conference, VTC2004-Fall IEEE 60th, Vol. 6, pp. 4175 – 4179, Sep. 26-29 2004.

[Bolcskei et al., 2002] H. Bölcskei, D. Gesbert and A. Paulraj. On the capacity of OFDM-based spatial multiplexing systems. IEEE Transaction on Communications, Vol. 50, No. 2, pp. 225–234, Feb. 2002.

[Brink, 2001] S. t. Brink. Convergence Behaviour of Iteratively Decoded Parallel Concatenated Codes. IEEE Transactions on Communications, Vol. 49, pp. 1727–1737, Oct. 2001.

[Brueninghaus et al., 2005] K. Brueninghaus, D. Astely, T. Salzer, S. Visuri, A. Alexiou, S. Karger and G. A. Seraji. Link performance models for system level simulations of broadband radio access systems. Personal, Indoor and Mobile Radio Communications, 2005. PIMRC 2005. IEEE 16th International Symposium, Vol. 4, pp. 2306 – 2311, Sep. 11-14 2005.

[Caire et al., 1998] G. Caire, G. Taricco and E. Biglieri. Bit-Interleaved Coded Modulation. IEEE Transactions on Information Theory, Vol. 44, No. 3, pp. 927–946, May 1998.

[Cheng et al., 2004] V. W. Cheng and C.-H. L. *. The Design of the Soft Decoder of the Interleaved Convolutional Code Used in IEEE 802.11a, 2004. Department of Computer Science and Information Engineering, Graduate Institute of Communication Engineering, National Chi Nan University.

[Cioffi et al., 1995] J. M. Cioffi, G. P. Dudevoir, M. V. Eyuboglu and G. D. Forney. MMSE decision-feedback equalizers and coding - Part I: Equalization results. IEEE Transactions on Communications, Vol. 43, pp. 2582 – 2594, Oct. 1995.

[Costello et al., 1999] D. Costello and O. Y. Takeshita. On the Packet Error rate of Convolutional Codes. ITW, Metsovo, 1999.

[Ericsson, 2003B] Ericsson. System-level evaluation of OFDM - further considerations. 3GPP, Vol. TSG-RAN WG1, No. 35 R1-031303, , Nov. 17-21 2003.

[Ericsson, 2003A] Ericsson, S. Tsai and A. Soong. Effective-SNR mapping for modelling frame error rates in multiple-state channels, 3GPP2-C30-20030429-010, Ericsson. Standardization Document, 3rd generation partnership project 2 3GPP2, 2003.

[FITNESS, 2000] I.-.-. F. P. FITNESS. MTMR baseband transceivers needs for intra-system and inter-system (UMTS/WLAN) reconfigurability Deliverable D3.3.1. Standardization Document, 2000.

[Fleury, 2006] B. H. Fleury. Channel Characterization and Measurement, 2006. Lecture notes for 9th semester SIPCOM 2006, AAU.

[Fleury, 2007] B. H. Fleury. Project discussion on channel modeling, 2007.

[Foschini, 1996] G. J. Foschini. Layered Space-Time Architecture for Wireless Communication in a Fading Environment when using Multi-Element Antennas. Bell Labs Technical Journal, 1996.

[Frenger et al., 1998] P. Frenger, P. Orten, T. Ottosson and A. Svensson. Multirate convolutional codes, 1998. Dpt. of Signals and Systems, Communication Systems Group, Chalmers University of Technology.

[Freudenthaler et al., 2007] K. Freudenthaler, A. Springer and J. Wehinger. Novel SINR-to-CQI Mapping Maximizing the Throughput in HSDPA. In Wireless Communications and Networking Conference, WCNC, pp. 2231–2235, March 2007.

[Gesbert et al., 2002] D. Gesbert, J. R. W. Heath, S. Catreux and V. Erceg. Adaptive modulation and MIMO coding for broadband wireless data networks. IEEE Communications magazine,, Vol. 40, No. 10.1109/MCOM.2002.1007416, pp. 108–115, June 2002.

[Globecom, 2003] E. P. Globecom and R. Stacey. IEEE 802.11n: Throughput, Robustness, and Reliability Enhancements to WLANs, 2003. T14 tutorial.

[Goldsmith et al., 1997] A. J. Goldsmith and P. Varaiya. Capacity of Fading Channels with Channel Side Information. IEEE Transaction on Information Theory, Vol. 43, No. 6, pp. 1986–192, November 1997.

[Gresset, 2006] N. Gresset. Transmission techniques over MIMO channels for 802.11n, 2006. Internal presentation, Wipro-Newlogic.

[Hara et al., 2004] B. Hara and A. Petrick. IEEE 802.11 Handbook - A Designer's Companion. IEEE, 2004.

[Hassibi and Vikalo, 2005] B. Hassibi and H. Vikalo. On the Sphere Decoding Algorithm: Part I and Part II. IEEE Transactions on Signal Processing, Vol. 53, pp. 2806–2834, Aug. 2005.

[IEEE802.11n] IEEE P802.11n/D2.00. IEEE 802.11 Working Group, Feb 2007.

[Jones et al., 2002] C. Jones, T. Tian, A. Matache, R. Wesel and J. Villasenor. Robustness of LDPC codes on periodic fading channels. Global Telecommunications Conference, GLOBECOM. IEEE, Vol. 2, pp. 1284–1288, Nov 2002.

[Kim, 1997] M. G. Kim. On systematic punctured convolutional codes. IEEE Trans. Communications, Vol. 45, No. 2, pp. 133–139, Feb 1997.

[Kim et al., 2006] Y. Kim, J. M. Cioffi and K. Holt. Low Complexity BICM-OFDM based MIMO Receiver using Successive Interference Cancellation, Apr. 2006.

[Lamarca et al., 2005] M. Lamarca and F. Rey. Indicators for PER prediction in wireless systems: A comparative study. Vehicular Technology Conference, VTC 2005-Spring, Vol. 2, No. 30, pp. 792–796, May-June 2005.

[Lampe, 2003] A. Lampe. Multiuser Detection and Channel. IEEE, 2003.

[Lampe et al., 2003] M. Lampe, T. Giebel, H. Rohling and W. Zirwas. Per-prediction for PHY mode selection in OFDM communication systems. Global Telecommunications Conference, GLOBECOM '03. IEEE, Vol. 1, pp. 25 – 29, Dec. 1-5 2003.

[Land et al., 2004] I. Land, P. A. Hoeher and S. Gligorevic. Computation of Symbol-Wise Mutual Information in Transmission Systems with LogAPP Decoders and Application to EXIT Charts, 2004.

[Larry et al., 1992] W. Larry, R. Lee and A. Rossmiller. Time-Variant Throughput Versus Delay Characteristics and Communication Reliability of a Wireless Local Area Network. pp. 30–37. IEEE Conference on Wireless LAN Implementation, Sept. 1992.

[Manshaei, 2005] M. H. Manshaei. Cross Layer Interactions for Adaptive Communications in IEEE 802.11 Wireless LANS. PhD thesis, Universit´e de Nice - Sophia Antipolis, 2005.

[Nanda et al., 1998] S. Nanda and K. M. Rege. Frame Error Rates for Convolutional Codes on Fading Channels and Concept of Effective E_b/N_0. IEEE Transactions on Vehicular Technology, Vol. 47, No. 4, pp. 1245–1250, November 1998.

[Prasad et al., 2000] R. V. Nee and R. Prasad. OFDM for Wireless Multimedia Communications. Artech House Publishers, 2000.

[Paulraj et al., 2005] A. Paulraj, R. Nabar and D. Gore. Introduction to Space-Time Wireless Communication. Cambridge University Press, 2005.

[Peng et al., 2007] F. Peng, J. Zhang and W. E. Ryan. Adaptive Modulation and Coding for IEEE 802.11n. IEEE Wireless Communications and Networking Conference, 2007.

[Proakis, 2001] J. G. Proakis. Digital Communications. McGraw-Hill, Fourth Edition edition, 2001.

[Rappaport, 2002] T. S. Rappaport. Wireless Communications Principles and Practice. Prentice Hall, 2002.

[S. Lin and D. Costello, 1983] S. Lin and D. J. C. Jr. Error Control Coding: Fundamentals and Applications. Prentice Hall, First Edition edition, 1983.

[Sayana et al., 2007] K. Sayana and J. Zhuang. Link Performance Abstraction Based on Mean Mutual Information per Bit (MMIB) of the LLR Channel, IEEE C802.16m-07/097, Motorola. Standardization Document, IEEE 802.16 Broadband Wireless Access Working Group, 2007.

[Schumacher, 2003] L. Schumacher. WLAN MIMO Channel Matlab program, 2003.

[Seethaler et al., 2004] D. Seethaler, G. Matz and F. Hlawatsch. An Efficient MMSE-Based Demodulator for MIMO Bit-Interleaved Coded Modulation. Global Telecommunications Conference, IEEE GLOBECOM-04, Vol. 4, pp. 2455 – 2459, Nov. 29 - Dec. 3 1998.

[Simoens et al., 2001] S. Simoens and D. Bartolome. Optimum performance of link adaptation in HIPERLAN/2 networks. Vehicular Technology Conference, VTC Spring, IEEE VTS 53rd, Vol. 2, pp. 1129 – 1133, May 2001.

[Simoens et al., 2005] S. Simoens, S. Rouquette-Léveil, P. Sartori, Y. Blankenship and B. Classon. Error prediction for Adaptive Modulation and Coding in Multiple-Antenna OFDM Systems. IEEE doc.:, Vol. IEEE, No. 802.11-03/940r4, , May 2004.

[TGn IEEE802.11] I. . C. M. S. C. TGn. TGn Channel Models for IEEE 802.11 WLANs. IEEE doc.:, Vol. IEEE, No. 802.11-03/940r4, , May 2004.

[Tse et al., 2005] D. Tse and P. Viswanath. Fundamentals of Wireless Communication. Cambridge University Press, 2005.

[WINNER, 2003] WINNER. Assessment of advanced beamforming and MIMO technologies, IST-2003-507581, D2.7 ver1.0. Standardization Document, EU project, Information society technologies, 2003.

[Yan et al., 2007] L. Yan and W. E. Ryan. Robustness of LDPC Codes on Periodic Fading Channels. IEEE Transactions On Wireless Communications, Vol. 6, No. 5, pp. 1670–1680, May 2007.

[Yoon et al., 2000] D. Yoon, K. Cho and J. Lee. Bit Error Probability of M-ary Quadrature Amplitude Modulation. IEEE VTC, 2000.

[Zehavi, 1992] E. Zehavi. 8-PSK Trellis Codes for a Rayleigh Channel. IEEE Transactions on Communications, Vol. 40, pp. 873–884, May 1992.

[Zelst, 2004] A. V. Zelst. MIMO OFDM for Wireless LANs. CIP-DATA Library Technische Universitei Eindhoven, the Netherlands, 2004.

Unbiased MMSE Estimation

A

To give a brief introduction of an unbiased MMSE based estimation, a MIMO system with single carrier modulation can be contemplated such that the signal model can be given as

$$\boldsymbol{y} = \mathbf{H}\boldsymbol{x} + \boldsymbol{n} \tag{A.1}$$

where $\boldsymbol{y}$ is a $N_{\mathrm{R}} \times 1$ received signal vector, $\mathbf{H}$ is a $N_{\mathrm{R}} \times N_{\mathrm{T}}$ channel matrix, $\boldsymbol{x}$ is a $N_{\mathrm{T}} \times 1$ transmitted (complex) data symbol vector and $\boldsymbol{n}$ $N_{\mathrm{R}} \times 1$ is a zero mean circularly symmetric complex Gaussian noise vector having variance N_0.

As it was discussed in Section 3.4.3 that the unbiased MMSE estimation should fulfill the following condition

$$\mathbb{E}\left\{\hat{\boldsymbol{x}} - \boldsymbol{x}\right\} = 0. \tag{A.2}$$

So, the unbiased MMSE estimation can be written as [Seethaler et al., 2004]

$$\hat{\boldsymbol{x}}^j = \left(\frac{\left[\left(\mathbf{H}\mathbf{H}^H + N_0\mathbf{I}_{N_{\mathrm{R}}}\right)^{-1}\boldsymbol{H}_j\right]^H}{\underbrace{\boldsymbol{H}_j^H\left[\left(\mathbf{H}\mathbf{H}^H + N_0\mathbf{I}_{N_{\mathrm{R}}}\right)^{-1}\boldsymbol{H}_j\right]}_{\text{scalar}}} \right) \boldsymbol{y} \quad \forall\, j = 1, 2, \cdots, N_{\mathrm{T}} \tag{A.3}$$

where, $\mathbf{H}$ is $N_{\mathrm{R}} \times N_{\mathrm{T}}$,

$$\mathbf{H} = \begin{bmatrix} \boldsymbol{H}_1 & \boldsymbol{H}_2 & \cdots & \boldsymbol{H}_j & \cdots & \boldsymbol{H}_{N_T} \end{bmatrix} \tag{A.4}$$

and $\boldsymbol{H}_j$ is $N_{\mathrm{R}} \times 1$.

Modulation and Coding for IEEE 802.11n

B

B.1 Modulation in IEEE 802.11n

Four modulation types is used in 802.11n, BPSK, QPSK, 16QAM and 64QAM. For preamble, rotated BPSK is also used. For a single stream the modulation is the same for all the subcarriers. There is no bitloading in frequency where the different subcarriers can be loaded with different modulation. However, different streams can have different modulation, called unequal modulation.

RawBER (bit error probability without decoding) for different modulation is derived. Bit error probability for a AWGN channel is well known for BPSK and QPSK. The expression for 16QAM and 64QAM is given in Equation (B.1) (B.3) [Yoon et al., 2000].

$$P_{b,16QAM} = \frac{3}{4}Q\left(\sqrt{\frac{1}{5}\frac{E_s}{N_0}}\right) + \frac{1}{2}Q\left(3\sqrt{\frac{1}{5}\frac{E_s}{N_0}}\right) - \frac{1}{4}Q\left(5\sqrt{\frac{1}{5}\frac{E_s}{N_0}}\right)$$
$$\approx \frac{3}{4}Q\left(\sqrt{\frac{1}{5}\frac{E_s}{N_0}}\right) \tag{B.1}$$

$$P_{b,64QAM} = \frac{7}{12}Q\left(\sqrt{\frac{1}{21}\frac{E_s}{N_0}}\right) + \frac{1}{2}Q\left(3\sqrt{\frac{1}{21}\frac{E_s}{N_0}}\right) - \frac{1}{12}Q\left(5\sqrt{\frac{1}{21}\frac{E_s}{N_0}}\right)$$
$$- \frac{1}{12}Q\left(9\sqrt{\frac{1}{21}\frac{E_s}{N_0}}\right) - \frac{1}{12}Q\left(13\sqrt{\frac{1}{21}\frac{E_s}{N_0}}\right) \tag{B.2}$$
$$\approx \frac{7}{12}Q\left(\sqrt{\frac{1}{21}\frac{E_s}{N_0}}\right) \tag{B.3}$$

with approximation accurate for high SNR. The accurate and the approximation are calculate for the AWGN and compared with simulations shown in Figure B.1. The simulation matches the accurate results very nicely for the entire range. The approximations are accurate for RawBER ≤ 0.1.

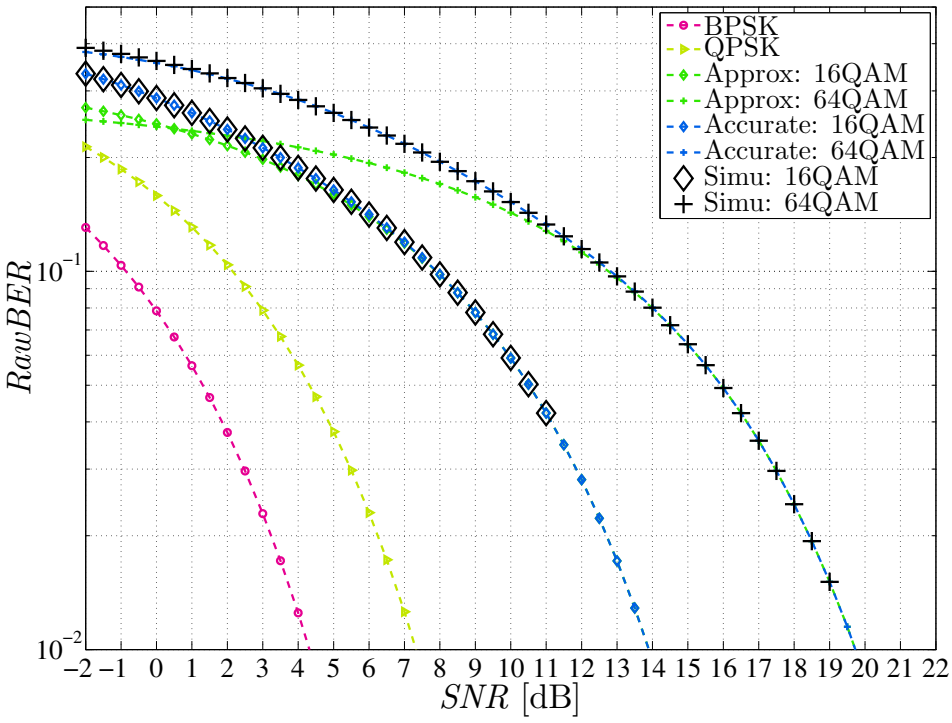

Figure B.1: *Simulations and theoretical calculations for RawBER.*

B.2 Coding in IEEE 802.11n

For IEEE 802.11n two different FEC is used. A mandatory convolutional code and a optional LDPC code. LDPC is not supported by Wipro 11n modem. The $(2, 1, 7)$ convolutional code with the generator polynomials $(133, 171)$ is utilized. The code rate is $1/2$ and can be adjusted to $2/3$, $3/4$ and $5/6$ by puncturing. Up to two spatial streams is multiplexed to share a single encoder/decoder.

B.3 Modulation and Coding Schemes

Modulation and coding schemes is a combination of a modulation and a code rate. The allowed combinations are defined in the standard [IEEE802.11n, sec.21.6] and the MCS for $N_{ss} = 1, 2$ are given in the Table B.1.

B.4 BER and PER in the AWGN Channel

In this section the performance of MCS $0 - 7$ is investigated for the AWGN channel. Also bounds for the BER are obtained from [Peng et al., 2007] to ensure the correct-

Table B.1: *Examples of modulation and coding schemes [IEEE802.11n, Sec21.6]. Data rate is for guard interval GI* $= 800\,\mathrm{ns}$ *and* $20\,\mathrm{MHz}$ *bandwidth. The dash "-" means that the second data stream is not employed.*

MCS	Modulation		Code	MCP	Data	No. of spatial
	Stream 1	Stream 2	Rate		Rate [Mb/s]	streams, N_{ss}
0	BPSK	-	$1/2$	0.5	6.5	1
1	QPSK	-	$1/2$	1	13.0	
2	QPSK	-	$3/4$	1.5	19.5	
3	16QAM	-	$1/2$	2	26.0	
4	16QAM	-	$3/4$	3	39.0	
5	64QAM	-	$2/3$	4	52.0	
6	64QAM	-	$3/4$	4.5	58.5	
7	64QAM	-	$5/6$	5	65.0	
8	BPSK	BPSK	$1/2$	1	13.0	2 Equal modulation
9	QPSK	QPSK	$1/2$	2	26.0	
10	QPSK	QPSK	$3/4$	3	39.0	
11	16QAM	16QAM	$1/2$	4	52.0	
12	16QAM	16QAM	$3/4$	6	78.0	
13	64QAM	64QAM	$2/3$	8	104.0	
14	64QAM	64QAM	$3/4$	9	117.5	
15	64QAM	64QAM	$5/6$	10	130.0	
33	16QAM	QPSK	$1/2$	3	39.0	2 Unequal modulation
34	64QAM	QPSK	$1/2$	4	52.0	
35	64QAM	16QAM	$1/2$	5	65.0	
36	16QAM	QPSK	$3/4$	4.5	58.5	
37	64QAM	QPSK	$3/4$	6	78.0	
38	64QAM	16QAM	$3/4$	7.5	97.5	

ness of the simulations.

The union bound for BER P_b for a punctured convolutional code with rate $R = k_0/n_0$ is [Peng et al., 2007]

$$P_b \leq \frac{1}{k_0} \sum_{d=d_{\mathrm{free}}}^{\infty} C_d P_d \tag{B.4}$$

where C_d is the number of bit errors for the hamming weight d path and P_d is the probability for choosing a weight d sequence over the all-zero sequence. *PER* can be

obtained by first calculating the codeword error probability as in Equation (B.5)

$$P_{cw} \leq \sum_{d=d_{\text{free}}}^{\infty} A_d P_d \tag{B.5}$$

with A_d the number of weight d codewords. Assuming that P_{cw} is independent, *PER* can be bounded as in Equation (B.6) [Manshaei, 2005, p.39]

$$PER \leq 1 - (1 - P_{cw})^{PL} \tag{B.6}$$

with PL the packet length in bits. BER and PER is clarified and we now consider how to calculate P_d for different modulations. For BPSK, P_d can be obtained as [Proakis, 2001, p.487]

$$P_{d,\text{BPSK}} = Q\left(\sqrt{\frac{2dE_s}{N_0}}\right). \tag{B.7}$$

For QPSK in-phase and quadrature-phase processing is independent and $P_{d,\text{QPSK}}$ is simply

$$P_{d,\text{QPSK}} = Q\left(\sqrt{\frac{dE_s}{N_0}}\right). \tag{B.8}$$

The bounds are a more complicated for higher order QAM signals. Tight bounds are derived in [Peng et al., 2007]. Note that for 16QAM there is an error in the original paper which was sorted out by contacting the authors. So, the correct formula is

$$P_{d,16\text{QAM}} \approx \frac{1}{I_d} \sum_{k=0}^{\lfloor d/3 \rfloor} \sum_{m=0}^{\lfloor (d-3k)/4 \rfloor} \binom{\lfloor d/3 \rfloor}{k} \binom{\lfloor (d-3k)/4 \rfloor}{m} Q\left(\sqrt{\frac{d+2k+4m}{5}\frac{E_s}{N_0}}\right) \tag{B.9}$$

with

$$I_d = \sum_{k=0}^{\lfloor d/3 \rfloor} \sum_{m=0}^{\lfloor (d-3k)/4 \rfloor} \binom{\lfloor d/3 \rfloor}{k} \binom{\lfloor (d-3k)/4 \rfloor}{m}. \tag{B.10}$$

Further, the 64QAM expression was obtained contacting the authors [Peng et al., 2007].

$$\begin{aligned} P_{d,16\text{QAM}} \approx & \frac{1}{I_d} \sum_{k_1=0}^{d} \sum_{k_2=0}^{L_2} \sum_{k_3=0}^{L_3} \sum_{k_4=0}^{L_4} \sum_{k_5=0}^{L_5} \sum_{k_6=0}^{L_6} \sum_{k_7=0}^{L_7} \binom{d}{k_1} \prod_{i=2}^{7} \binom{L_i}{k_i} \times \\ & Q\left(\sqrt{\frac{d+8k_1+2k_2+2_k3+10k_4+4k_5+24k_6+44k_7}{21}\frac{E_s}{N_0}}\right) \end{aligned} \tag{B.11}$$

$$
\begin{aligned}
L_2 &= \left\lfloor \frac{d+k_1}{2} \right\rfloor \\
L_3 &= \left\lfloor \frac{d+k_1-2k_2}{3} \right\rfloor \\
L_4 &= \left\lfloor \frac{d+k_1-2k_2-3_k3}{3} \right\rfloor \\
L_5 &= \left\lfloor \frac{d+k_1-2k_2-3_k3-3k_4}{4} \right\rfloor \\
L_6 &= \left\lfloor \frac{d+k_1-2k_2-3_k3-3k_4-4k_5}{5} \right\rfloor \\
L_7 &= \left\lfloor \frac{d+k_1-2k_2-3_k3-3k_4-4k_5-5k_6}{6} \right\rfloor \qquad \text{(B.12)}
\end{aligned}
$$

$$
\text{and} \quad I_d = \sum_{k_1=0}^{d} \sum_{k_2=0}^{L_2} \sum_{k_3=0}^{L_3} \sum_{k_4=0}^{L_4} \sum_{k_5=0}^{L_5} \sum_{k_6=0}^{L_6} \sum_{k_7=0}^{L_7} \binom{d}{k_1} \prod_{i=2}^{7} \binom{L_i}{k_i} . \qquad \text{(B.13)}
$$

To calculate P_b, the code dependent parameters C_d and A_d are obtained from [Kim, 1997] and [Frenger et al., 1998, p.54] for the constraint length 7 $(133, 171)$ convolutional code with the punctured patterns used in IEEE 802.11n. The simulation of the BICM as described in 802.11n [IEEE802.11n] is conducted in the AWGN channel and compared with the bounds obtained. The BER results are shown in Figure B.2. For the simulation in the AWGN channel the 802.11n $40\,\mathrm{MHz}$ interleaver is used. This is because interleaving will have some effect on higher order modulation such as 16QAM and 64QAM. Here 2 and 3 bits are processed each for the inphase and quadrature phase component of the received symbol and these bits are hence not independent (cf. Figure 5.8). Interleaving might degrade the error performance [Cheng et al., 2004, p.27]. Also, interleaving influence both the capacity and cutoff rate for the AWGN channel [Caire et al., 1998].

The BER bounds obtained matches very well the results given in [Peng et al., 2007] when the summation in Equation (B.4) is from $d_{\text{free}} \rightarrow d_{\text{free}} + 10$. The simulations has in general a lower BER for the same SNR when comparing with the results [Peng et al., 2007] and hence, the bounds are not as tight. This could be because the Viterbi decoder used for the simulations is with full trace back whereas it is not clear what Viterbi decoder that are used in [Peng et al., 2007]. The bounds for the PER results are given in Figure B.3.

The bounds in Figure B.2 and B.3 are in general tight for MCS $0, 1, 2, 7$ and not as tight for the other MCSs. The performance in the AWGN channel of different MCS is ordered systematic with respect the MCS index. First BPSK (MCS 0), QPSK (MCS $1-2$), 16QAM (MCS $3-4$) and at last 64QAM (MCS $5-7$) regardless of the rate.

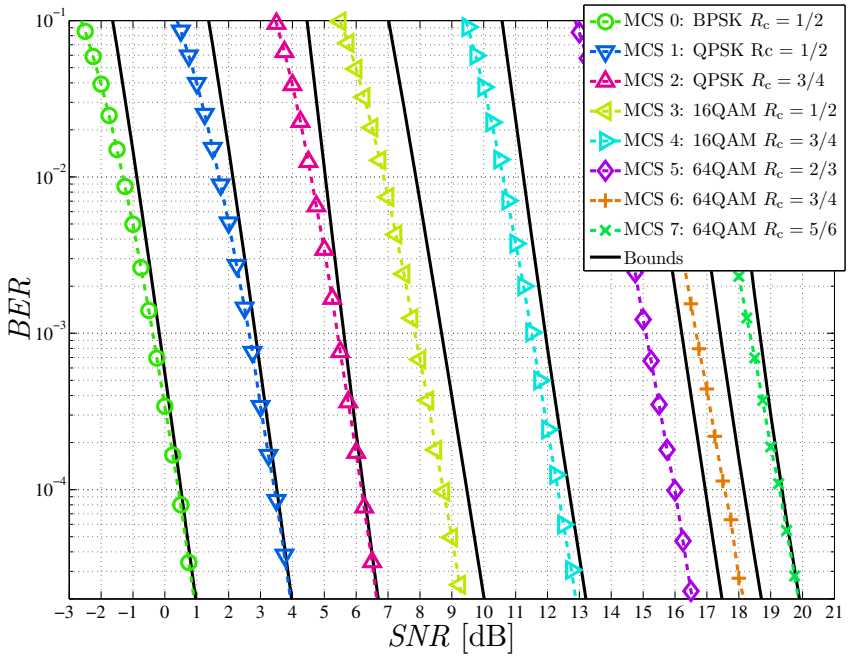

Figure B.2: *BER simulations and bounds for MCS* $0 \rightarrow$ *MCS* 7 *for the BICM sytem in the AWGN channel. MaxLog mapper, full trace back Viterbi decoder, info packet length PL* $=$ $1024\,\mathrm{Bytes}$ *and* $40\,\mathrm{MHz}$ *interleaver used for simulation.*

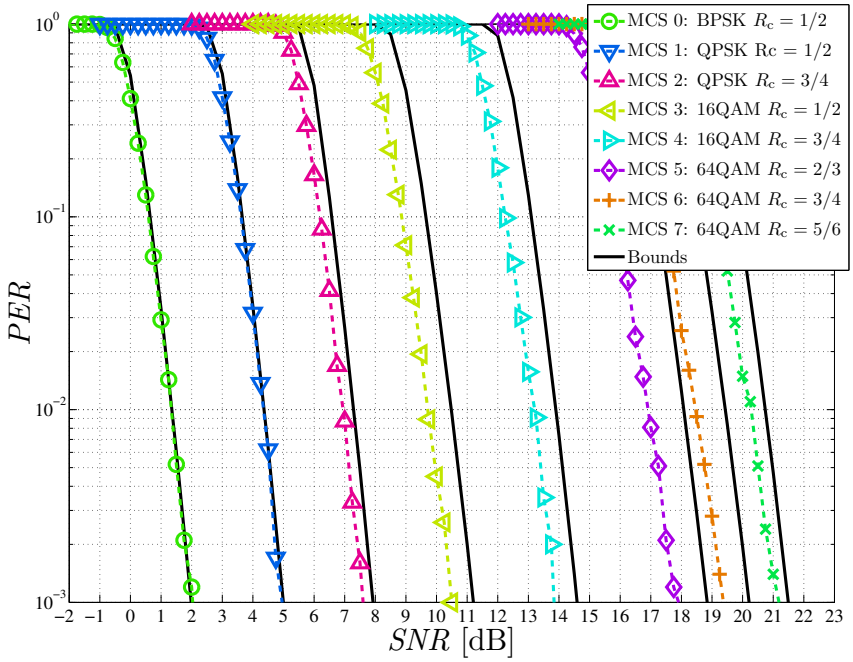

Figure B.3: *PER simulations and bounds for MCS 0* $\rightarrow$ *MCS 7 for the BICM system in the AWGN channel. MaxLog mapper, full trace back Viterbi decoder, info packet length PL* $=$ $1024\,\mathrm{Bytes}$ *and* $20\,\mathrm{MHz}$ *interleaver used for simulation.*

Formulas for Unequal Modulation

C

One method to combine the streams with different modulations is to consider the PER of each stream individually and then combine them into a single PER by

$$PER = 1 - (1 - PER_1)(1 - PER_2) \tag{C.1}$$

for the case of two streams. This indicates that the PER_1 and PER_2 are independent. But the two streams are multiplexed into a single stream where they share the same decoder and the independence assumption is not valid. Using this formula for combining equal modulation has also shown inaccurate PER estimation results.

We will however assume that the PER is independent of modulation but only dependent on the code rate in the PER versus RawBER domain as suggested in [Peng et al., 2007]. This is not a true assumption as discussed in Section 5.2.3. It can also be assumed in the PER versus MI domain [Sayana et al., 2007]. But by considering Figure 5.7 for RawBER or 5.15 for MI we observe that for $R_c = 3/4$ the curves are overlapping but this is not true for $R_c = 1/2$ where some inaccuracy then must be expected. However, we see no other possibility for combining the streams to estimate the PER. By assuming independence of the modulation in RawBER and MI domain, we obtain the following different formulas.

- **[MMIBM and MMIRM]**

$$\mathcal{I}_{\text{mean}}^{\text{symbol}} = \frac{\frac{1}{N_{\text{sd}}} \sum_{j=1}^{N_{\text{ss}}} b_j \sum_{k=1}^{N_{\text{sd}}} \mathcal{I}_j^{\text{symbol}}[k]\,(SINR_j[k])}{\sum_{j=1}^{N_{\text{ss}}} b_j} \tag{C.2}$$

- **[EESM]** For this method we also assume that

$$\mathit{RawBER}_j[k] \approx Errf(M, \mathit{SINR}_j[k]) \approx a \exp\left(\frac{\mathit{SINR}_j[k]}{b}\right) \tag{C.3}$$

for the modulation M. The effective SNR can then be obtained as

$$\mathit{SNR}_{\text{eff}} = -\beta_{\text{MCS}(n)} \log\left(\frac{\frac{1}{N_{\text{sd}}}\sum_{j=1}^{N_{\text{ss}}} b_j \sum_{k=1}^{N_{\text{sd}}} \exp\left(-\frac{\mathit{SINR}_j[k]}{\beta_{\text{MCS}(j)}}\right)}{\sum_{j=1}^{N_{\text{ss}}} b_j}\right) \tag{C.4}$$

where the variable $\text{MCS}(n)$ should then be used as the MCS for the look-up on the regression curve. Alternatively, combine the streams in the mutual information domain [Ericsson, 2003A]

$$\mathcal{I}_{\text{EESM}} = \frac{\frac{1}{N_{\text{sd}}}\sum_{j=1}^{N_{\text{ss}}} b_j \sum_{k=1}^{N_{\text{sd}}} \left(1 - \exp(\mathit{SINR}_j[k])\right)}{\sum_{j=1}^{N_{\text{ss}}} b_j} \tag{C.5}$$

where $1 - \exp(\mathit{SINR}_j[k])$ is the exponential information measure.

- **[MIESM]**

$$\mathit{SNR}_{\text{eff}} = \gamma_{\text{MCS}(n)} \left[J^{-1}\left(\frac{\frac{1}{N_{\text{sd}}}\sum_{j=1}^{N_{ss}} b_j \sum_{k=1}^{N_{\text{sd}}} J\left(\sqrt{\frac{\mathit{SINR}_j[k]}{\gamma_{\text{MCS}(j)}}}\right)}{\sum_{j=1}^{N_{\text{ss}}} b_j}\right)\right]^2 . \tag{C.6}$$

Additional Numerical Results

D

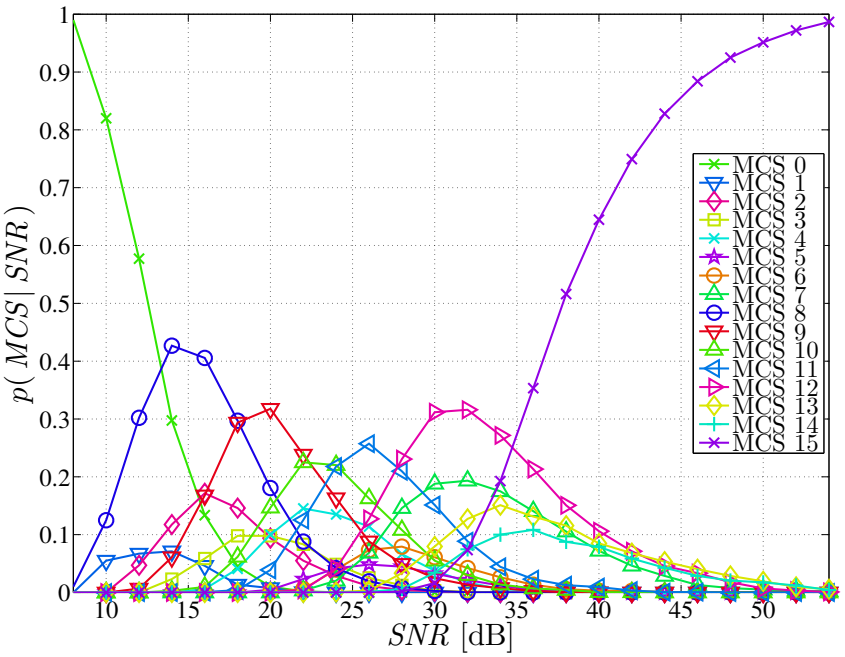

Figure D.1: *The probability for a MCS to be selected given a certain SNR for the MIESM method, channel B,* $20\,\mathrm{MHz},\ 2{\times}2$.